International
Progress Report

IPR-02-29

Äspö Hard Rock Laboratory

TRUE Block Scale project

Channel network and discrete fracture network analysis of hydraulic interference and transport experiments and prediction of Phase C experiments

W. Dershowitz
K. Klise
A. Fox
Golder Associates Inc.

S. Takeuchi
M. Uchida
JNC

December 2002

Svensk Kärnbränslehantering AB
Swedish Nuclear Fuel
and Waste Management Co
Box 5864
SE-102 40 Stockholm Sweden
Tel +46 8 459 84 00
Fax +46 8 661 57 19

Äspö Hard Rock
Laboratory

Report no.
IPR-02-29
No.
F56K
Author
W. Dershowitz
K. Klise
A. Fox
S. Takeuchi
M. Uchida
Date
Dec 2002
Checked by
Anders Winberg
Date
June 2003
Approved
Christer Svemar
Date
2004-02-12

Äspö Hard Rock Laboratory

TRUE Block Scale project

Channel network and discrete fracture network analysis of hydraulic interference and transport experiments and prediction of Phase C experiments

W. Dershowitz
K. Klise
A. Fox
Golder Associates Inc.

S. Takeuchi
M. Uchida
JNC

December 2002

Keywords: Fractured rock modelling, FracMan, tracer transport, TRUE Block Scale

Foreword

This report describes channel network and discrete fracture network analysis of hydraulic interference and tracer tests at the 100-meter scale in fractured granite, within the context of the Äspö TRUE Block Scale Project. This work was carried out by the JNC/Golder team, sponsored by the Japan Nuclear Cycle Development Institute (JNC), in Tono, Japan.

The modeling is based on a hydro-structural model developed from a combination of geological, geophysical, and hydrogeological data. This model was used to predict conservative tracer transport, and was then refined and re-calibrated for sorbing tracer transport (Phase C tracer tests).

Abstract

This report describes channel network (CN) and discrete fracture network (DFN) flow and transport modeling by the JNC/Golder team for the Äspö TRUE Block Scale project Tracer Testing Stage (TTS). The fracture network model combines the deterministic structures of the Revised March 2000 Hydro-structural model (Hermanson and Doe, 2000) and the by Dershowitz stochastically generated background fractures, cf. Andersson et al., 2002a

The DFN/CN modeling described in this report was carried out to improve the understanding of flow and transport in fracture networks at the 50 to 100 meter scale. This was achieved by testing the hydro-structural models against hydraulic responses, and using the results of conservative tracer experiments to derive transport properties for prediction of sorbing tracer transport. Particular emphasis was placed on understanding of the differences between transport in single fractures and in fracture networks. The models used include special elements developed to model fracture intersection zone (FIZ) effects.

To facilitate testing of hypotheses, this work was carried out within the framework of the existing hydro-structural model, with only minor modifications. Initial simulations were purely hydrologic, resulting in minor adjustments to the hydro-structural model. The modified hydro-structural model was then used to simulate conservative tracer transport. Transport parameters derived from conservative tracer transport simulations were used to predict the “Phase C” sorbing tracer transport experiments. Transport parameters adjusted based on conservative tracer transport experiments performed prior to Phase C included matrix porosity, diffusion distance, dispersion length, and transport aperture.

The experimental data used in this study were as follows. Phase A Tests A4 and A5 were used to test the hydro-structural model. Simulated distance-drawdown data were compared to experimental drawdown data to analyze the transmissivity and connectivity of deterministic structures. Tracer recovery was then used to evaluate FIZ pipes properties. The result of the distance-drawdown and FIZ evaluation of the preliminary model resulted in minor changes to the hydro-structural model. With the updated model, Phase B Tests B2g and B2d, and PT4 conservative tracer tests were simulated to provide transport properties. The transport parameters derived from these tests were then used in Phase C "blind" predictions of sorbing tracer transport. Once the predictions were completed, the experimental sorbing tracer breakthrough data were compared to the predictions. Several predictions produce good matches to the measured breakthrough. For the tracers that were not as well matched, additional supplementary simulations were carried out to derive appropriate sorption parameters to explain the observed tracer retention. In general, tracer retention along the tested pathways was greater than predicted, indicating either greater reactive surface areas or more porous fracture infillings than were observed in the TRUE-1 experiments.

Sammanfattning

Denna rapport beskriver modellering utförd av JNC/Golder inom ramen för TRUE Block Scale-projektet med en beskrivning av berget som diskreta nätverk (DFN) och som nätverk av kanaler (CN). Nätverksmodellen kombinerar de deterministiska strukturerna i den reviderade hydrostrukturella modellen från mars 2000 (Hermanson och Doe, 2000) och de av Dershowitz stokastiskt genererade bakgrundsprickorna (Andersson et al., 2002).

Den DFN/CN-modellering som redovisas i denna rapport utfördes med syfte att öka förståelsen av flöde och transport i ett nätverk av sprickor på en skala av 50-100 m. Detta åstadkoms genom att testa den upprättade hydrostrukturella modellen, implementerad i den numeriska modellen, mot mätta hydrauliska responser i borrhål, och genom utnyttjande av resultat från icke-sorberande spårförsök för att bestämma transportparametrar, att senare utnyttjas för förutsägelser av transport av sorberande spårämnen. Speciell betoning gavs till att söka förstå skillnaden mellan transport i en enskild spricka och i ett nätverk av sprickor. Modellerna inkluderade speciella beräkningselement för att adressera effekter av skärningszoner mellan sprickor (FIZ).

För att möjliggöra tester av olika hypoteser genomfördes denna studie inom ramen för den aktuella hydrostrukturella modellen, endast med mindre modifieringar. De initiala simuleringarna var rent hydrauliska, som resulterade i smärre justeringar i den hydrostrukturella modellen. Den senare hydrostrukturella modellen utnyttjades sedan för att simulera icke-sorberande spårämnestransport. Transportparametrar erhållna från simuleringen av icke-sorberande transport användes för att göra förutsägelser av försök med sorberande spårämnen inom ramen för ”Phase C”. De transportparametrar som justerades på basis av simulering av icke-sorberande spårförsök, inkluderade matrisporositet, diffusionslängd, dispersionslängd och transportapertur.

De experimentella data som utnyttjades i denna studie var följande: Resultat från testerna A4 och A5 (Phase A) utnyttjades för att testa den hydrostrukturella modellen. Beräknade avstånd-avsänkningsdata jämfördes med experimentella data för analys av deterministiska strukturers transmissivitet och konnektivitet. Erhållen massa (tracer mass recovery) utnyttjades sedan för att utvärdera egenskaper hos kanaler motsvarande FIZ-zoner. Utfallet av analysen av avstånd-avsänkning och FIZ-zoner med den preliminära modellen resulterade endast i mindre förändringar i den hydrostrukturella modellen. Med utnyttjande av testerna B2d och B2g (Phase B) samt PT4 användes den uppdaterade modellen för att bestämma transportparametrar som sedan utnyttjades för att göra förutsägelser om försök med sorberande spårämnen (Phase C). När modellprediktionerna var färdiga jämfördes resultatet med experimentella data. Många av modellprediktionerna visade god överensstämmelse med mätta genombrottsdata. För de spårämnen där ingen god överensstämmelse noterades, genomfördes kompletterande beräkningar för att söka bestämma acceptabla sorptionsparametrar som kunde förklara den noterade retentionen. Generellt befanns retentionen längs de undersökta flödesvägarena vara större än vad förutsägelserna visade. Detta indikerar att större area finns tillgänglig för diffusion/sorption , alternativt att sprickfyllnaderna är mer porösa än vad som observerades inom ramen för TRUE-1 experimentet.

Table of Contents

List of Figures

List of Tables

1 Introduction

This report describes the development and testing of a discrete fracture network/channel network (DFN/CN) model for the TRUE Block Scale site, and the use of this model for "blind" predictions of sorbing tracer breakthrough. The channel network model described in this report explores the Revised March 2000 Äspö Hydro-structural Model (Hermanson and Doe, 2000) combined with stochastically generated background fractures based on Dershowitz (2000).

To test hypotheses concerning "Fracture Intersection Zone" (FIZ) channels, special elements were included at the intersection of conductive structures where they could potentially influence solute recovery. These FIZ channels were assigned higher transmissivity and aperture. Generic FIZ studies reported in Winberg (ed) (2000) indicate that the primary effect of FIZ channels is in reducing mass recovery by providing pathways to alternative sinks within the rock mass.

The development and testing of the Revised March 2000 Äspö Hydro-structural Model begins with a hydraulic interference test to check the validity of the DFN structure transmissivity and connectivity. Tracer test A4 was used in the distance-drawdown comparison. Calibration to the A4 drawdown resulted in modifications to the models transmissivity and connectivity. The model was then used to run simulations of Tracer Tests B2g, B2d, and PT4. Non-sorbing tracer breakthrough was calibrated for each test and the resulting transport parameters were used for future "blind" predictions of sorbing tracers. The sorbing tracer predictions were carried out using both TRUE-1 and TRUE-Block Scale sorbing parameters, K_d and K_a. Once the sorbing tracer prediction was complete, the experimental sorbing tracer breakthrough data was released to compare the "blind" predictions with the in-situ data. Calibration to the sorbing tracer breakthrough data was then completed by modifying the sorbing parameters.

2 DFN and CN implementation of hydro-structural model

One of the goals of the TRUE Block Scale project is to test the validity of the derived hydro-structural model. The hydro-structural model used to develop DFN/CN models is described in Andersson et al. (2002a). Figure 2-1 and Figure 2-2 illustrates the TRUE Block Scale hydro-structural model at the scale of the Äspö Hard Rock Laboratory, and in the detailed region where tracer tests were performed. The model was synthesized on the basis of hydrological interpretations of pressure interference to drilling (Figure 2-3), Posiva flow logs (Figure 2-4), and hydraulic interference logs responses (Figure 2-5). The structural model also includes background fracturing based primarily on a combination of BIPS borehole imaging (Figure 2-6) and Posiva flow logs. For more information on the construction of the hydro-structural model see Andersson et al. (2002a).

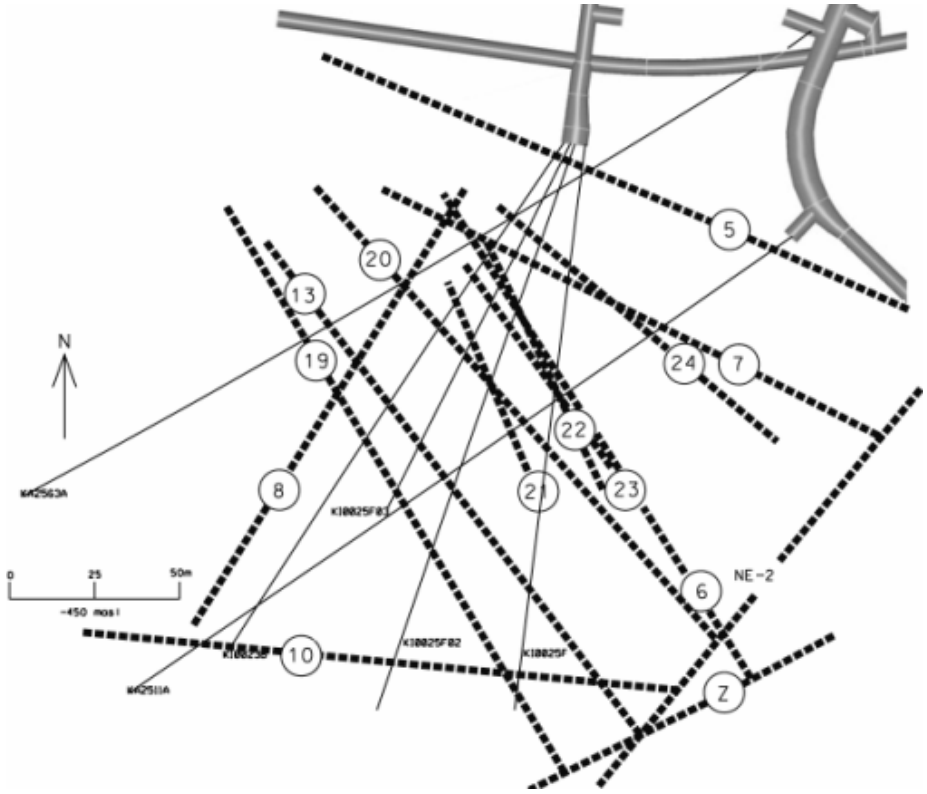

Figure 2-1 *Plan view of Äspö TRUE Block Scale site including tracers of boreholes and interpreted structures (Hermanson and Doe, 2000) (Dashed lines represent interpreted deterministic structures, thin solid lines represent boreholes)*

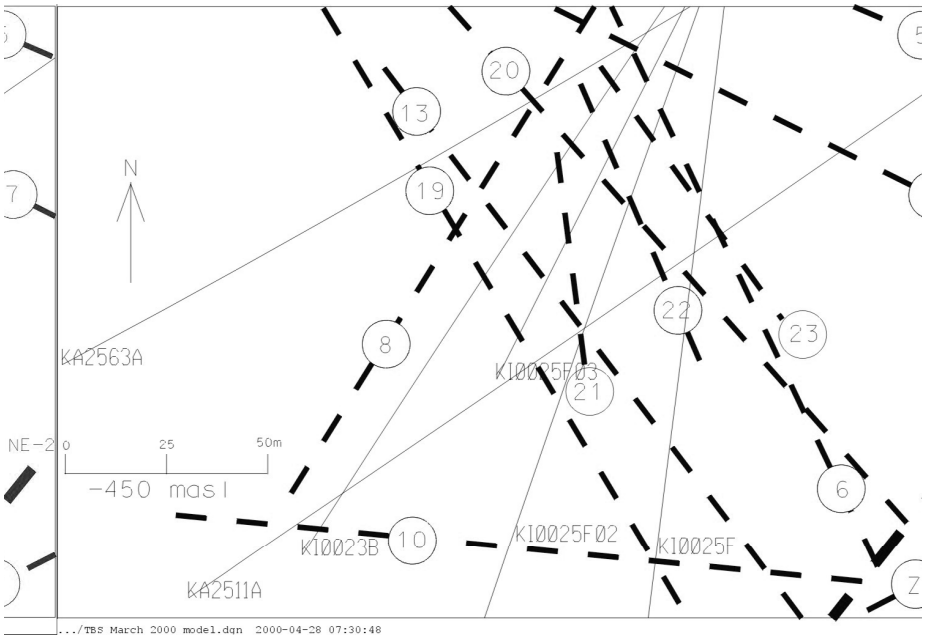

Figure 2-2 *Hydro-structural model – detail (Andersson et al., 2002b)*

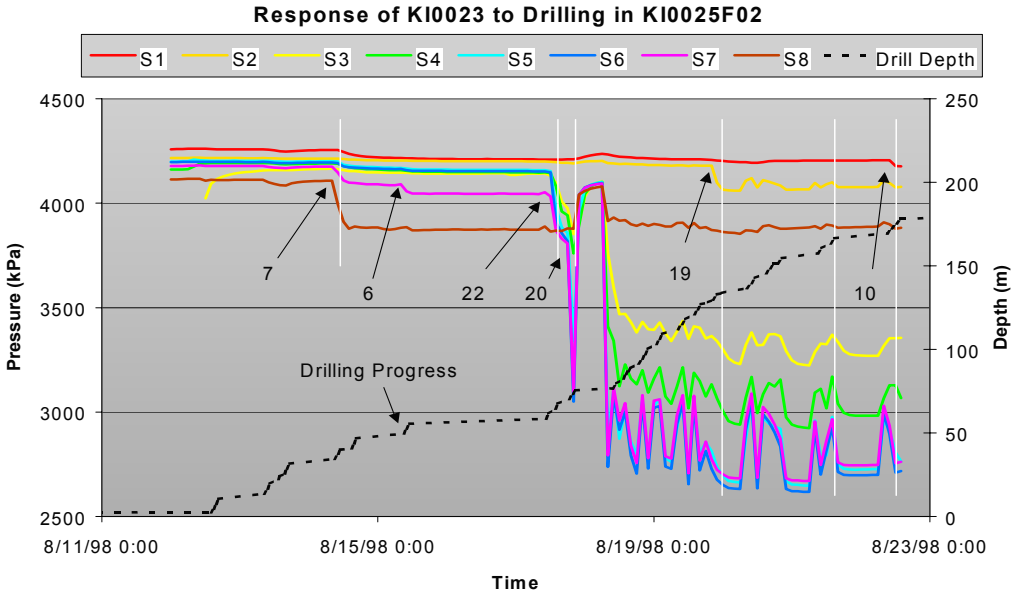

Figure 2-3 *Pressure response in KI0023B due to drilling of KI0025F02 (Andersson et al. (2002a)*

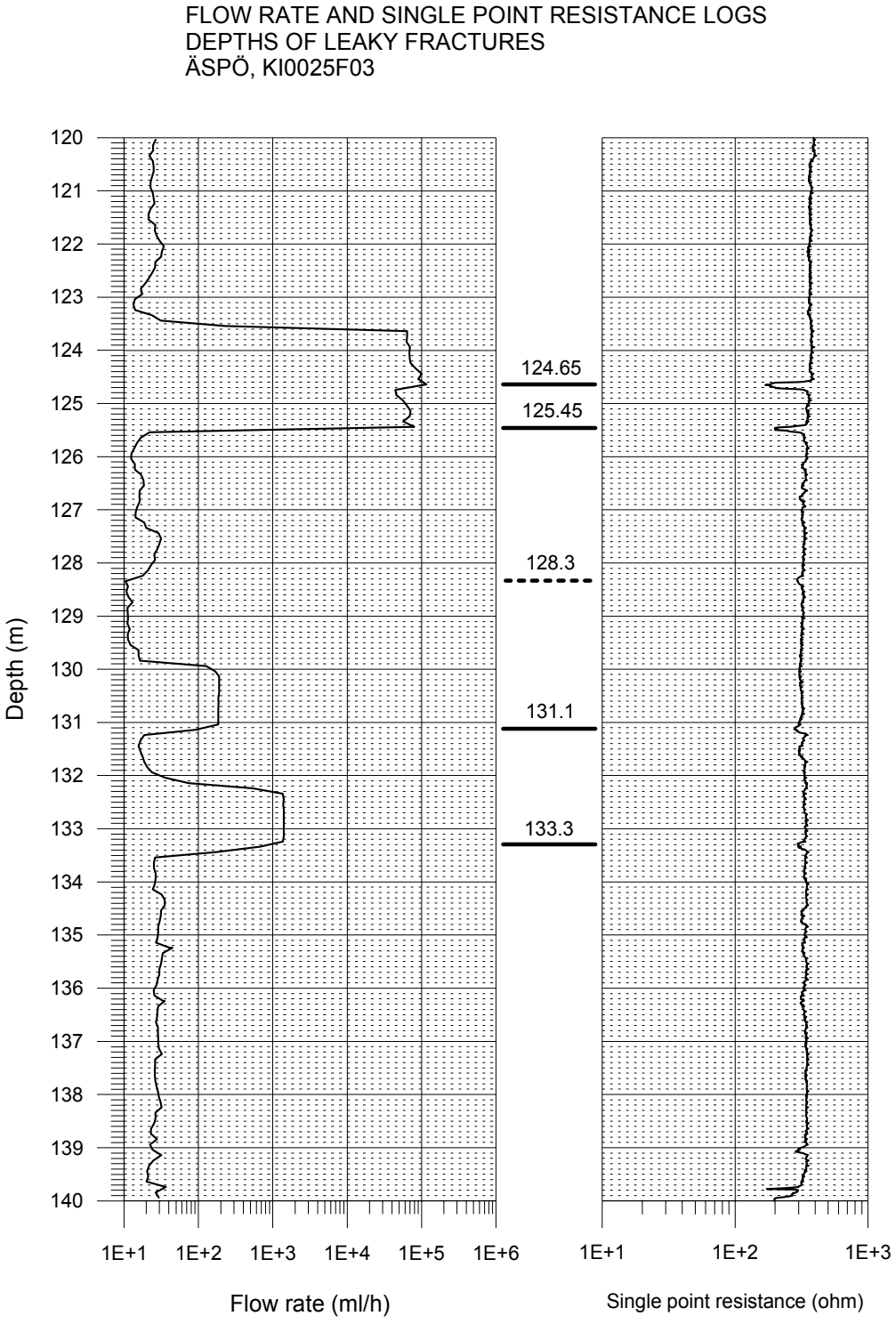

Figure 2-4 *Example of Posiva Flow Log - KI0025F03*

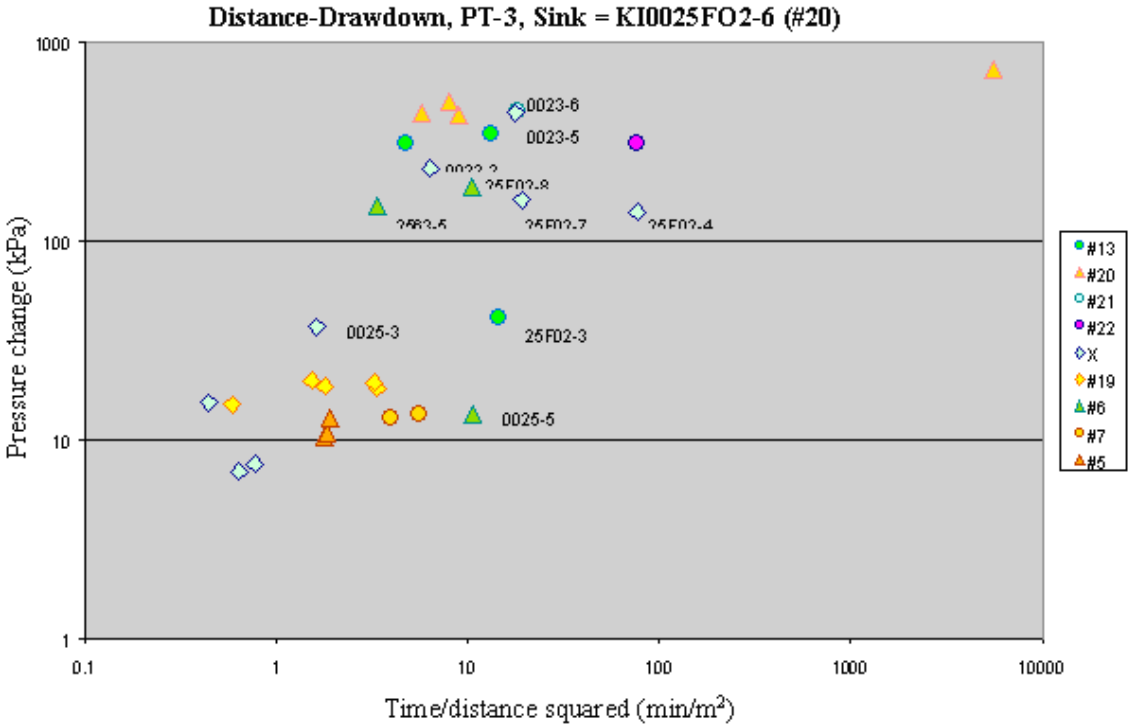

Figure 2-5 *Test PT-3 Plot of Distance-Drawdown (Structure #20)*

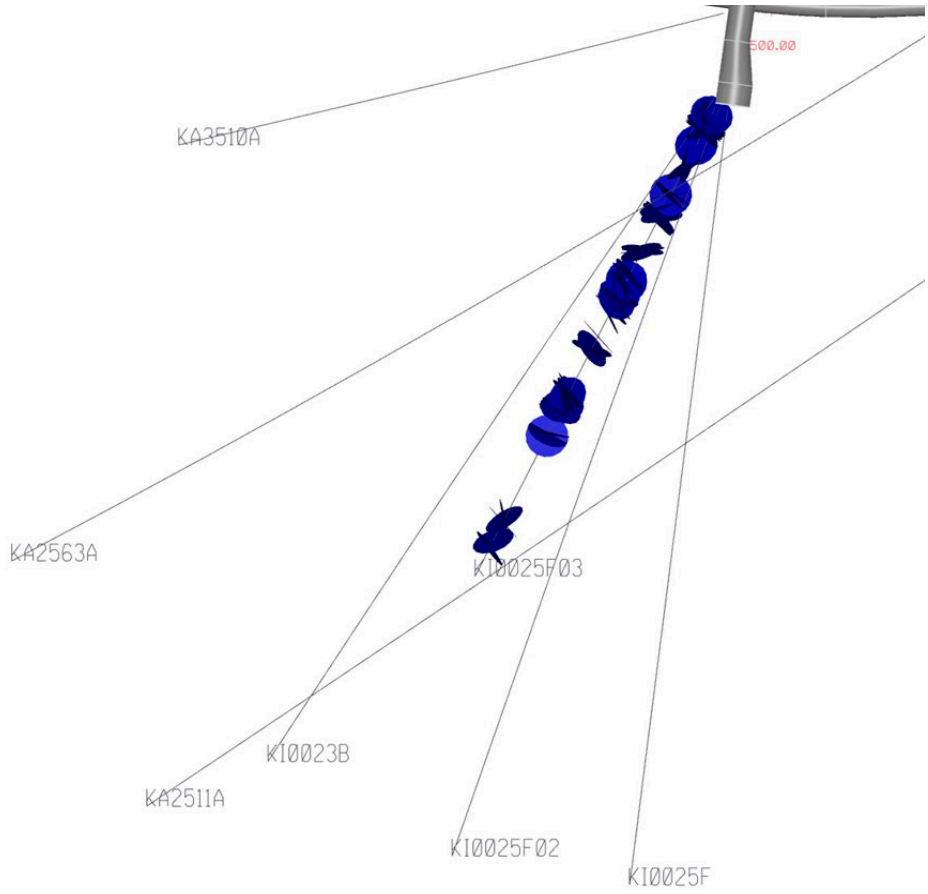

Figure 2-6 *Interpreted BIPS Structures in Borehole KI0025F03*

The DFN/CN model incorporates the deterministic structures contained in the Revised March 2000 Äspö Hydro-structural Model (Hermanson and Doe, 2000), and smaller, stochastically generated background fractures conditioned to borehole observations from the individual information from Borehole KI0025F03 (Andersson et al., 2002a).

2.1 Deterministic structures

Deterministic structures were defined by implementing the Revised March 2000 Hydro-structural Model (Hermanson and Doe, 2000). The model was implemented within a 500m x 500m x 500m cube, centered at 1900m, 7170m, -450masl in Äspö coordinates. Figure 2-7 shows a plan map view of the traces of the structures of this model at 450 meters below the surface. Figure 2-8 provides a three-dimensional visualization. Table2-1 contains a summary of the structures and their properties as incorporated into this model.

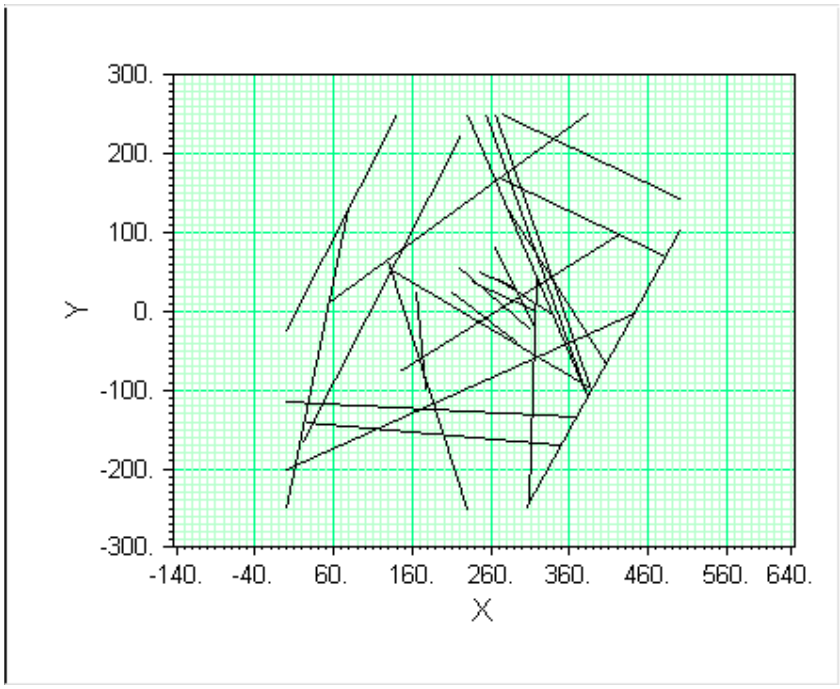

Figure 2-7 *Trace Map of Revised March 2000 Hydro-structural Model (Hermanson and Doe, 2000) Depth = 450m below surface (masl)*

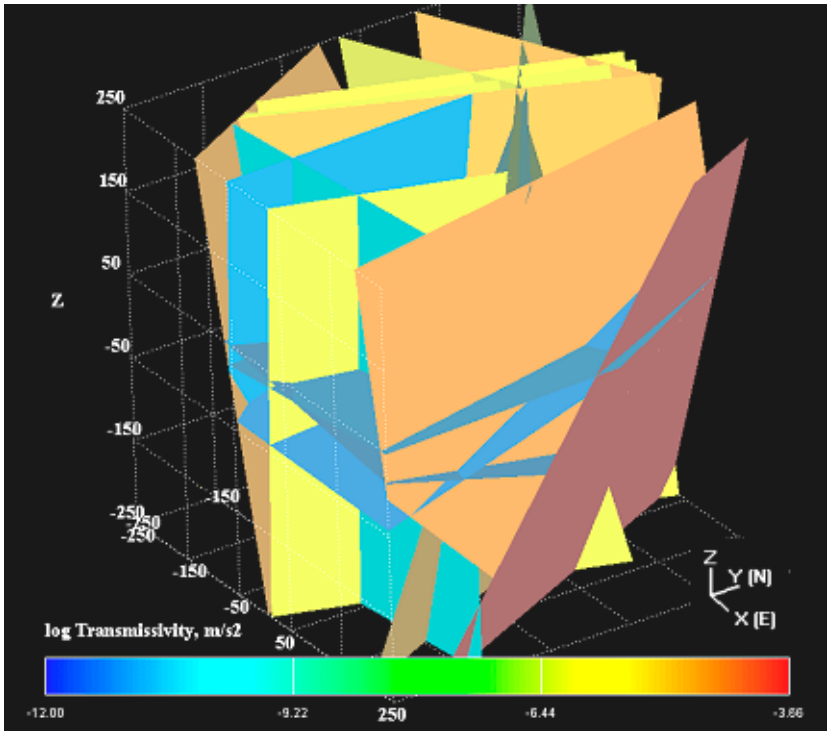

Figure 2-8 *Revised March 2000 Hydro-structural Model (Hermanson and Doe, 2000)*

2.2 Conditioned stochastic background fractures

In addition to the larger deterministic structures of the Revised March 2000 Hydro-structural Model, the DFN/CN model contains stochastic background fractures conditioned to borehole data. These fractures are modeled on a smaller scale, and are present within a 150m x 150m x 150m cube inside the larger model. This cube is also centered at 1900m, 7170m, -450 masl in Äspö coordinates. The 150 m cube accounts for the volume of the rock affected by the performed interferece and tracer tests.

Conditioning on borehole data adjusts stochastically generated fractures to match specific fracture observations in boreholes (Dershowitz et al., 1999). This allows for the development of models that precisely describe fracture geometry and properties where they are most important (i.e. at tracer injection holes, tunnel faces/walls and observation wells).

The background fractures in this channel network model are derived from drill core logs, flow logging, and downhole camera logs (BIPS) from boreholes KA2511A, KA3510A, KA2563A, KI0025F, and KI0023B. In addition, preliminary Posiva flow logs from KI0025F02 were incorporated into the model.

Table 2-2 presents a summary of properties for the stochastic background fractures; Figure 2-9 illustrates a realization of the stochastically generated fractures in the model.

Table 2-1: Deterministic Structures (after Hermanson and Doe, 2000)

Structure	Strike (°)	Pole Trend (°)	Pole Dip (°)
#6	327.50	237.50	88.6
#7	116.50	26.50	81.4
#13	322.80	232.80	66.4
#19	329.20	239.20	89.3
#20	318.50	228.50	84.93
#21	156.74	66.74	71.21
#22	154.64	64.64	69.02
#23	137.2	47.20	90
#24	130.24	40.24	81.62

Structure		Corner Coordinates of Interpreted Structures (m)					
		1	2	3	4	5	6
#6	Easting	1784.327	1799.417	2118.921	2103.975		
	Northing	7420.639	7420.527	6919.361	6919.26		
	Elevation	-199.361	-700.79	-700.639	-199.507		
#7	Easting	1649.361	2150.793	2150.639	1649.45		
	Northing	7392.688	7143.232	7058.112	7307.397		
	Elevation	-199.361	-199.472	-700.639	-700.825		
#13	Easting	1842.699	2150.675	2150.66	1947.787	1649.385	1649.317
	Northing	7420.705	7014.25	6919.278	6919.305	7313.005	7420.613
	Elevation	-700.692	-700.551	-569.251	-199.295	-199.263	-347.88
#19	Easting	1730.108	1737.527	2036.671	2029.388		
	Northing	7420.649	7420.528	6919.351	6919.252		
	Elevation	-199.351	-700.793	-700.649	-199.502		
#20	Easting	1678.12	1737.532	2150.532	2150.665	2121.151	
	Northing	7420.609	7420.579	6953.287	6919.262	6919.338	
	Elevation	-199.481	-700.692	-700.674	-447.995	-199.461	
#21	Easting	1915.555	2130.957	1945.342	1729.951		
	Northing	7420.706	6919.275	6919.294	7420.487		
	Elevation	-199.294	-199.517	-700.706	-700.73		
#22	Easting	1936.065	2150.537	2150.52	1960.907	1723.467	
	Northing	7420.802	6968.196	6919.227	6919.378	7420.507	
	Elevation	-199.417	-199.457	-254.175	-700.782	-700.68	
#23	Easting	1720.653	1720.748	2150.533	2150.601		
	Northing	7420.575	7420.472	6956.347	6956.274		
	Elevation	-199.379	-700.765	-700.621	-199.533		
#24	Easting	1753.722	1649.372	1649.422	2150.684	2150.684	
	Northing	7420.443	7420.403	7411.863	6987.775	7084.454	
	Elevation	-199.168	-656.728	-700.739	-700.518	-199.444	

Table 2-2 Properties of stochastic background fractures (Andersson et al., 2002a)

Parameter	Basis	Set #1	Set #2
Orientation Distribution	Two Fitted Sets to BIPS camera logs (NeurISIS)	Fisher Distribution Mean Pole (Trend, Plunge) = (211°, 0.6°) Fisher Dispersion = 9.4	Fisher Distribution Mean Pole (Trend, Plunge) = (250°, 54°) Fisher Dispersion = 3.8
Intensity P_{32}	Posiva Log Structures 0.29 m^2/m^3 total	0.16 m^2/m^3 (55.2% of fractures)	0.13 m^2/m^3 (44.8% of fractures)
Transmissivity	Posiva Log Structures, OxFilet Analysis of Packer Tests	Lognormal Distribution $\log_{10}$ mean = -8.95$\log_{10}$ m^2/s st.dev = 0.93$\log_{10}$ m^2/s	Lognormal Distribution $\log_{10}$ mean = -8.95$\log_{10}$ m^2/s st.dev = 0.93$\log_{10}$ m^2/s
Size Equivalent Radius	Hermanson et al. (1997)	Lognormal Distribution mean = 6 m st.dev. = 3 m.	Lognormal Distribution mean = 6 m st.dev. = 3 m.
Spatial Pattern	Fractal and Geostatistical Analyses	Baecher Model in TTS Region Fractal (D≈2.6) for larger scale blocks.	Baecher Model in TTS Region Fractal (D≈2.6) for larger scale blocks.

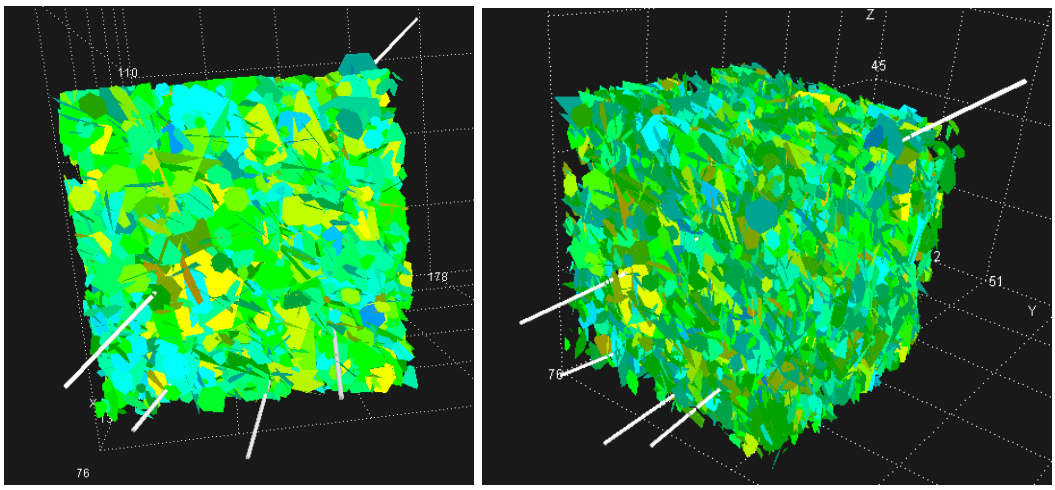

Figure 2-9 *Conductive Background Fractures. Conductive background fractures (N=7415), colored by $\log_{10}$ Transmissivity (m^2/s). Cube is 150 m x 150 m x 150 m, centered at 7170m, 1900m, -450 masl in Äspö coordinates.*

2.3 Channel network (CN) model

2.3.1 Transformation of DFN model to CN model

Fracture networks represent a three-dimensional flow and transport regime made up of interconnected two-dimensional structures (fractures). The channel networks method reduces the complexity of flow and transport solutions within fracture systems. This improves computational efficiency and the representation of channeling processes along fracture planes and fracture intersections. A channel network model transforms a 3D discrete fracture network into a network of 1D pipes. Pipes are geometric connections between fracture traces formed by the intersection of two or more fractures (Dershowitz et al. 1998). They reduce flow and transport to a one-dimensional process along "stream tubes", which can significantly reduce processing time.

The pipes that make up the pathways within a channel network are, at the very basic level, derived from continuum streamlines defined by pressure contours. However, since both connectivity and flow in most fractured rocks are controlled by fractures, a smooth, continuous field of streamlines may not accurately define the flow field. A channel network takes these variations due to geometry into account. Each fracture intersection is reduced from a line connecting two points to a single node. Channels, or "pipes", simply become lines connecting nodes. Pathways are composed of multiple pipes. Pipe properties, such as aperture, transmissivity, roughness and mineral infillings are either derived from the fractures themselves or are specified independently. Figure 2-10 illustrates the basic methodology behind the channel network approach.

A discrete fracture network model is converted to channels through the use of the PAWorks software package (Dershowitz et. al., 1998). A 3-D network of fractures is first converted into a 1-D pipe network mesh. The finite-element code MAFIC (Miller et al., 1999) is then used to calculate heads and fluxes at all nodes to produce a flow solution for the network. The PAWorks module analyzes transport pathways based on a search algorithm. Transport with PAWorks channel networks can be solved using the Laplace Transform Galerkin algorithm, which provides for advection-dispersion, sorption onto the fracture surface, diffusion into the rock matrix and stagnant (non-flowing) water adjacent to the flowing fracture, and for radionuclide decay.

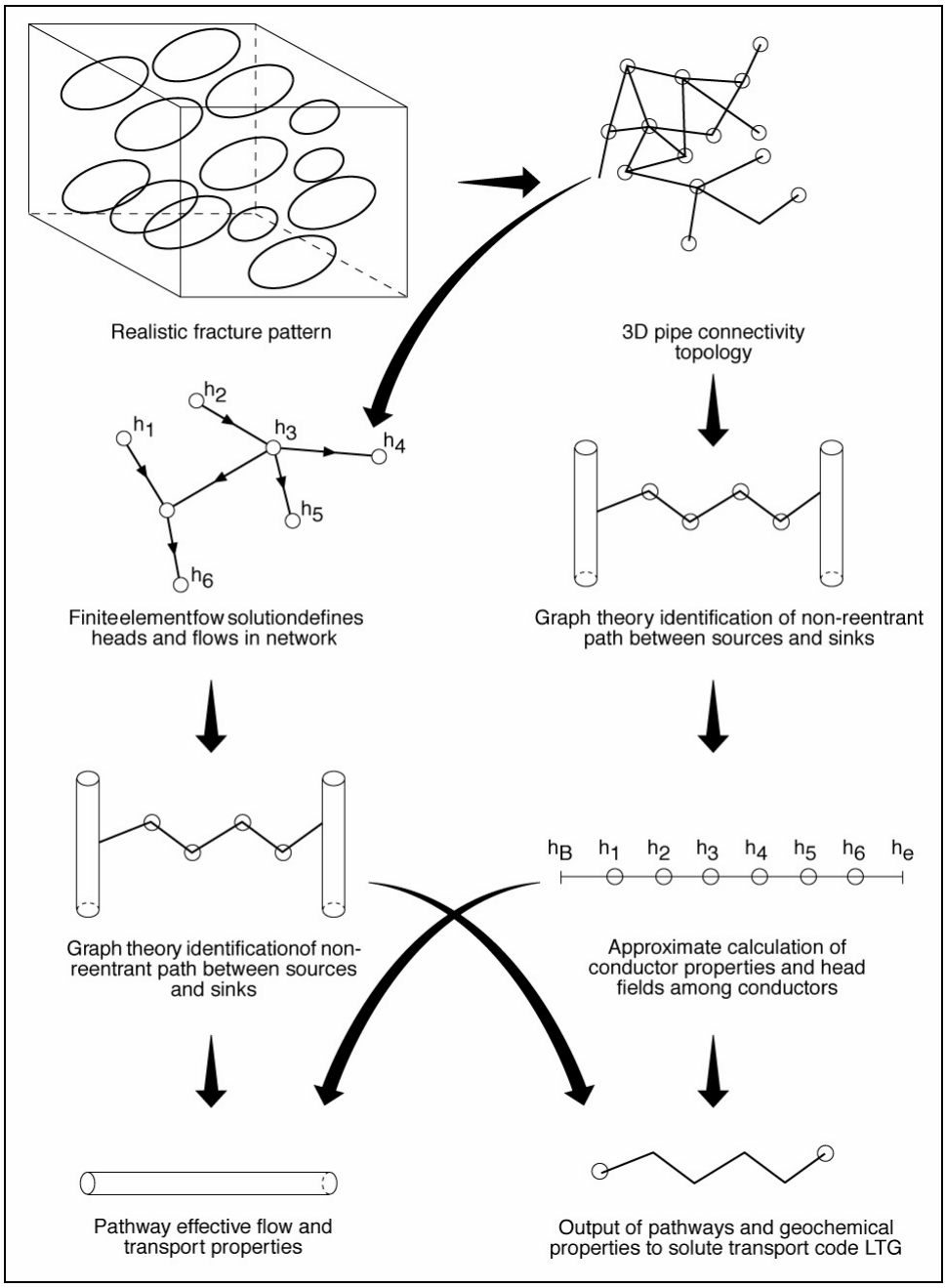

Figure 2-10 *PAWorks approach to channel network modeling*

2.3.2 CN model implementation of the Äspö TRUE Block Scale DFN model

The DFN described earlier in this report forms the basis of the channel network model. The DFN model contains 29 deterministic structures and approximately 7600 stochastically generated background fractures that reside in a 150m x 150m x 150m cube within the larger 500m x 500m x 500m scale hydro-structural model.

Fractures contained within the DFN model are converted to CN pipes based on the assumptions described below. Figure 2-11 illustrates the parameters used in the calculation of pipe widths within PAWorks.

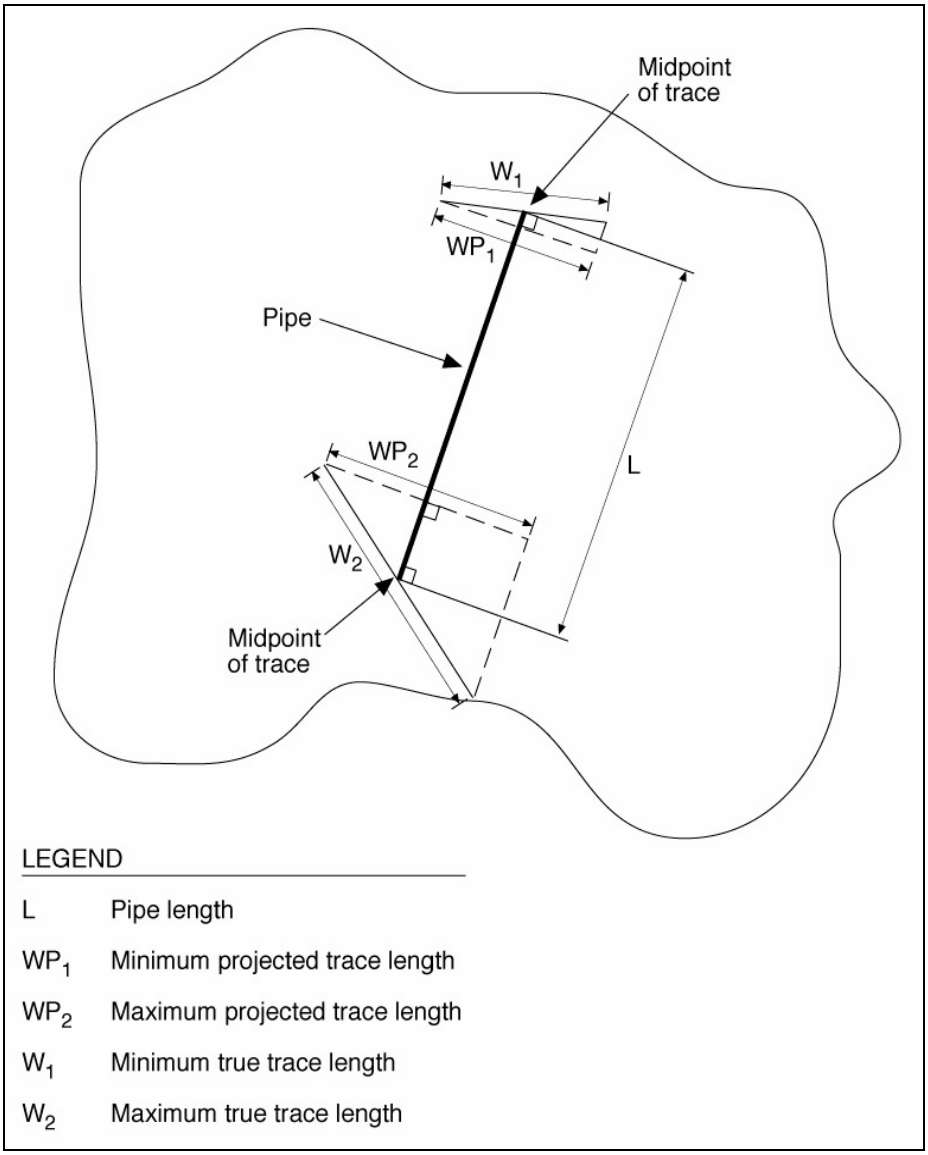

Figure 2-11 *Parameters for Pipe Width Calculation*

- Effective Pipe Generation:
  Pipes cannot overlap each other. Pipes cannot cross fracture traces on a given fracture surface. All traces on a fracture are connected, preventing isolated pipe clusters within a fracture. In addition, to prevent excessively long pathways, additional pipes are added so that the tortuous distance between two nodes does not exceed the effective pipe factor times the Cartesian distance. The CN model effective pipe factor is assigned to 1.2 to avoid large pipe lengths as compared with the Cartesian length between nodes.

- Pipe "Aperture":
  Pipe aperture is derived from fracture transmissivity using a power-law relationship of Equation 1. CN model aperture parameters are initially assigned as A = 2 and B = 0.5 based on Dershowitz et al. (2000).

$$\text{Pipe Aperture} = A \bullet T^{B} \qquad \textbf{Eq 1}$$

Where pipe aperture is in meters and transmissivity is in m^2/s

- Pipe Width:
  The pipe flow width for a pathway is calculated from the width of the fracture intersections forming the pipe. Pipe width is calculated from the trace length (Dershowitz et al., 1998). The CN model pipe width used for these analyses was calculated from Equation 2:

$$W_i' = W_{af} \bullet W_i \ / \ W_{area} \qquad \textbf{Eq 2}$$

Where:
W_i' = pipe width corrected for W_{af}
W_{af} = width to area correction factor
W_i = width of pipe *i*
W_{area} = sum of $\{W_i \bullet L_i\} / A_f$

$$W_i = W_{area} \bullet (X_{min} \bullet L_{min} + W_{max} \bullet L_{max}) \qquad \textbf{Eq 3}$$

Where:
W_{area} = effective pipe width multiplier
X_{min} = pipe width multiplier for shorter trace length
X_{max} = pipe width multiplier for longer trace length

All three multipliers for the CN model are set equal to 1 in this study. A value of W_{af} equal to 1 gives an equivalence of total pipe and fracture area.

- Merge Distance:
  Any nodes that are closer together than the merge distance are merged together into one node. The CN model merge distance is assigned to 0.0001 m

- Minimum Fracture Transmissivity:
  Any fracture with a transmissivity less than this value is eliminated from the CN model. The CN model minimum transmissivity is assigned to $1.00 \bullet 10^{-10}$ m^2/s

- External Model Boundaries:
  The external boundary of the preliminary CN model are the edges of the 500m x 500m x 500m cube of the March 2000 structural model. All external boundaries are modeled as constant head, and are set to the conditioned head field values presented by Holton (2001).

- Internal Boundaries:
  Two types of internal boundaries were used in the model: source zones and sink zones. Zones are described as the area between two packers (i.e. a "packer interval"). Sources and sinks were modeled as having a constant group flux.

2.3.3 Fracture Intersection Zones (FIZ)

In a fracture network, the intersection between two fractures may be more conductive than the surrounding fracture area, and as a result, may behave as a distinct flow channel. Alternatively, gouge materials formed at fracture interaction may act as flow barriers. Fracture intersection zones (FIZ) can therefore act as highly permeable flow channels, as flow barriers, or as a combination of flow channels and flow barriers. FIZs are defined by having different hydraulic properties other then their associated fractures. The locations of the flow channels on any fracture surface are normally not known. In the case of deterministic structures, whose locations are known, the location of the FIZ can be determined. This provides the opportunity to design hydraulic borehole tests in a way that the FIZ will be part of the flow channel network.

To establish the connection between the FIZ and the boreholes, pipes are added to the channel network running from the FIZ to each borehole location on the two intersecting structures. Each new node, where the added channel intersects the FIZ, is then connected. FIZs are terminated on the regional bounding structures (NE-2, and EW-1) to improve the connection within the TRUE block. Channels established within the intersection zone are added to the channel network prior to calculating the head field.

FIZ pipes are assigned a transmissivity of 10 times greater than the higher transmissivity of the two intersecting structures defining the FIZ. This results in corresponding FIZ transport apertures as calculated using Eq 1. FIZs are linked to the CN model by adding pipes that connect the injection and withdrawal borehole sections to the FIZ pipes at the intersection of the deterministic structures associated with the test. These pipes are assigned the same transmissivity as the structures that contain them.

FIZ pipes have the potential to change tracer transport through several mechanisms. Where the gradient along the FIZ causes the tracer to deviate from the associated structure, increased path length and changes in travel velocity result in longer travel times. FIZ sections also provide a large volume for tracer dilution. Tracer tests crossing fracture intersection zones may experience mass loss due to enhanced retardation and/or diffusion, and/or by transporting tracer mass to alternative sinks.

FIZ pipes were added to CN models to model the intersection of Structure 20 and 21 and the intersection of Structures 13 and 21. Figure 2-12 illustrates a generic pathway generated by the CN model and a pathway generated through the additional FIZ pipes.

Figure 2-13 illustrates the location of the FIZ zone associated with each structure intersection. Figure 2-14 illustrates location of low hydraulic head in tracer Test A4, which support the concept of mass loss through FIZ pipes to alternative sinks.

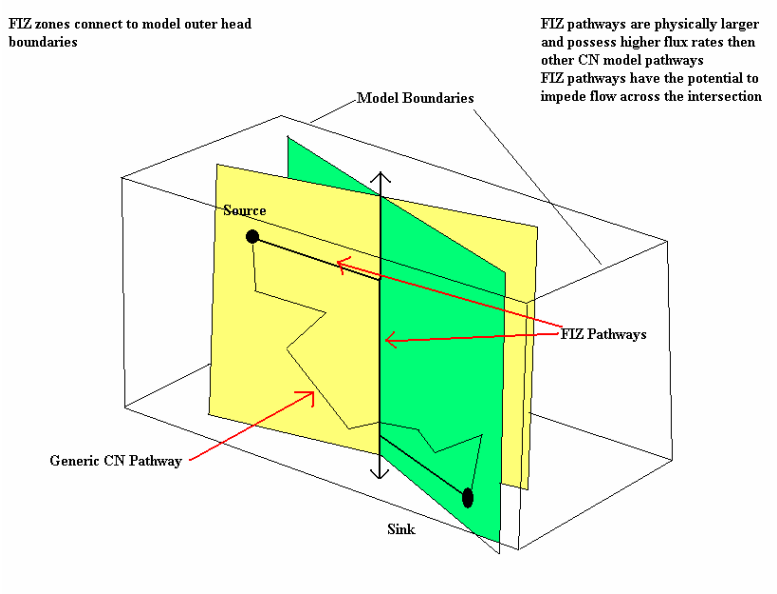

Figure 2-12 *Generic FIZ Model*

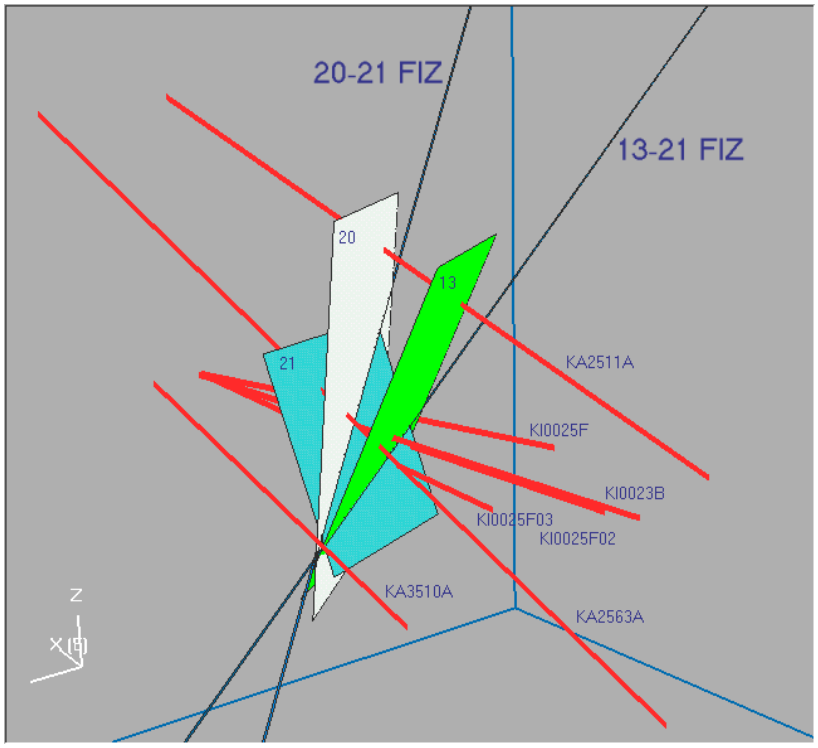

Figure 2-13 *Location of #20/#21 FIZ and #13/#21 FIZ*

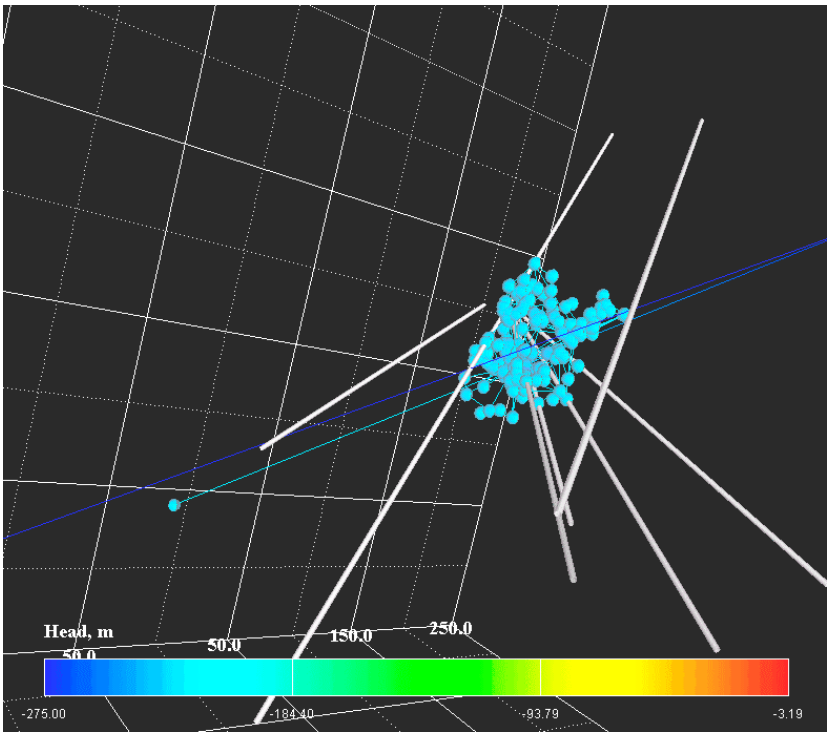

Figure 2-14 *Location of low heads during a Phase A Test A4 tracer test (including #20/#21 FIZ zone)*

3 Simulations using March 2000 hydro-structural model

The first simulations carried out tested the Hermanson and Doe (2000) updated hydro-structural model. The preliminary parameters of the DFN deterministic structure are summarized in Table 3-1, while stochastically generated background fracture properties are shown in Table 2-2. The structure numbers in Table 3-1 refer to the hydro-structural model of Winberg et al. (2001). The preliminary DFN model of deterministic structures had a constant storativity of $1.00 \bullet 10^{-6}$ and flow aperture parameters A = 2, B = 0.5 (See Eq 1).

This section describes the simulation of hydraulic interference tests to evaluate the viability of the hydro-structural model for flow, and transport simulations to evaluate the sensitivity of tracer transport to immobile zone properties. Tracer Test A4 was used in the following simulations. Parameters related to tracer test A4 are listed in Table 3-2.

Table 3-1 Preliminary Deterministic Structure Parameters (Hermanson and Doe, 2000)

Structure	Transmissivity (m^2/s)	Normal Vector to Plane			Area (m^2)
		nx	ny	nz	
1	$1.00 \cdot 10^{-6}$	-0.419	0.897	0.139	193.22
2	$1.00 \cdot 10^{-6}$	0.95	-0.33	0.017	242.99
3	$1.00 \cdot 10^{-6}$	-0.93	0.34	-0.151	247.42
4	$1.00 \cdot 10^{-6}$	0.84	-0.53	-0.146	189.08
5	$1.00 \cdot 10^{-6}$	-0.92	0.39	-0.008	248.74
6	$1.50 \cdot 10^{-8}$	0.61	-0.80	0.047	5663.25
7	$1.70 \cdot 10^{-6}$	0.93	-0.37	0.098	43539.19
8	$1.00 \cdot 10^{-10}$	0.50	0.80	-0.352	222.4
9	$1.00 \cdot 10^{-8}$	-0.84	0.54	-0.035	308.13
10	$5.30 \cdot 10^{-8}$	0.95	-0.09	-0.311	13096.46
11	$1.00 \cdot 10^{-6}$	-0.95	0.30	0.035	229.7
12	$1.00 \cdot 10^{-10}$	-0.09	1.00	0	226.46
13	$5.00 \cdot 10^{-8}$	0.63	-0.75	-0.213	9358.65
15	$2.00 \cdot 10^{-11}$	-1.00	-0.04	0.035	203.12
16	$2.00 \cdot 10^{-11}$	-0.02	0.31	-0.952	261.28
17	$2.00 \cdot 10^{-11}$	0.08	0.04	-0.996	255.86
18	$1.00 \cdot 10^{-6}$	-0.11	-0.25	-0.962	250.75
19	$1.70 \cdot 10^{-6}$	0.53	-0.84	0.138	17958.34
20	$9.60 \cdot 10^{-7}$	0.67	-0.74	-0.088	14966.42
21	$8.10 \cdot 10^{-7}$	0.14	-0.98	-0.172	6663.6
22	$2.60 \cdot 10^{-7}$	0.41	-0.89	-0.2	7289.85
Z	$5.00 \cdot 10^{-6}$	-0.87	-0.44	0.225	243.55
EW-1	$1.20 \cdot 10^{-5}$	-0.86	-0.48	-0.199	255.91
EW-3	$1.70 \cdot 10^{-5}$	-0.96	-0.20	-0.191	221.5
NE-1	$2.20 \cdot 10^{-4}$	0.85	0.44	-0.301	227.04
NE-2	$1.20 \cdot 10^{-7}$	-0.57	-0.79	-0.225	242.73
NNW-7	$7.50 \cdot 10^{-6}$	0.42	-0.90	-0.087	199.74

Table 3-2 Tracer Test A4 Basic Data

Tracer	Source	Structures Tested
Uranine	KI0023F03: P5 (66.5 - 74 m)	20
Amino G Acid	KI0023F03: P6 (59.5 - 65.5 m)	22
Rhodamine WT[2]	KI0023F03: P7 (55 - 58.5 m)	23
Sink Location	KI0023B:P6 (70.4 - 71.4 m) Structure 21/(20)	
Pumping Rate	2.30 l/min	
Pumping Duration	17370 minutes (~ 12 days)	

3.1 Distance-drawdown simulations for hydro-structural model evaluation

Comparisons between the distance-drawdown results measured in the field, and as computed in the preliminary CN model, were used to refine the hydrologic properties assigned to the major structures. The external boundaries of the modeled region were the edges of the 500m x 500m x 500m cube. All external boundaries were modeled using a constant head boundary condition, and were set to the conditioned head field values presented by Holton (2001). Connectivity between the deterministic structures and the outer boundary establish the steady state head field across the CN model. The finite-element code MAFIC was used to compute the flow solution. Heads prior to the start of tracer Test A4 across the $500m^3$ block are displayed in Figure 3-1. Figure 3-2 displays a contour map of heads prior to Test A4 at the model's center, looking towards the Äspö HRL tunnel. Figure 3-3 and Figure 3-4 display hydraulic head distribution after Test A4 across the TRUE Block Scale region.

Figure 3-5 compares in-situ experimental and predicted distance-drawdown data. While most of the intervals are well modeled, simulated drawdowns is too large for Structures #19, #20, and #13. This indicates that the hydro-structural model may be over-connected for these structures, or the structures may be connected to hydraulic boundaries that reduce their sensitivity to the A4 pumping. In general, however, the hydro-structural model appears to perform well enough to be useful at the scale of the tracer tests to be carried out in Phase C. Future studies will address possible refinements to the hydro-structural models to address the discrepancies between measured and modeled drawdown.

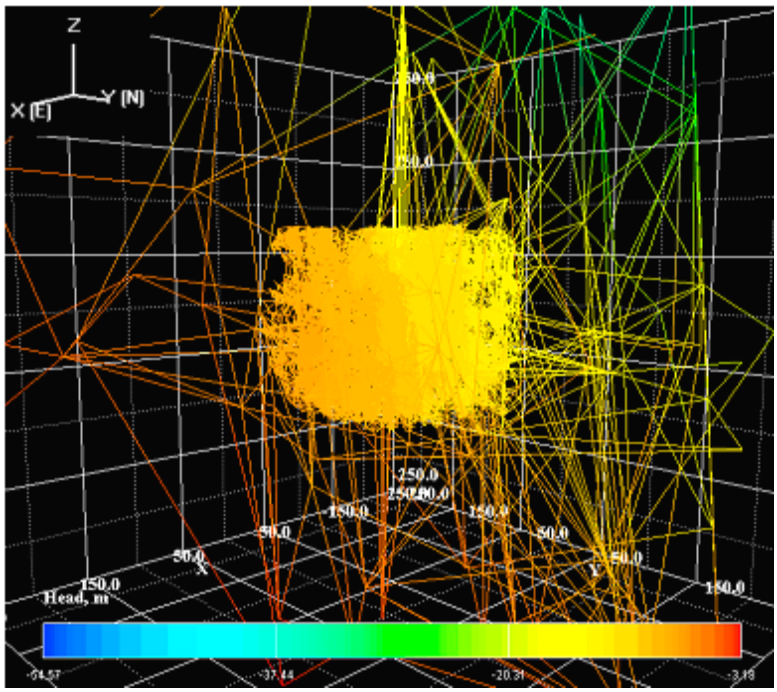

Figure 3-1 *TTS Test A4: Heads prior to start of Tracer Test A4. CN Model Mesh, with pipes colored by head (masl)*

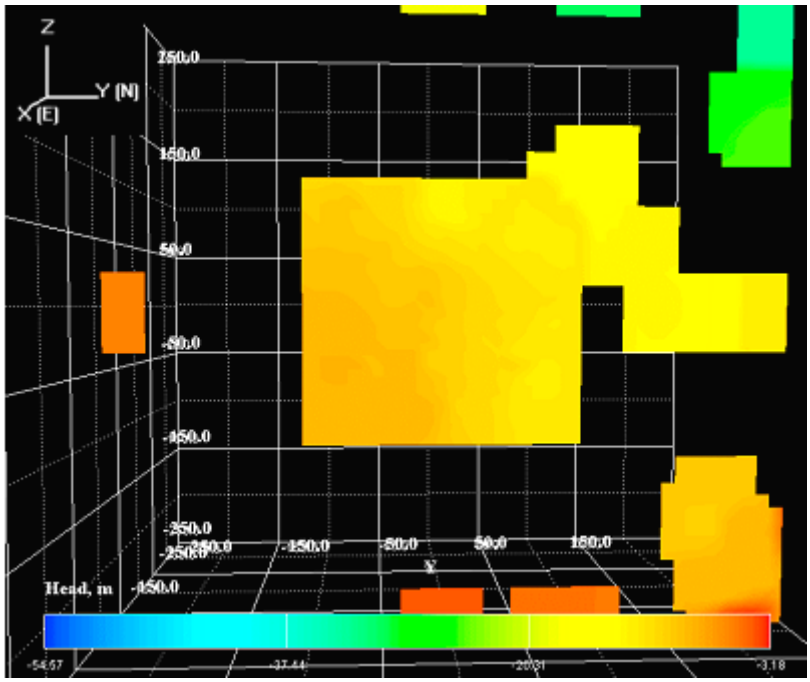

Figure 3-2 *TTS Test A4: Contour map of heads prior to start of Tracer Test A4. Vertical trace map view at model center looking towards Äspö HRL tunnel. Grid colored by head (masl)*

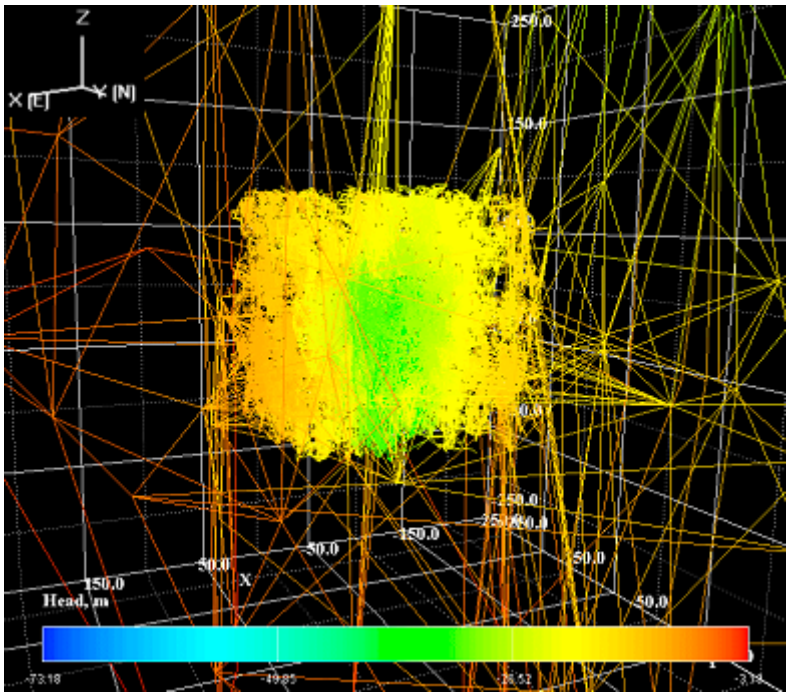

Figure 3-3 *TTS Test A4: Head values after tracer Test A4. CN Model Mesh, with pipes colored by head (masl)*

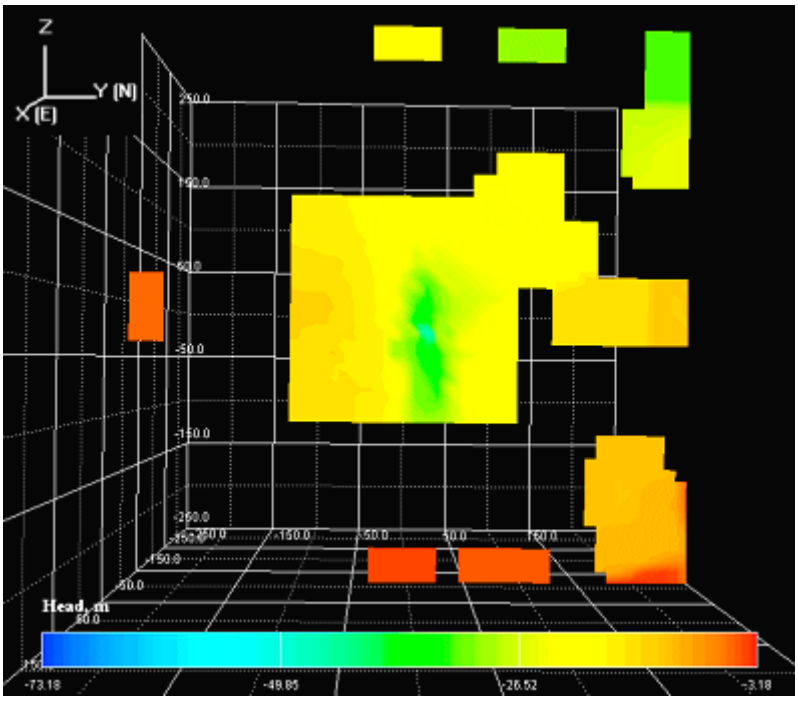

Figure 3-4 *TTS Test A4: Contour map of head values after tracer Test A4. Vertical trace map view at model center looking towards Äspö HRL tunnel. Grid colored by head (masl)*

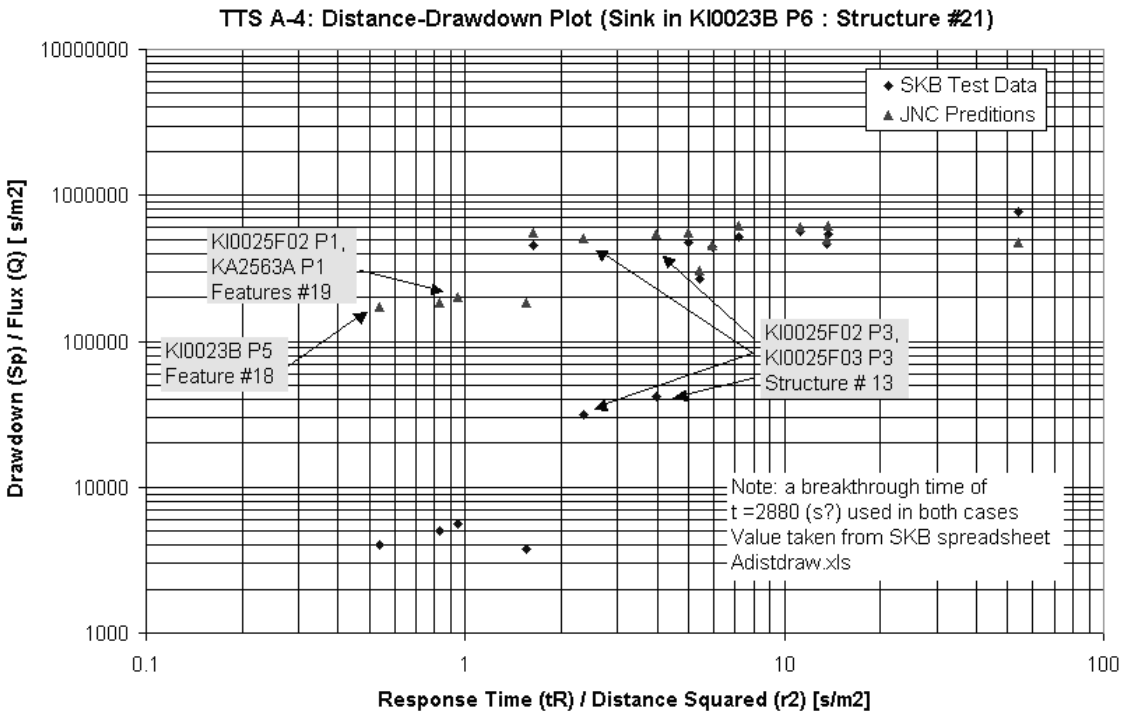

Figure 3-5 *TTS Test A4: In-situ Distance-Drawdown data compared with TTS Test A4 Distance-Drawdown resulting from CN model simulation.*

3.2 Simulation of tracer tests for evaluation of immobile zone properties

Using the March 2000 Hydro-structural Model (Hermanson and Doe, 2000), tracer Test A4 was tested against experimental data to evaluate appropriate immobile zone properties. Simulations were carried out using the Laplace Transform Galerkin transport code (Dershowitz et al, 1998).

Three simulations were carried out (A, B, and C). Figure 3-6 through Figure 3-10 shows the breakthrough and recovery for tracers Uranine, Rhodamine WT, and Amino G Acid. Note the multiple peaks of the Amino G Acid breakthrough curve, caused by a multiple pathway network. Table 3-3 details the parameters used for each calibration. All three simulations share the following parameters: aperture parameters A = 2, B = 0.5 (Eq 1), dispersion length = 1.5 m. Simulation A had no immobile zones included. Simulations B and C are identical to Simulation A with the addition of immobile zones. Simulation B has a matrix porosity of 2% and maximum diffusion distance of 0.1 m, Simulation C has matrix porosity and diffusion distance of 2% and 1 m respectively. The ensuing Figures 3-6 through 3-10 show that the increasing the diffusion distance improves the initial breakthrough time match to the measured breakthrough of Uranine and Amino G Acid. The addition of immobile zones in calibration B and C also decreases the mass recovery of the tracer during the test. The matches are still not perfect, and could clearly be improved by further calibration. For the present purposes, however, it was sufficient to demonstrate that the hydro-structural model and transport parameters could provide an approximate representation of the transport pathway and transport properties.

Table 3-3 Tracer Test A4: Simulations Varying Immobile Zone Parameters. Transport aperture is a function of transmissivity.

Simulation	Matrix Porosity (%)	Diffusion Distance (m)	Dispersion Length (m)	Transport Aperture (m)
A	0%	0	1.5	$2 \bullet T^{1/2}$
B	2%	0.1	1.5	$2 \bullet T^{1/2}$
C	2%	1	1.5	$2 \bullet T^{1/2}$

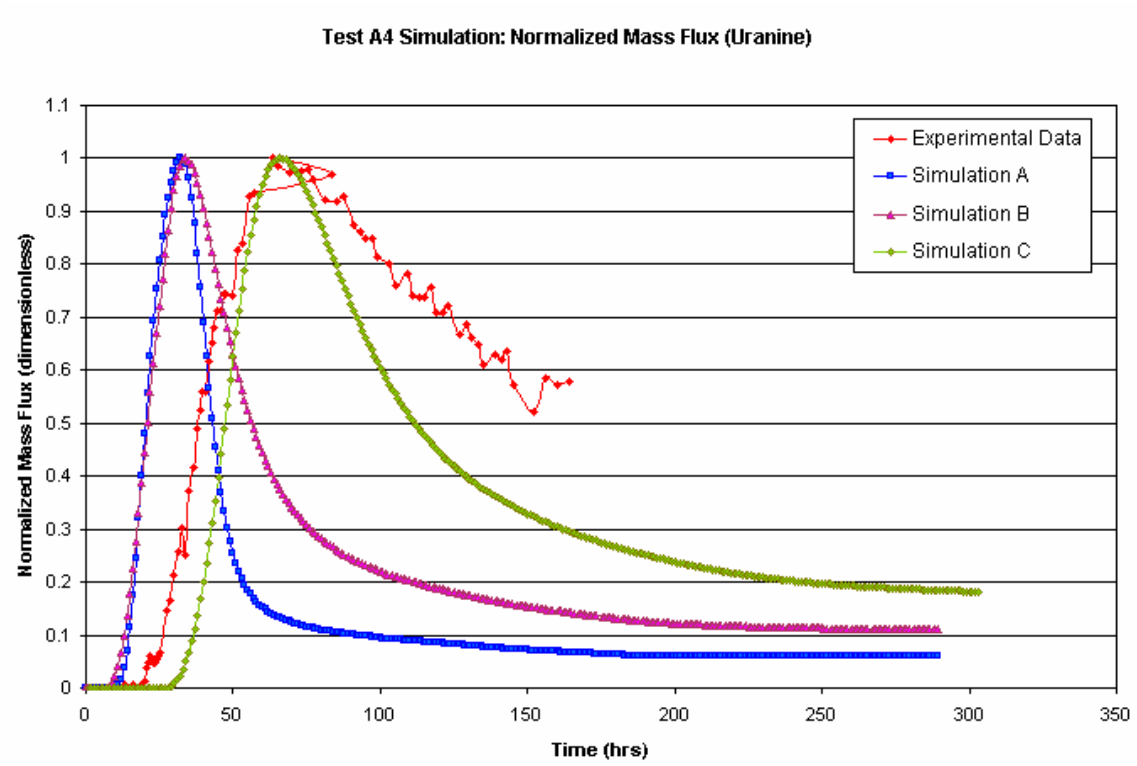

Figure 3-6 *TTS Test A4: Uranine breakthrough results compared with experimental data.*

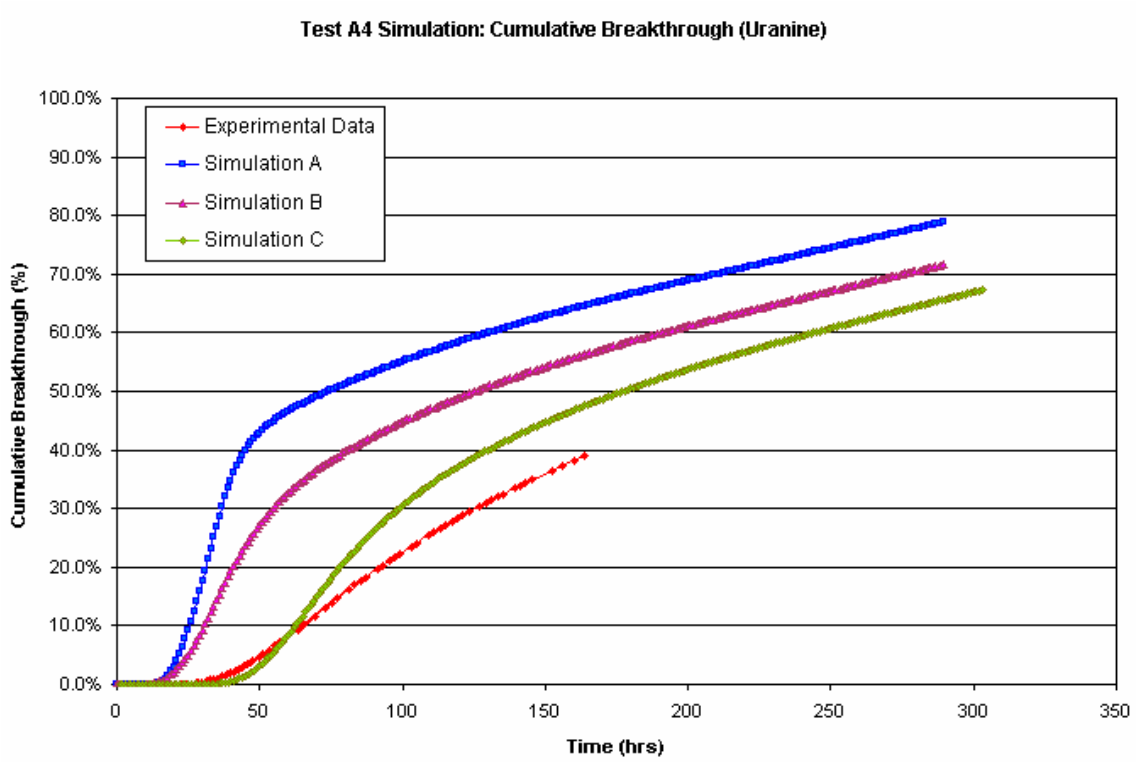

Figure 3-7 *TTS Test A4: Uranine cumulative recovery simulations compared with experimental data.*

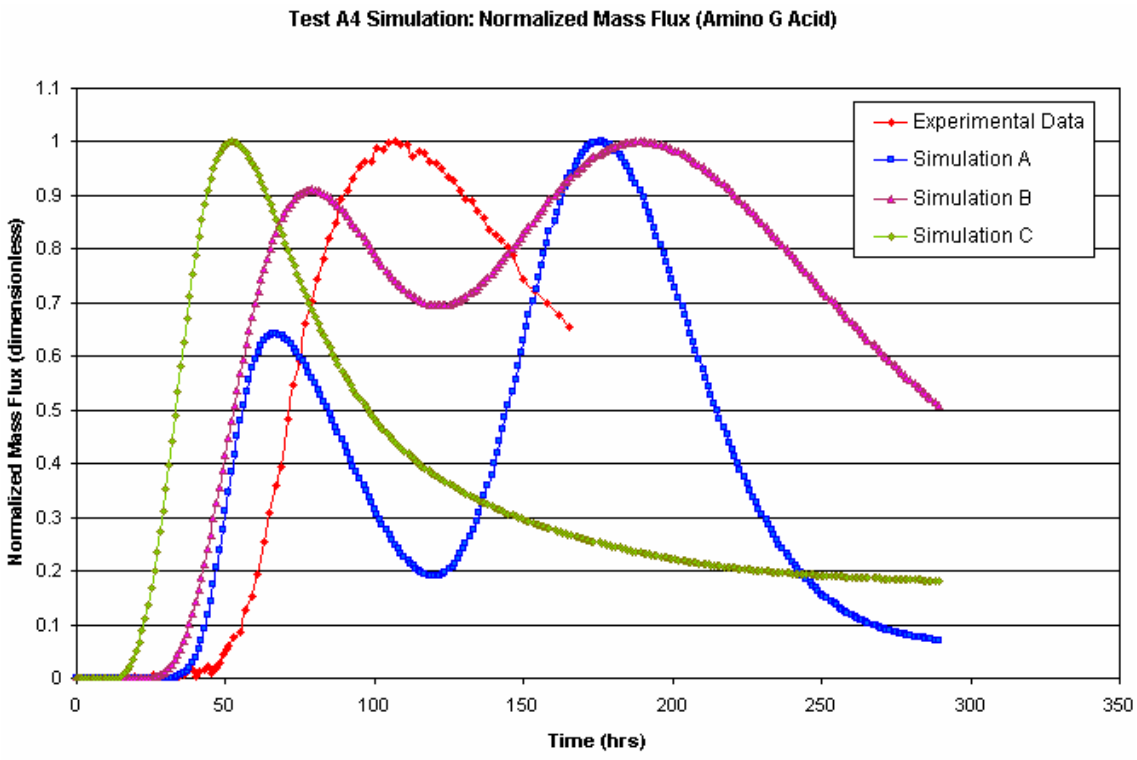

Figure 3-8 *TTS Test A4: Amino Acid breakthrough simulations compared with experimental data.*

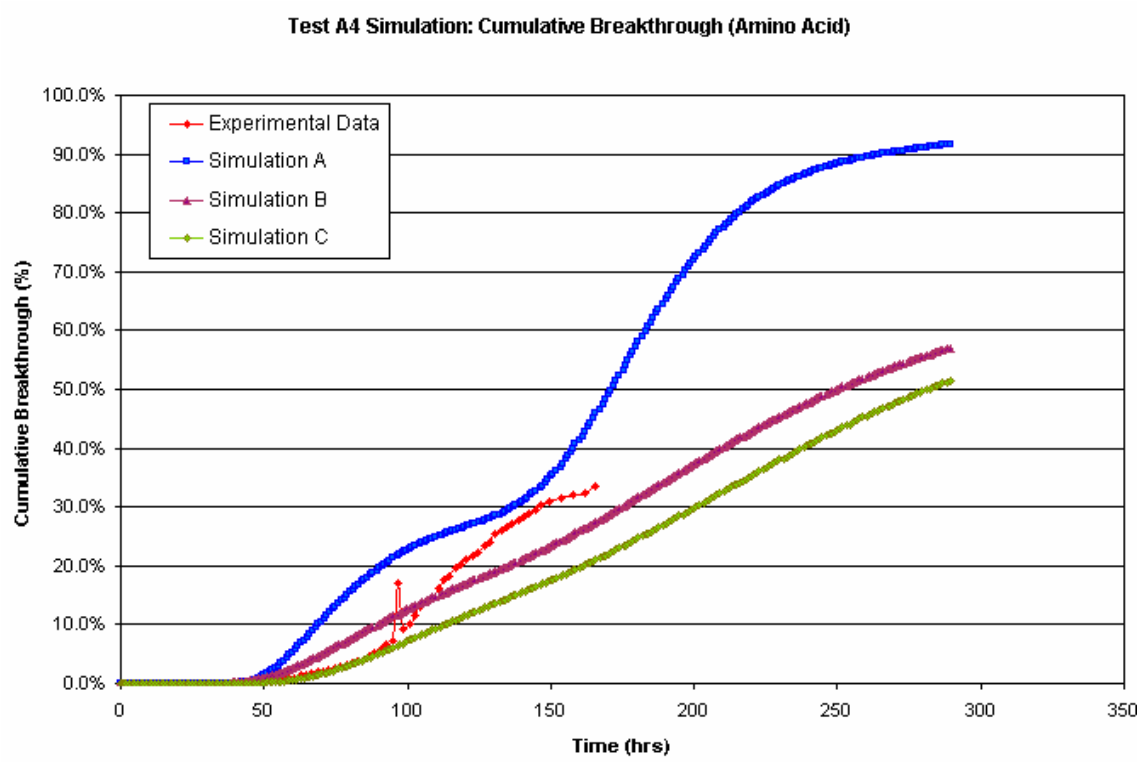

Figure 3-9 *TTS Test A4: Amino Acid cumulative recovery results compared with experimental data.*

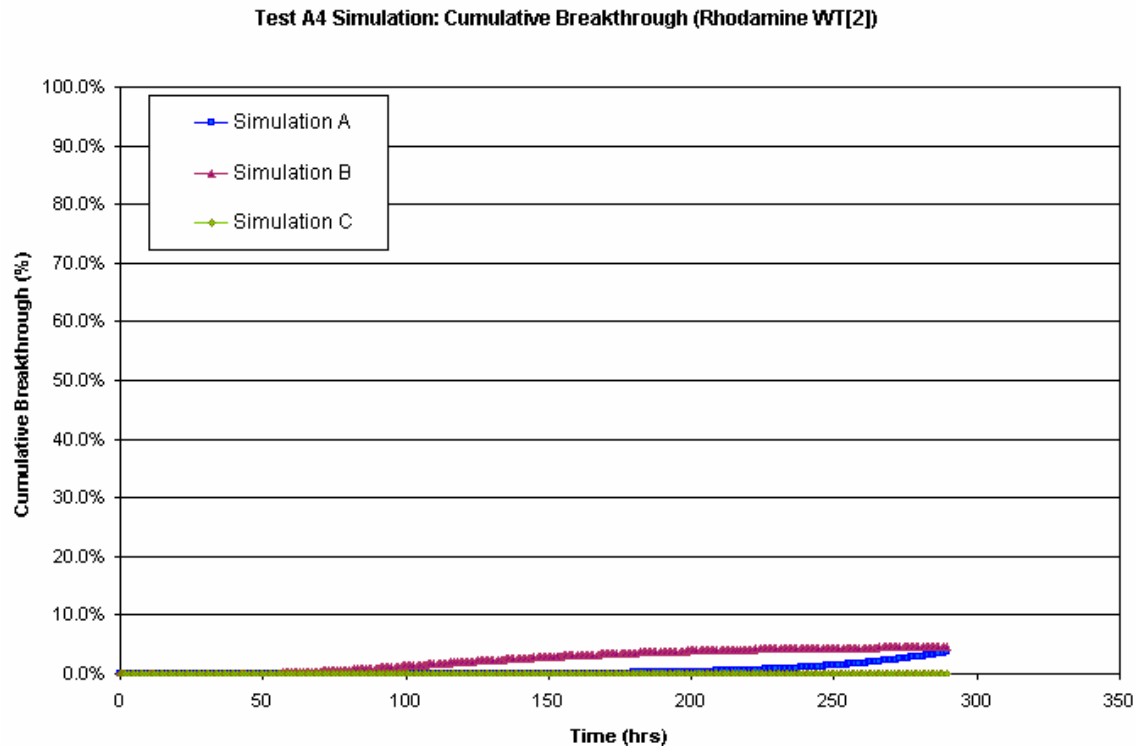

Figure 3-10 *TTS Test A4: Rhodamine WT cumulative recovery simulations compared with experimental data*

3.3 Hydro-structural model implementation

Distance-drawdown simulations of Section 3.1 and tracer test simulations of Section 3.2 confirm that the hydro-structural model can approximately reproduce the observed in-situ hydrogeologic behavior. However, the parameters used in the simulation do not produce exact matches to in-situ measurements indicating a need for changes to the model implementation. Comparison between the experimental distance-drawdown data and the distance-drawdown established from Test A4 with the preliminary CN model shows good late time matches. Early time drawdown associated with Structures #13, 18, and 19 results in greater discrepancy between the in-situ and simulated data. Simulated drawdowns appear to be an order of magnitude higher than those observed in-situ. Possible approaches to improving the distance-drawdown matches could include changing the internal connectivity of Structure 13 and modifying the transmissivities of Structures 18 and 19.

Transport simulation of Test A4 was used to evaluate whether immobile zones should be included in the model. Simulation of Uranine transport showed improvements in $T_5/T_{50}/T_{95}$ matches when immobile zones were added to each structure. In-situ Rhodamine recovery was below background levels; simulated Rhodamine recovery is below 5% both with and without immobile zones. The modeled Amino G Acid breakthrough was delayed by the presence of immobile zones; the slower breakthrough improves the match to the measured breakthrough time. Test A4 immobile zone simulations suggest that immobile zones should be included along tracer transport pathways, as they were for the TRUE-1 experiments.

4 Simulation of hydraulic interference

This chapter describes systematic CN simulations of hydraulic interference during tracer dilution Test A1 using the March 2000 Hydro-structural Model (Hermanson and Doe, 2000) and the stochastic background fractures (Dershowitz, 2000). These simulations were carried out to determine what changes were necessary to the hydro-structural model considering hydraulic conductivity and diffusivity.

Table 3-1 summarizes the deterministic structure parameters comprising the CN model. This model is considered as the base case hydro-structural model. Table 4-1 summarizes the tracer dilution Test A-1 configuration.

Table 4-1 Tracer Dilution Test A1: Basic Data

Sink Location	KI0025F03: P5 (66.5 - 74 m) Structure 20
Pumping Rate	2.05 l/min for the first 305 minutes of the test, 2.70 l/min for the remaining 3675 minutes.
Pumping Duration	3980 minutes (~ 3 days)

4.1 Test of the bace case hydro-structural model

A distance-drawdown plot was created to compare the in-situ and simulated drawdown at specified structures within the base structural model. Simulations of Test A1 compared drawdowns at Structures 6, 13, 19, 20, 21, and 22 to the in-situ measurements. The greatest amount of discrepancy between measured and simulated drawdown occurs along Structure 19. Figure 4-1 shows the distance-drawdown plot for Test A1.

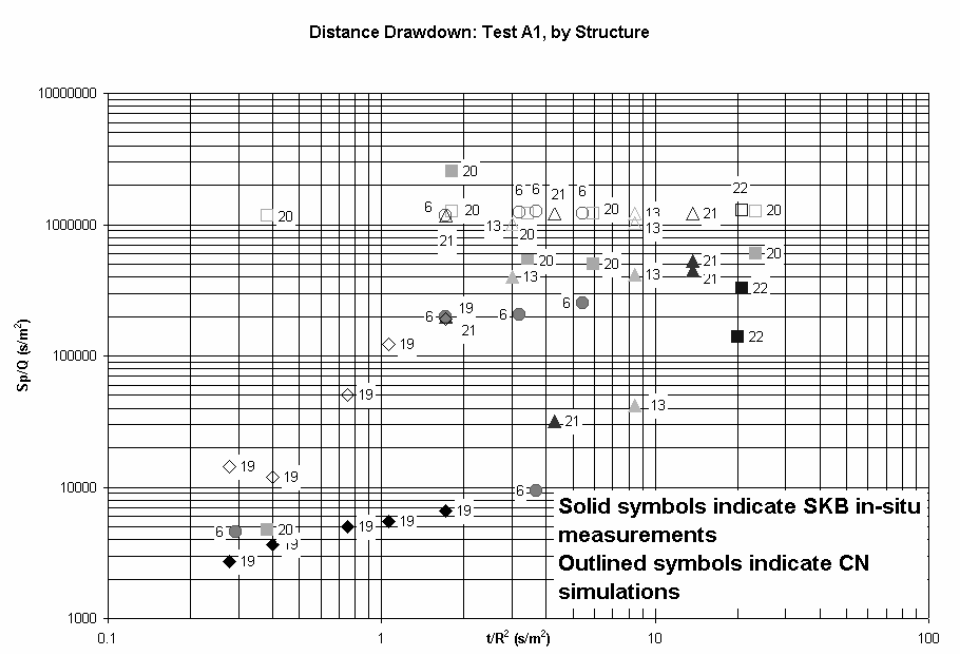

Figure 4-1 *Test A1 Distance-Drawdown. Comparison of the March 2000 Structural Model (Hermanson and Doe, 2000) to in-situ data.*

4.2 Adjustments of tansmissivity

To improve the distance-drawdown match, simulations were carried out with different transmissivity values assigned to deterministic structures. Since there is considerable doubt regarding the hydraulic significance of sub-horizontal structures, transmissivity of the sub-horizontal deterministic structures (Structures 16, 17, and 18) was decreased. Decreasing the transmissivity of the sub-horizontal structures was expected to result in less hydraulic connectivity between the vertical structures. The transmissivity of Structures 16, 17, and 18 was decreased by 3 orders of magnitude. Structure 16 transmissivity decreased from $1.00 \bullet 10^{-8}$ m^2/s to $1.00 \bullet 10^{-11}$ m^2/s. Structures 17 and 18 transmissivity decreased from $1.00 \bullet 10^{-11}$ m^2/s to $1.00 \bullet 10^{-14}$ m^2/s. Figure 4-2 illustrates the distance-drawdown plot with the modified transmissivities. In general, the distance-drawdown matches did not improve as a result of these changes.

Another test of the hydro-structural model was made by modifying Structures 5 and 16 to determine whether changes to structure transmissivity could improve the matches for hydraulic interference. Structure 5 transmissivity was increased from $1.00 \bullet 10^{-6}$ m^2/s to $1.00 \bullet 10^{-5}$ m^2/s to better represent the influence of the adjacent subparallel structures. Structure 16 transmissivity reduced from $1.00 \bullet 10^{-8}$ m^2/s to $1.00 \bullet 10^{-11}$ m^2/s to decrease network connectivity. Figure 4-3 illustrates the distance-drawdown matches with the transmissivities of Structures 5 and 16 modified. This modification to the March 2000 Hydro-structural model (Hermanson and Doe, 2000) resulted in improved drawdown matches to the in-situ data collected along Structures 6, 13, 20, 21, and 22. Responses in Structure 19 appear insensitive to these transmissivity modifications.

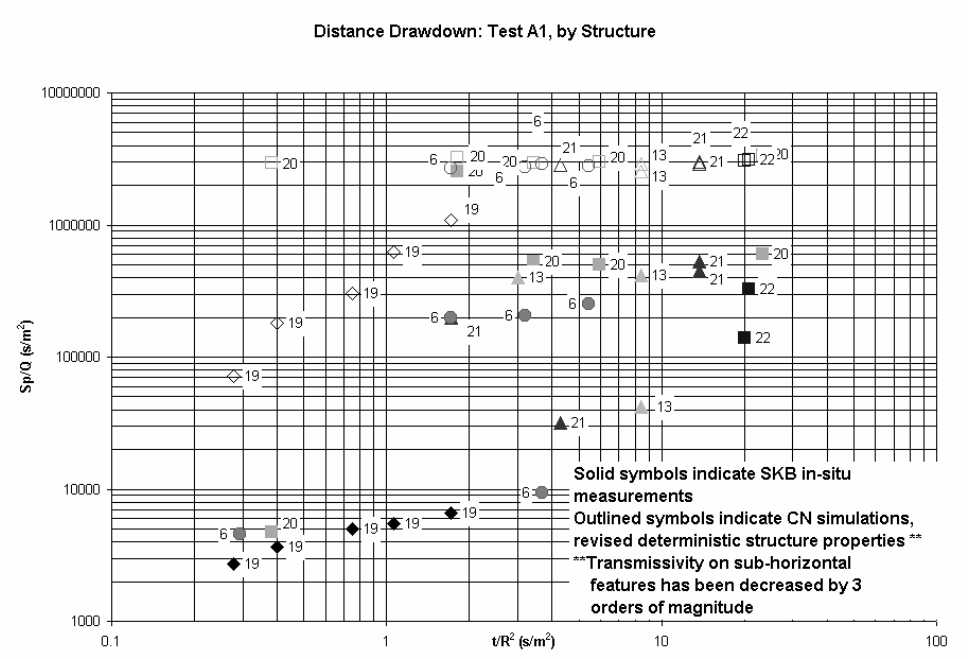

Figure 4-2 *Test A1 Distance-Drawdown. Transmissivity of Structures 16, 17, and 18 decreased by three orders of magnitude. Resulting fit of simulated drawdown to in-situ data is not improved.*

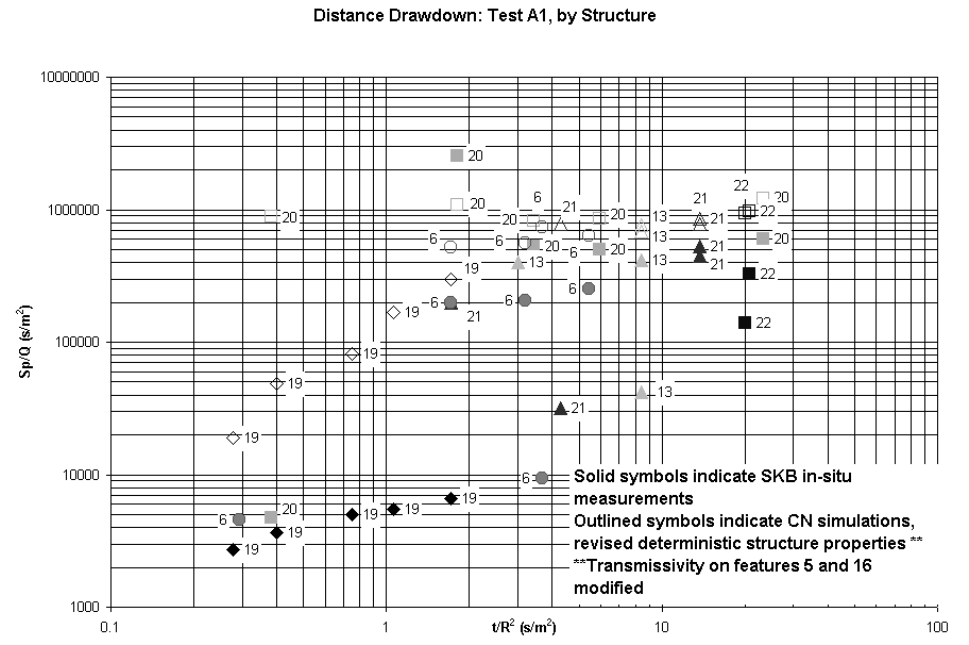

Figure 4-3 *Test A1 Distance-Drawdown. Transmissivity of Structures 5 was decreased by one order of magnitude; Structure 16 was decreased by three orders of magnitude. Resulting simulated drawdown improves the fit to in-situ at borehole monitoring intervals data in Structures 6, 13, 20, 21 and 22.*

4.3 Adjustments to connectivity of network

One of the difficulties in implementing the hydro-structural model involved the difference in levels of detail at different scales. The model is very detailed at the 150 m scale, but only includes major structures to the 500 m scale boundaries. In order to address this, Structures 19 was extended to connect with Structures EW-1 and NE-2, and Structure 6 was extended to connect with Structure 5. As illustrated in Figure 4-4, these modifications to the extents in the hydro-structural model result in minor improvements to the interference Tests A1 match. These improvements indicate that it should be possible to calibrate the existing hydro-structural model with relatively minor changes. Such calibration, however, is not part of the current scope.

4.4 Revised structural model implementation

The March 2000 Hydro-structural Model refinements described in Sections 4.2 and 4.3 were adapted for all the further flow and transport modeling described in this report. None of the refinements made were considered significant enough to be considered changes to the hydro-structure model itself. Rather, these are changes to the model implementation. Table 4-2 summarizes the changes in the Revised March 2000 Hydro-structural Model. Numbers in bold indicate changes from the transmissivity of the Preliminary DFN model described in Chapter 3. Figure 4-4 contains the distance-drawdown plot with the revised hydro-structural model implementation. Distance-drawdown simulations with the Revised March 2000 Hydro-structural Model result in less derivation from the experimental drawdown data. Specifically, the drawdown along Structures 6 and 19 were greatly improved. Structures 13 and 21, where drawdown matches with the preliminary model were poor, improved slightly, Structure 20 simulated drawdown remained largely unaffected by the changes to the imposed hydro-structural model.

Table 4-2 Deterministic Structures Parameters of the Revised March 2000 Hydro-structural Model (Hermanson and Doe, 2000), bold value indicate modified parameters

Structure	Transmissivity (m^2/s)	Normal Vector to the Plane			Area (m^2)
		nx	ny	nz	
1	$1.00 \cdot 10^{-6}$	-0.419	0.897	0.139	193.22
2	$1.00 \cdot 10^{-6}$	0.95	-0.33	0.017	242.99
3	$1.00 \cdot 10^{-6}$	-0.93	0.34	-0.151	247.42
4	$1.00 \cdot 10^{-6}$	0.84	-0.53	-0.146	189.08
5	**$1.00 \cdot 10^{-5}$**	-0.92	0.39	-0.008	248.74
6	$1.00 \cdot 10^{-7}$	-0.537	0.843	0.025	**6698.04**
7	$1.80 \cdot 10^{-5}$	-0.885	0.44	-0.15	12746
8	$1.00 \cdot 10^{-10}$	0.50	0.80	-0.352	222.4
9	$1.00 \cdot 10^{-6}$	-1	0	0	0.79
10	$5.30 \cdot 10^{-8}$	0.95	-0.09	-0.311	13096.46
11	$1.00 \cdot 10^{-6}$	-0.95	0.30	0.035	229.7

Structure	Transmissivity (m^2/s)	Normal Vector to the Plane			Area (m^2)
		nx	ny	nz	
12	$1.00 \cdot 10^{-10}$	-0.09	1.00	0	226.46
13	$1.70 \cdot 10^{-7}$	-0.554	0.73	0.4	15517.3
14	$1.00 \cdot 10^{-12}$	-1	0	0	0.03
15	$2.00 \cdot 10^{-11}$	-1.00	-0.04	0.035	203.12
16	**$1.00 \cdot 10^{-11}$**	-0.02	0.31	-0.952	261.28
17	$2.00 \cdot 10^{-11}$	0.08	0.04	-0.996	255.86
18	$1.00 \cdot 10^{-11}$	-0.11	-0.25	-0.962	250.75
19	$1.80 \cdot 10^{-7}$	-0.513	0.859	0.013	**46344.9**
20	$9.60 \cdot 10^{-7}$	-0.66	0.746	0.088	18938.3
21	$8.10 \cdot 10^{-7}$	-0.374	0.87	-0.322	8009.34
22	$3.70 \cdot 10^{-7}$	-0.4	0.844	-0.358	4648.02
23	$6.79 \cdot 10^{-9}$	-0.679	0.734	0	1203.66
24	$2.98 \cdot 10^{-8}$	-0.755	0.639	-0.146	1172.34
Z	$5.00 \cdot 10^{-6}$	-0.87	-0.44	0.225	243.55
EW-1	$1.20 \cdot 10^{-5}$	-0.86	-0.48	-0.199	255.91
EW-3	$1.70 \cdot 10^{-5}$	-0.96	-0.20	-0.191	221.5
NE-1	$2.20 \cdot 10^{-4}$	0.85	0.44	-0.301	227.04
NE-2	$1.20 \cdot 10^{-7}$	-0.57	-0.79	-0.225	242.73
NNW-7	$7.50 \cdot 10^{-6}$	0.42	-0.90	-0.087	199.74

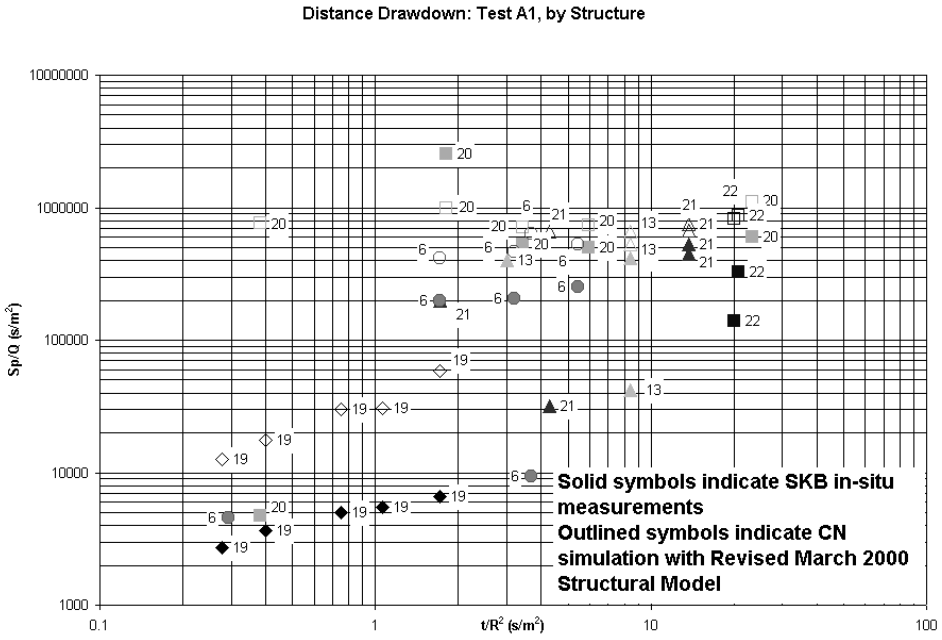

Figure 4-4 *Test A1 Distance-Drawdown. Comparison for the Revised March 2000 Structural Model (with numbered structures)*

5 Fracture Intersection Zone (FIZ) studies

Hypotheses number 2 of the TRUE Block Scale project (Winberg, 2000) concern whether fracture intersection zones (FIZ) have distinctive hydrologic properties that can be detected. The sub-hypothesis is that a FIZ could: a) provide a strong hydraulic connection to alternative sinks, decreasing tracer recovery; b) increase dilution; c) increase dispersion or travel time due to greater aperture or sorption properties; or d) serve as a flow barrier due to infilling materials. The magnitude of the FIZ effect on the tracer test largely depends on the transmissivity, aperture, geochemistry, geometry, and hydraulic gradient of the FIZ in relation to its surroundings. Tracer tests were simulated with and without FIZ pipes added to the CN model to establish the relationship between FIZ properties and the surrounding structures for possible detection of FIZ effects. Tests A4 and A5 were used to model the effects of the FIZs.

FIZ pipes were added to existing CN models by hand, and were connected directly to source and sink locations. FIZ pipes were extended to the external boundary and are therefore affected by the constant head field at the outer boundary established by Holton (2001). Figure 5-1 illustrates a generic pathway generated by the CN model and a pathway generated through the additional FIZ pipes. Multiple simulations using FIZ transmissivities greater than the "host" structure transmissivity were compared with the breakthrough and recovery of each tracer measured in the field.

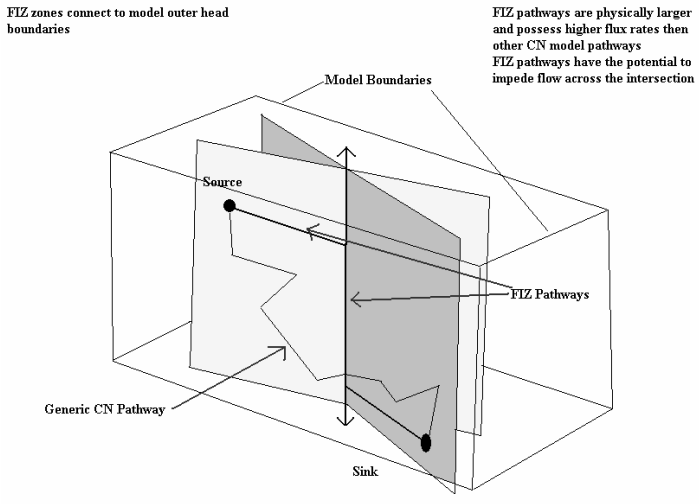

Figure 5-1 *FIZ Conceptual Model*

5.1 FIZ simulations

FIZ simulations were carried out using tracer Tests A4 and A5. The experimental recovery measured along with the predicted ultimate recovery and associated FIZ are listed in Table 5-1 for tracer Tests A4 and A5. Ultimate recovery for each test was estimated by visual extrapolation from the measured breakthrough curves. Several of these tests show a low estimated ultimate recovery, which might be explained by possible FIZ effects.

In Test A4, Rhodamine WT[2] crosses the 20/21 FIZ. Experimental breakthrough data shows no recovery above background levels from this tracer. The remaining tracers of Test A4, Uranine and Amino G Acid, both have high estimated ultimate recovery. The travel paths of Uranine and Amino G Acid do not cross a FIZ.

In Test A5, Rhodamine WT[1] and Uranine cross the 20/21 FIZ. The estimated ultimate recoveries for these tracers are 67% and less than background levels, respectively. The remaining three tracers associated with Test A5, Napthionate, Rhodamine WT[2], and Amino G Acid, do not cross a FIZ on their paths from source to sink.

Table 5-1 TTS Test A4 and Test: A5 Measured Recovery and Associated FIZ

Test / Tracer	Measured Recovery	Estimated Ultimate	Associated FIZ
A4 (Uranine)	38.9%	70%	No FIZ
A4 (Amino G)	50.8%	90%	No FIZ
A4 (Rhodamine WT[2])	Less than background	Less than background	20/21
A5 (Rhodamine WT[1])	65.7%	70%	20/21
A5 (Uranine)	Less than background	Less than background	13/21
A5 (Napth)	132.2%	132%	No FIZ
A5 (Rhodamine WT[2])	43.2%	55%	No FIZ
A5 (Amino G Acid)	94.9%	97%	No FIZ

5.1.1 Test A4: FIZ simulations

Conservative tracers injected into KI0023F03 as part of Test A4 include Uranine, Rhodamine WT[2], and Amino G Acid. The source and sink locations as well as associated structures and pumping rate for tracer Test A4 are listed in Table 5-2.

Table 5-2 Tracer Test A4: Basic Data

Tracer	Source	Structure
Uranine	KI0023F03: P5 (66.5 - 74 m)	20
Amino G Acid	KI0023F03: P6 (59.5 - 65.5 m)	22
Rhodamine WT[2]	KI0023F03: P7 (55 - 58.5 m)	23
Sink Location	KI0023B:P6 (70.4 - 71.4 m) Structure 21/20	
Pumping Rate	2.30 l/min	
Pumping Duration	17370 minutes (~ 12 days)	

A series of sensitivity studies were carried out to evaluate possible FIZ effects on Test A4. The initial simulation was run with the following parameters: dispersion length of 0.5 m, flow aperture parameters A = 2, B = 0.5 (See Eq 1) on both deterministic and background fracture, and no FIZ effects. When FIZ pipes were added to these models the match to measured breakthrough and recovery improved, possibly supporting the FIZ hypothesis. Early time measured recovery was improved with increased FIZ transmissivity. Table 5-3 presents the FIZ parameters used in the FIZ simulations for Test A4. Simulation 4, with a FIZ transmissivity of $2.0 \cdot 10^{-5}$ m^2/s, results in the best fit to the early time cumulative recovery data. The aperture of the FIZ in this calibration is $6.19 \cdot 10^{-3}$ m. From the aperture of $6.19 \cdot 10^{-3}$ m, a relationship between transmissivity and aperture is back calculated as A = 1.4, B = 0.5 (See Eq 1). Figure 5-2 and Figure 5-3 display the FIZ geometry used in the simulation of Test A4. Figure 5-2 shows pipes that connect boreholes to the 20/21 FIZ on Structure 20 and Figure 5-3 shows pipes that connect boreholes to the 20/21 and 13/21 FIZ on Structure 21. Figure 5-4 illustrates the effect of the FIZ on the breakthrough and recovery of Uranine in Test A4.

From Figure 5-4 it can be seen that models with or without FIZ pipes provides a good match to the high dispersion seen in the A4 Uranine breakthrough. It is expected, however, that this level of dispersion could also be obtained by calibrating longitudinal dispersion in X_L. However, the FIZ pipes and successively increased transmissivity in FIZ do show the expected reduction in tracer mass recovery, supporting the hypothesis.

Table 5-3 Parameters for FIZ Simulations (Test A4)

Simulation	Transmissivity of 20/21 FIZ (m^2/s)	Aperture of FIZ (m)
Simulation 1	$9.6 \cdot 10^{-6}$	$6.19 \cdot 10^{-3}$
Simulation 2	$9.6 \cdot 10^{-5}$	$6.19 \cdot 10^{-3}$
Simulation 3	$3.0 \cdot 10^{-5}$	$6.19 \cdot 10^{-3}$
Simulation 4	$2.0 \cdot 10^{-5}$	$6.19 \cdot 10^{-3}$

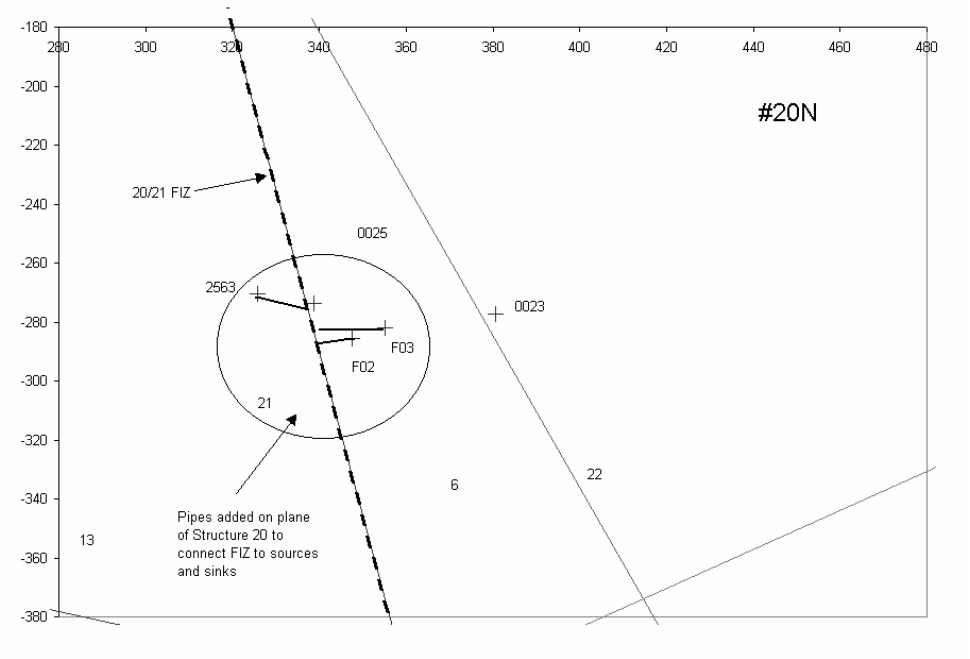

Figure 5-2 *FIZ Pipes in plane of Structure 20 (View North)*

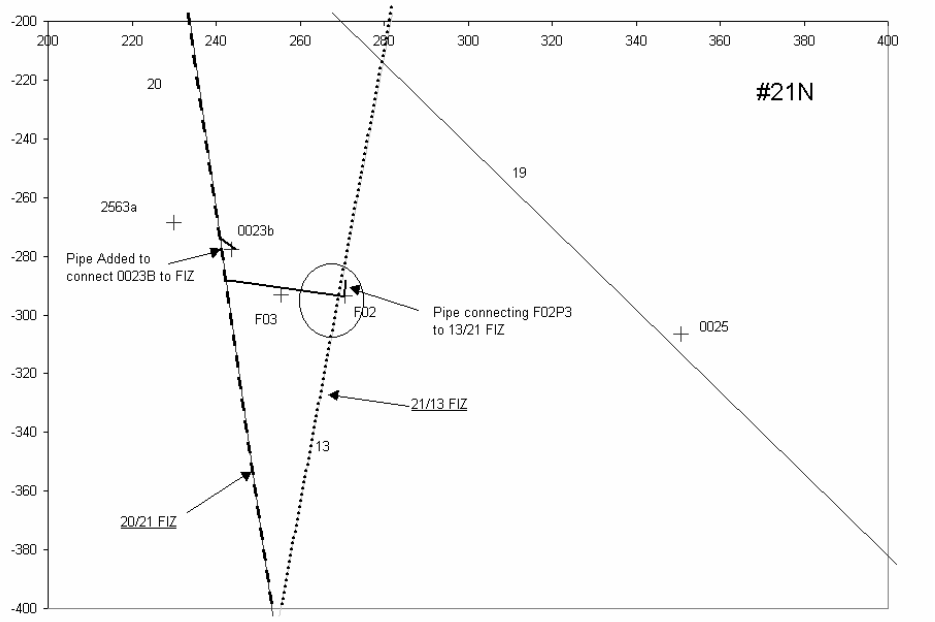

Figure 5-3 *FIZ pipes in plane of Structure 21 (View North)*

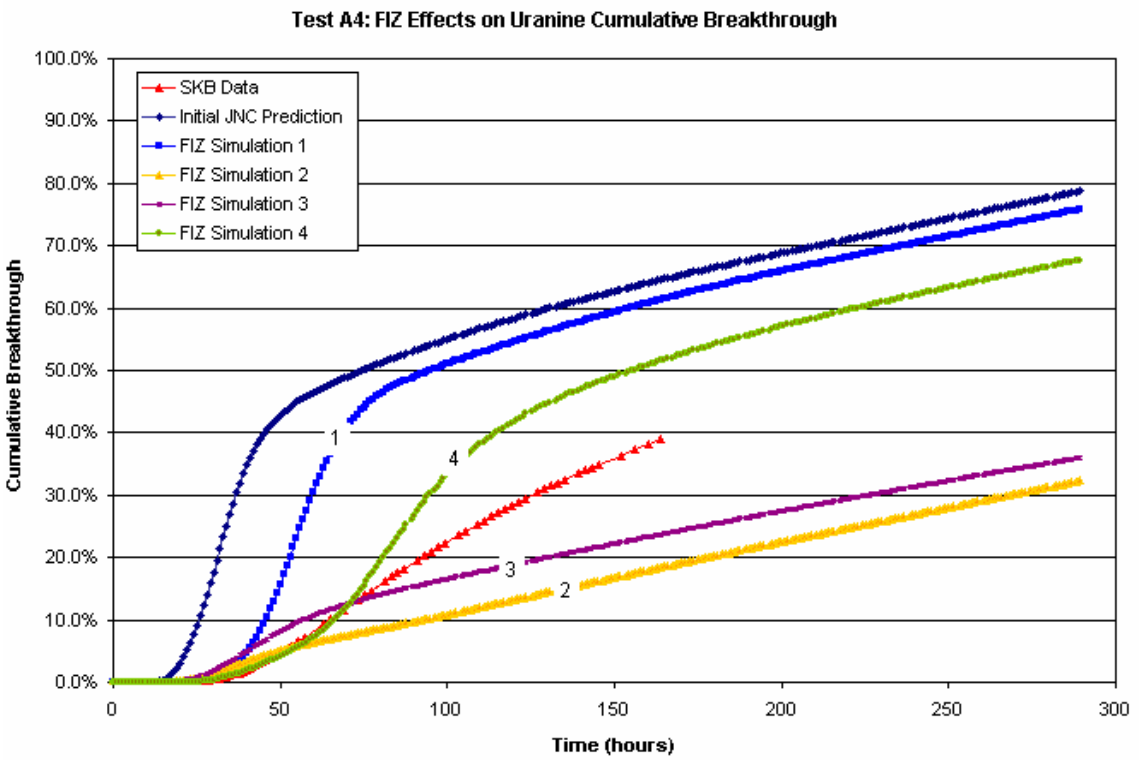

Figure 5-4 *TTS Test A4: Experimental Uranine cumulative recovery data compared with 'Initial JNC Prediction' (No FIZ effect) and four simulations that include FIZ pipes.*

5.1.2 Test A5: FIZ simulations

Conservative tracers injected into boreholes KA2563A, KI0025F02, and KI0025F03 as part of Test A5 include Rhodamine WT[1], Uranine, Napthionate, Rhodamine WT[2], and Amino G Acid. The source and sink locations for each tracer are noted in Table 5-4. Figure 5-5 and
Figure 5-6 display the post-test hydraulic head distributions across the tested region.

Table 5-4 Tracer Test A5: Basic Data

Tracer	Source	Structure
Rhodamine WT[1]	KA2563A: S4 (187.0 - 190.0 m)	20
Uranine	KI0025F02: P3 (94.4 - 99.25 m)	13, 21
Napthionate	KI0025F02: P5 (73.3 - 77.25 m)	20
Rhodamine WT[2]	KI0025F02: P6 (64.0 - 72.3 m)	22
Amino G Acid	KI0025F03: P6 (59.5 - 65.5 m)	22
Sink Location	KI0025F03: P5 (66.5 - 74.5 m) Structure 20	
Pumping Rate	2.60 l/min	
Pumping Duration	54380 minutes (~ 38 days)	

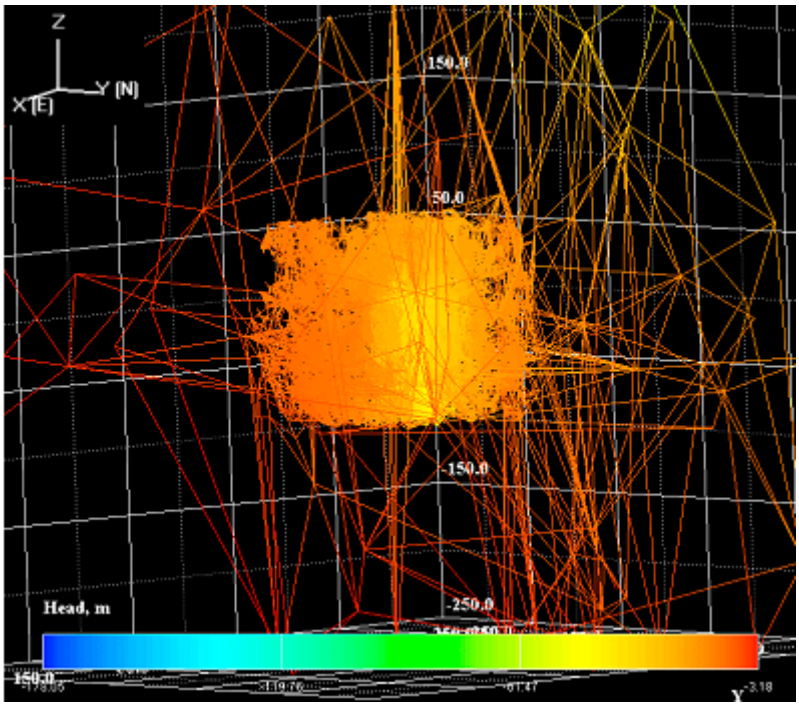

Figure 5-5 *TTS Test A5: Post-test Heads, CN Model Mesh, with pipes colored by head (masl)*

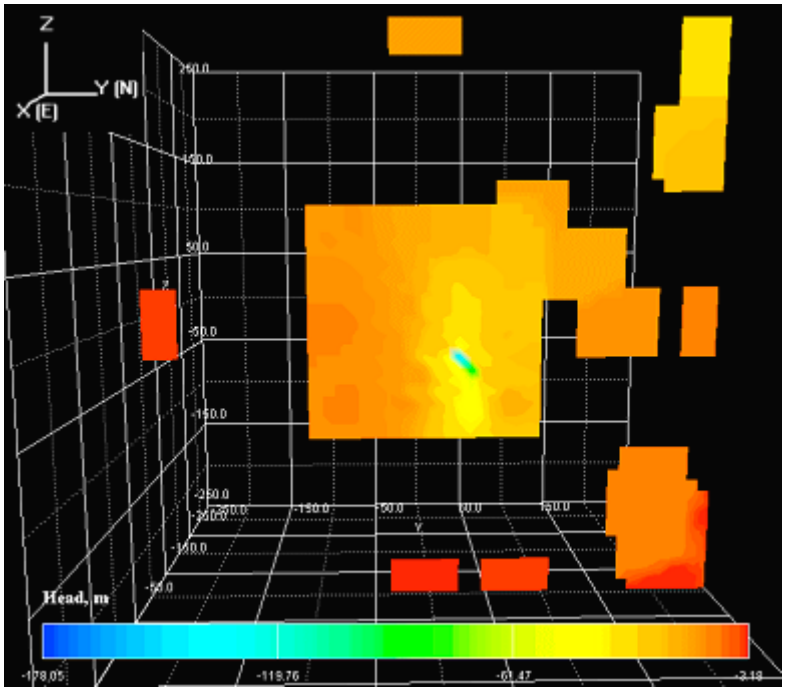

Figure 5-6 *TTS Test A5: Post-test Head Map. View is looking towards Äspö HRL tunnel. Vertical trace map view at model center looking towards Äspö HRL tunnel. Grid colored by head (masl)*

Simulations of Test A5 were carried out both with and without FIZ pipes. The results are shown in Figure 5-7 through Figure 5-15. The parameters assumed for the Structure 20/21 FIZ and the 13/21 FIZ are as follows; FIZ transmissivities were assigned values of $9.6 \cdot 10^{-6}$ m^2/s and $8.1 \cdot 10^{-6}$ m^2/s, respectively (10 times the transmissivity of the hosting fractures). The dispersion length was set to 1.5 m and the aperture of the FIZ followed the relationship in Eq 1 with A = 2 and B = 0.5.

As shown in Figure 5-7 through Figure 5-15, the FIZ models adopted for simulation of Test A5 were successful in reducing simulated recoveries when compared to models without FIZ pipes. No recovery of Uranine was observed during the test duration (639 hours): An addition of the 13/21 FIZ with the previously noted parameters reduced the simulated recovery of Uranine from 95% to 0%. Rhodamine WT[1] recovery reduced from 97% to 60%, Napthionate recovery reduced from 100% to 76%, Rhodamine WT[2] reduced from 96% to 45%, and Amino G Acid recovery decreased from 97% to 47%. Table 5-5 contains recovery data for Test A4. These results provide some support for the FIZ hypothesis, particularly for those tracer experiments with low estimated ultimate recovery. In addition, it is possible that other mechanisms are responsible for low ultimate recovery projections, including experimental error and heterogeneity in fracture planes not related to possible FIZ effects. Therefore, at most, the results can be considered as not refuting the hypothesis of FIZ zones affecting breakthrough and recovery.

Table 5-5 Percent Recovery, Measured versus Simulated

Tracer	Measured Recovery	Estimated Ultimate Recovery	Baseline Simulated Recovery	Simulated Recovery with FIZ 1
Rhodamine WT[1]	66%	70%	97%	60%
Uranine	0%	0%	95%	0%
Napthionate	132%	132%	100%	76%
Rhodamine WT[2]	43%	55%	96%	45%
Amino G Acid	95%	97%	97%	47%

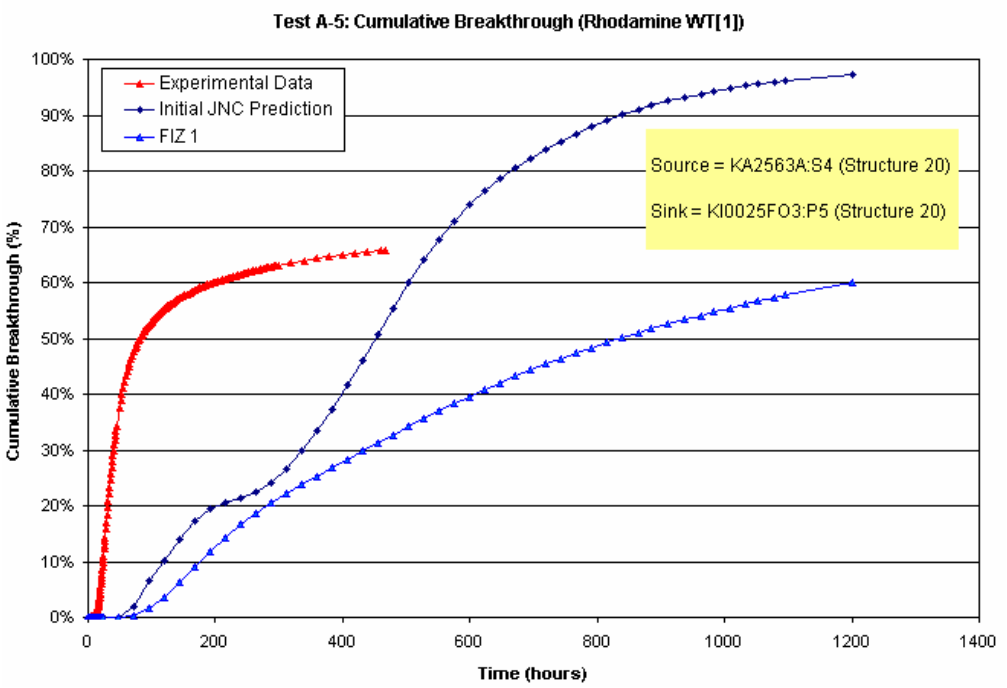

Figure 5-7 *TTS Test A5: FIZ effect on simulated Rhodamine WT[1] cumulative breakthrough compared with experimental data.*

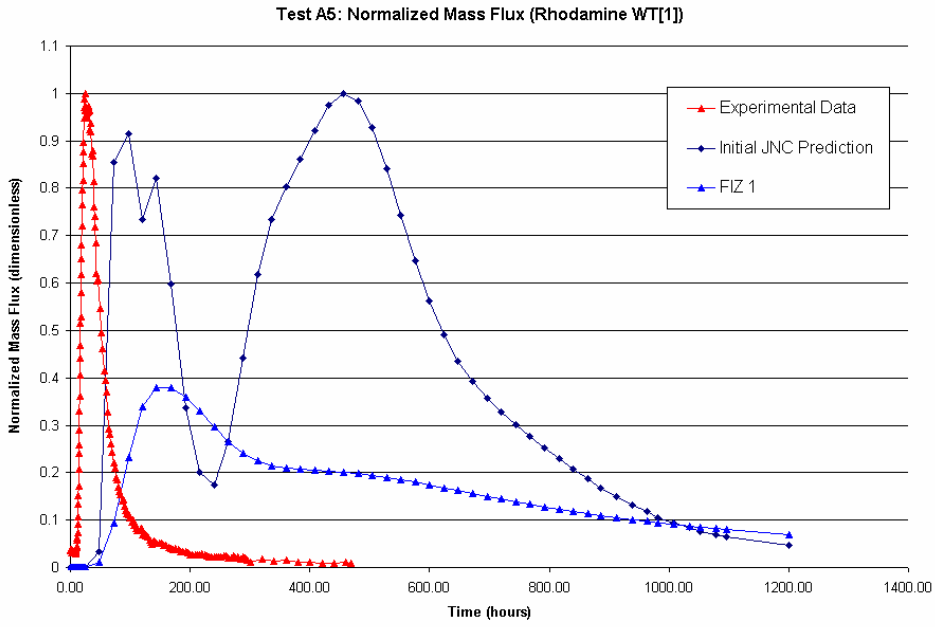

Figure 5-8 *TTS Test A5: FIZ effect on simulated Rhodamine WT[1] breakthrough compared with experimental data.*

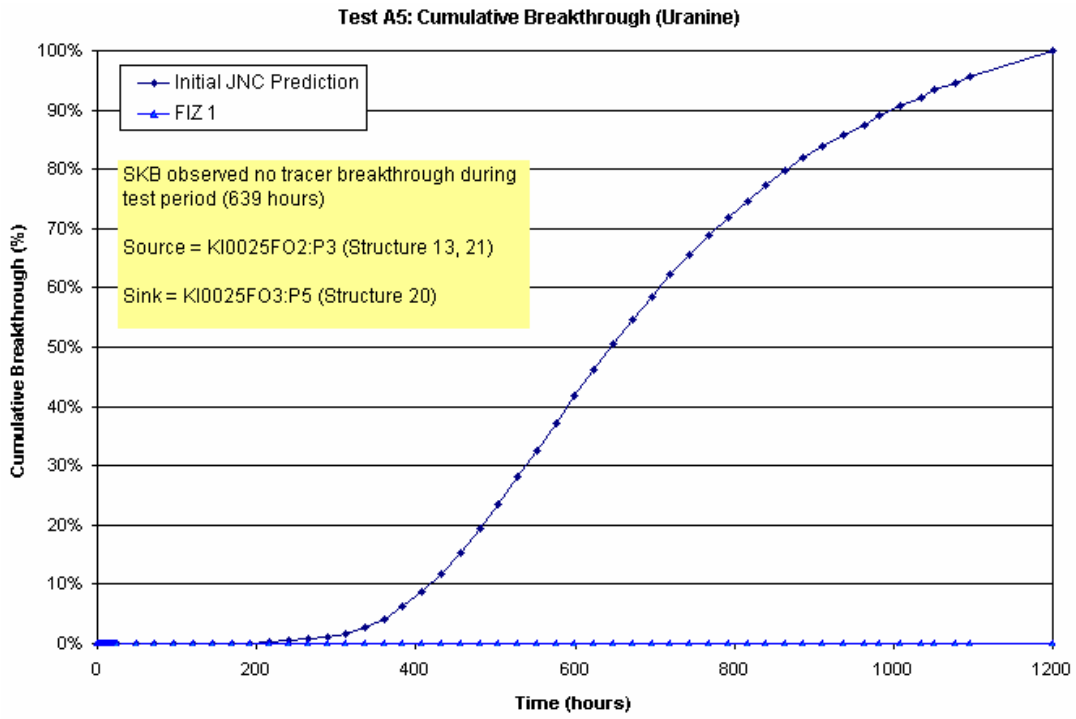

Figure 5-9 *TTS Test A5: FIZ effect on simulated Uranine cumulative breakthrough compared with experimental data.*

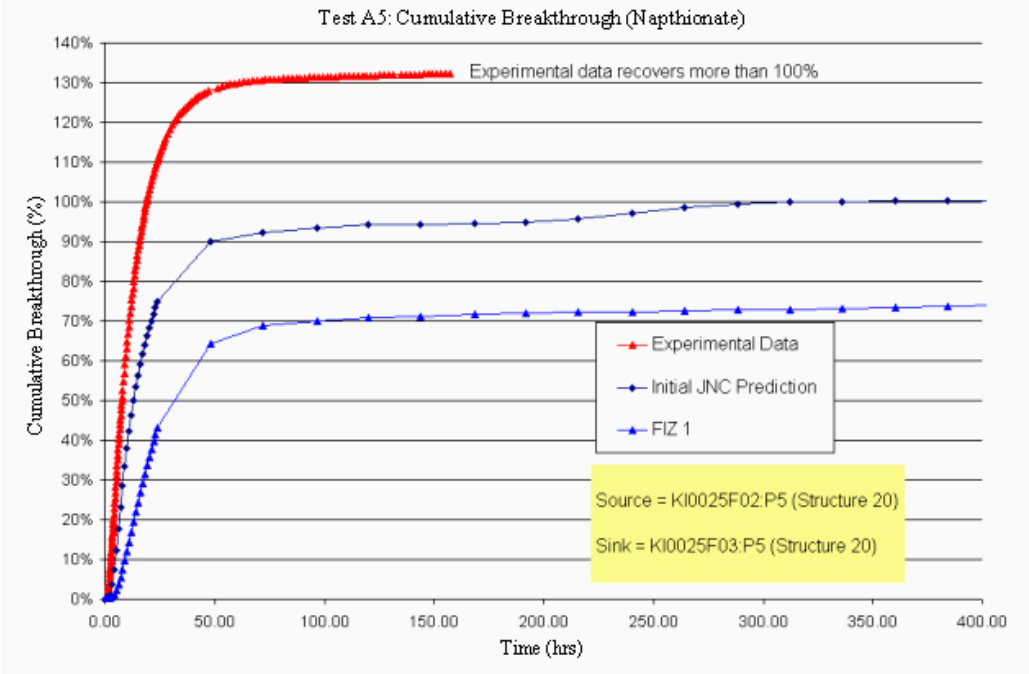

Figure 5-10 *TTS Test A5: FIZ effect on simulated Napthionate cumulative breakthrough compared with experimental data.*

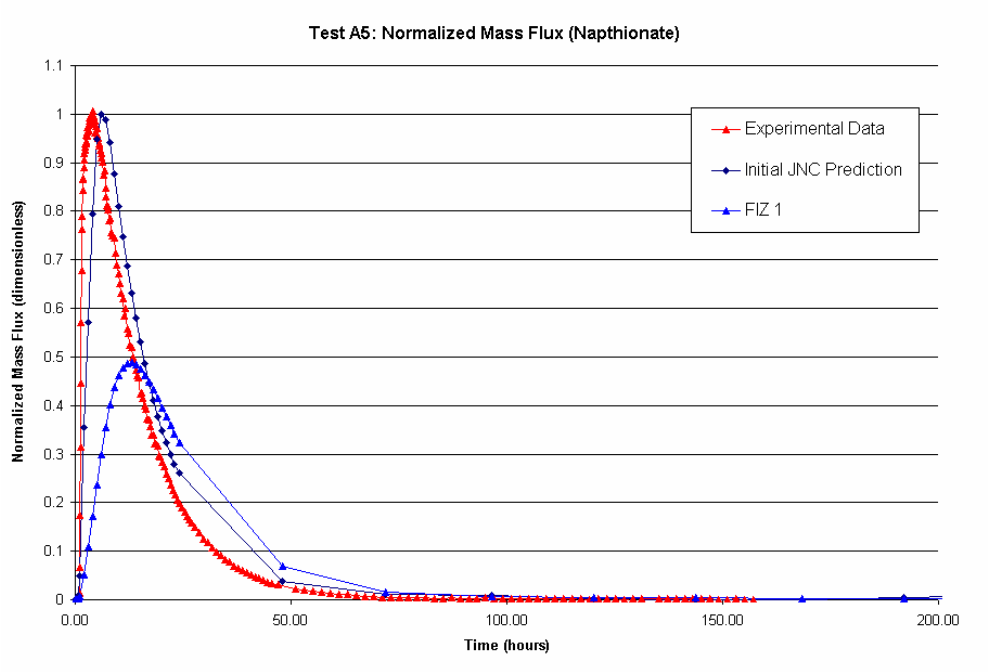

Figure 5-11 *TTS Test A5: FIZ effect on simulated Napthionate breakthrough compared with experimental data.*

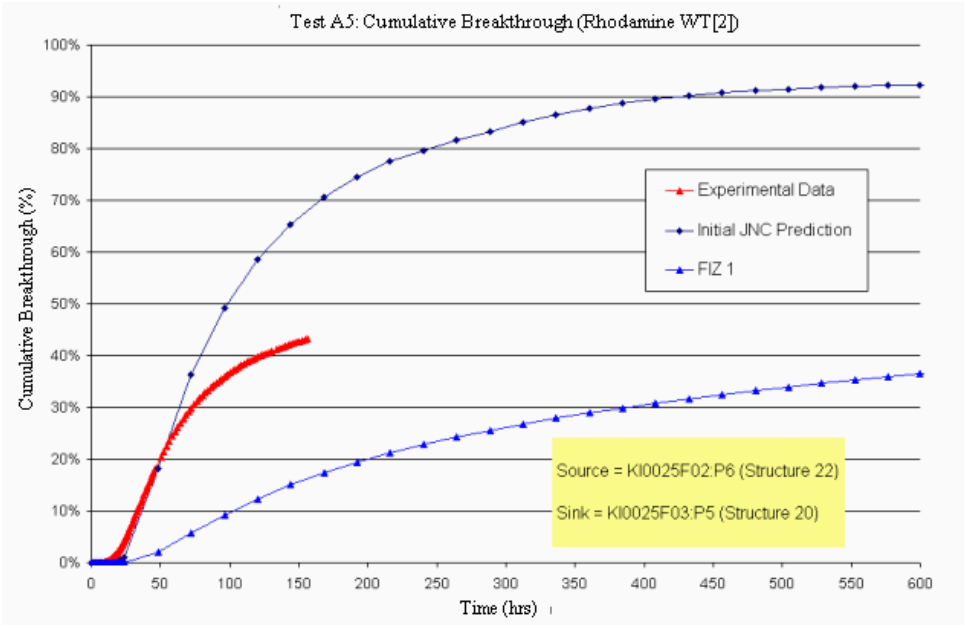

Figure 5-12 *TTS Test A5: FIZ effect on simulated Rhodamine WT[2] cumulative breakthrough compared with experimental data.*

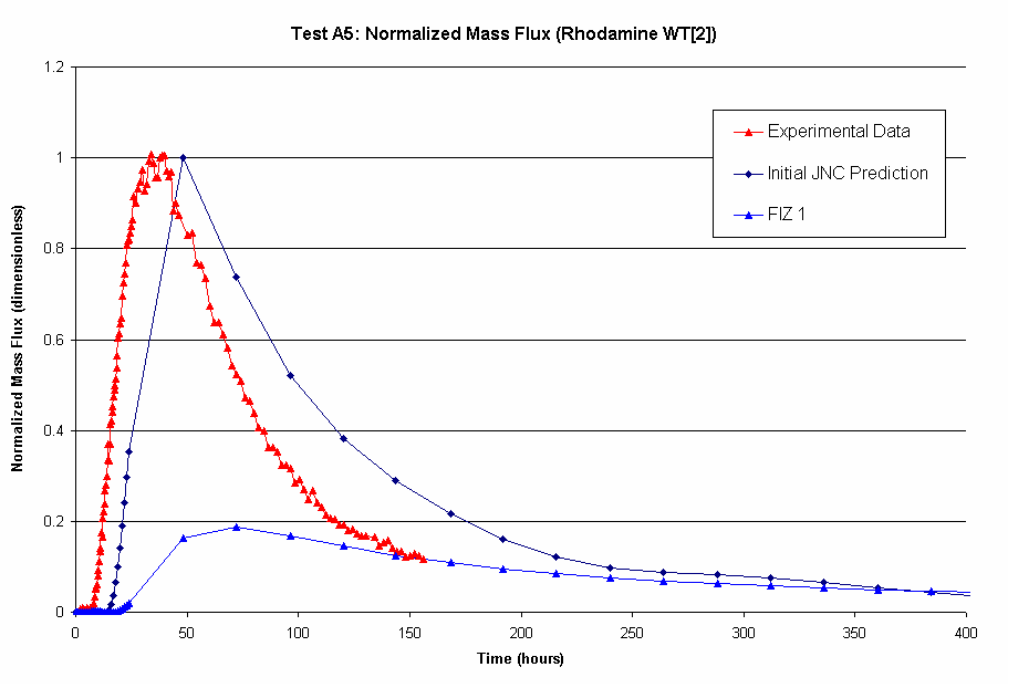

Figure 5-13 *TTS Test A5: FIZ effect on simulated Rhodamine WT[2] breakthrough compared with experimental data.*

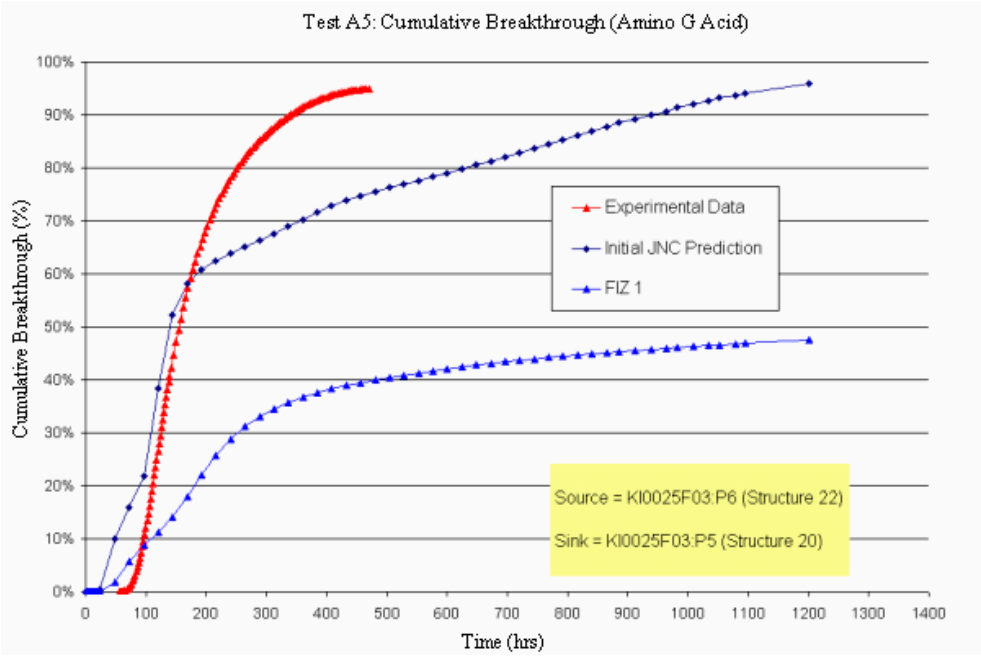

Figure 5-14 *TTS Test A5: FIZ effect on simulated Amino G Acid cumulative breakthrough compared with experimental data.*

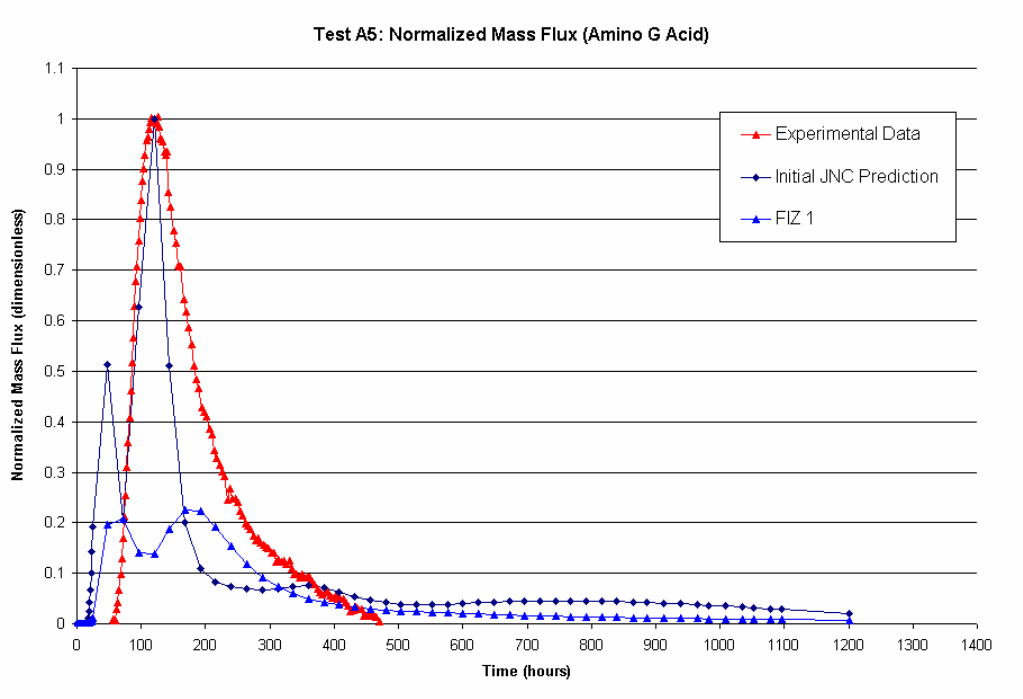

Figure 5-15 *TTS Test A5: FIZ effect on simulated Amino G Acid breakthrough compared with experimental data.*

6 Transport simulations and Phase C predictions

This chapter describes a series of sorbing and conservative tracer simulations carried out to provide a "blind" prediction for the "Phase C" tracer experiments. These predictions were "blind" in the sense that the predictions were made without any access to the sorbing tracer breakthrough measurements from the TRUE Block Scale Site, and therefore were a true test of model capabilities. The purpose of these simulations was to demonstrate the verisimilitude of the TRUE-Block Scale hydro-structural model and the transport conceptual model. Predictions were made for three pathways: C1, C2, and C3.

Each of these pathways was tested previously using conservative tracers. Transport parameters for these pathways were therefore derived for the conservative tracer tests in these pathways. Sorbing tracer transport parameters for predictions were taken directly from those obtained in TRUE-Block Scale 15-10 m scale tracer experiment (Dershowitz et al., 2000).

6.1 Pathway transport parameters

The three tracer tests, B2g, B2d, and PT4 were carried out along the same pathways as the Phase C sorbing tracer experiments C1, C2, C3, respectively. The former experiments were therefore used to derive pathway specific values for matrix porosity, diffusion distance, dispersion length, and transport aperture. The matrix porosity values are reflecting the damaged, or gauged, zone on either side of the fracture together with possible fracture infilling materials. The diffusion distance is the maximum distance solute can be transported into the rock or non-flowing pore space. Dispersion length refers to the longitudinal dispersion length reflecting the variability of advective velocities along the pathway. Transport aperture is reported as a percentage of the flow aperture. The aperture of the FIZ region is specified as being 10 times the aperture of the deterministic structures and background fractures. Table 6-1 presents the conservative transport parameters used in the simulations. Pathway transport parameters derived based on B2g, B2d, and PT4 tests are shown in bold.

Table 6-1 Transport Parameters for Simulation of Tracer Tests PT4, B2d, and B2g. Parameters derived based on conservative tracer breakthrough and recovery and displayed in bold.

Transport Parameters	Assumption
Transport Width	Set equal to flow width
Free Water Diffusion (D_w)	D_w of Helium-3 = $2.50 \cdot 10^{-9}$ m^2/s (based on particle size) D_w of all other conservative tracers = $1.00 \cdot 10^{-9}$ m^2/s
Decay Constant (λ)	Conservative tracers decay constant set to 0
Matrix partition Coefficient (K_d)	Set equal to 0 m^2/yr for conservative tracers
Surface Sorption Coefficient (Ka)	Set equal to 0 m for conservative tracers
Metal Complex Properties	Transport properties of metal complexes assumed to be the same as fluorescent dyes (Andersson, 2000)
Matrix porosity	Ranges from the bulk measured matrix porosity to values several percentage points higher than the bulk value, and represents damage zones along large-scale structures (Kamppainen et al, 2001).
Diffusion Distance	Deterministic and background fractures can have different diffusion distances.
Longitudinal Dispersion Length	Range = 0.25m to 2m
Transport Aperture	Defined as a percentage of the flow aperture. Flow aperture is defined in Eq 1 where A = 2 and B = 0.5 in deterministic structures and background fractures. A = 0.2 and B = 0.5 for FIZ pipes

6.2 Pathway transport property simulations

Two sets of simulations were carried out to derive pathway-specific conservative transport properties. The first set of simulations derived matrix porosity, diffusion distance, dispersion distance, and transport aperture based on conservative tracer Tests B2g, B2d, and PT4 without constraints on matrix porosity. These simulations are described in sections 6.2.1, 6.2.2, and 6.2.3, respectively.

The second set of simulations was constrained to use diffusion distance and matrix porosity derived by Dershowitz et al. (2000) for TRUE-1 STT-2 (Task4F). The diffusion distance of 0.01 m and matrix porosity of 3% calibrated from TRUE-1 STT-2 (Task 4F) were held constant while dispersion length and transport aperture were modified to find the best fit to the in-situ measurements. These simulations are described in section 6.2.4.

Table 6-2 lists the source and sink locations for each test, the deterministic structure associated with the packed off section of the source and sink, injection and pumping rates for each test, the projected path length, and the associated Phase C sorbing tracer test. The pumping rate is known from experimental data. The injection rate is estimated by multiplying the measured experimental concentration by an estimated injection rate until the cumulative mass injection falls within the margin of error established for the in-situ injected mass. Injection rates were established for all tracers that fell within the margin or error.

Table 6-2 Tracer Test Configuration and Associated Phase C Test

Test	Injection Location and Associated Structure	Injection Rate	Pumping Location and Associated Structure	Pumping Rate	Projected Path Length	Associated Phase C Test
B2g	KI0025F03:P5 Structure 20	7.50 x 10^{-7} m^3/s (0.0450 l/min)	KI0023B:P6 Structures 21/20	3.43 x 10^{-5} m^3/s (2.05 l/min)	17.9 m	C1 (Pathway 1)
B2d	KI0025F03:P7 Structure 23	0.67 x 10^{-7} m^3/s (1.02 l/min)	KI0023B:P6 Structures 21/20	3.43 x 10^{-5} m^3/s (2.05 l/min)	66.9 m	C2 (Pathway II)
PT4	KI0025F02:P3 Structure 21	4.00 x 10^{-8} m^3/s (0.00240 l/min)	KI0023B:P6 Structures 21/20	3.33 x 10^{-5} m^3/s (2.00 l/min)	32.5 m	C3 (Pathway III)

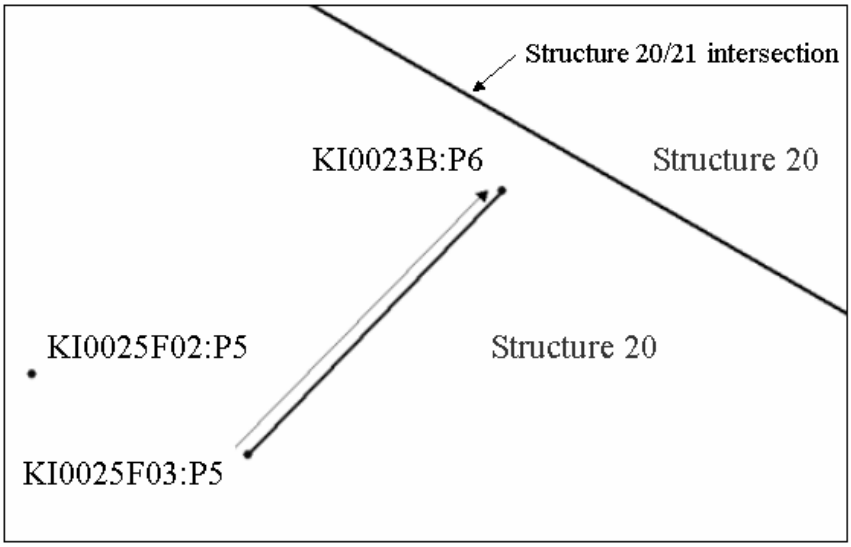

Figure 6-1 *Pathway I Visualization*

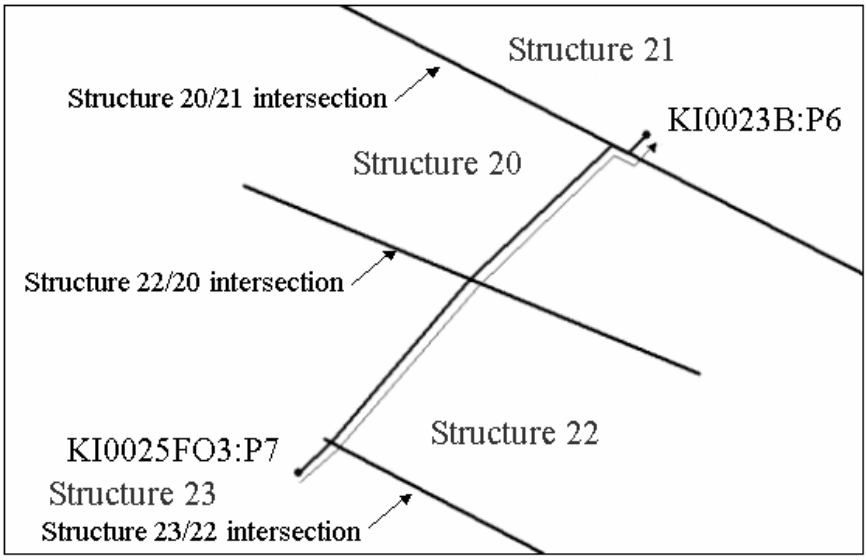

Figure 6-2 *Pathway II Visualization*

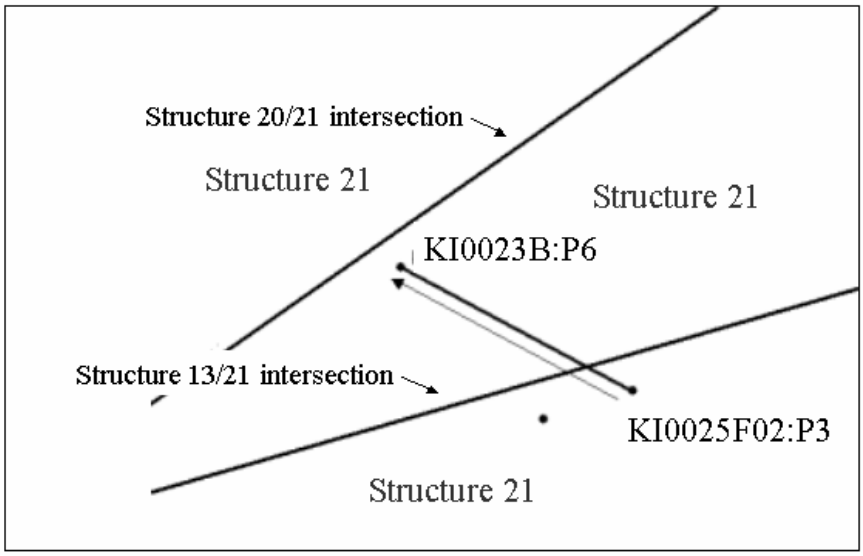

Figure 6-3 *Pathway III Visualization*

6.2.1 Pathway I (KI0025F03:P5 to KI0023B:P6) Test B2g

The B2g conservative tracers Napthionate and Helium-3 were used to derive transport parameters for the C1 pathway (Andersson et al., 2002b). The two tracers were injected into borehole KI0025F03 section P5 and were recovered at borehole KI0023B section P6 (Table 6-3). The tracers differed by their diffusivity value: Napthionate has a diffusivity value of $1 \cdot 10^{-9}$ m^2/s, while the diffusivity of Helium-3 equals $2.5 \cdot 10^{-9}$ m^2/s. The pathway of Test B2g travels for the most part on Structure 20. The experimental recovery of conservative tracer and breakthrough measurements were best matched by Simulation #2 (Table 6-3). The matrix porosity in Simulation #2 differs between the background fractures and the deterministic structures, 0.001% and 0.5% respectively. The diffusion distance is set to 0.1 mm for the background fractures and 1 cm for the deterministic structures. The transport aperture is 25% of the flow aperture and the dispersion length is 1 m.

Table 6-3 displays the input parameters for the simulations. Figures 6-1 through 6-4 show breakthrough and recovery comparisons between measured and simulated data.

Table 6-3 Pathway I Simulations (Test B2g)

Simulation	Matrix Porosity (%)	Diffusion Distance (m)	Dispersion Length (m)	Transport Aperture (m)
1	1%	0.01	1	flow aperture
2	0.001% on background fractures, 0.5% on deterministic fractures	0.0001 on background fractures, 0.01 on deterministic fractures	1	0.25•flow aperture
4	0.5% on background fractures, 0.001% on deterministic fractures	0.01 on background fractures, 0.0001 on deterministic fractures	1	0.25•flow aperture

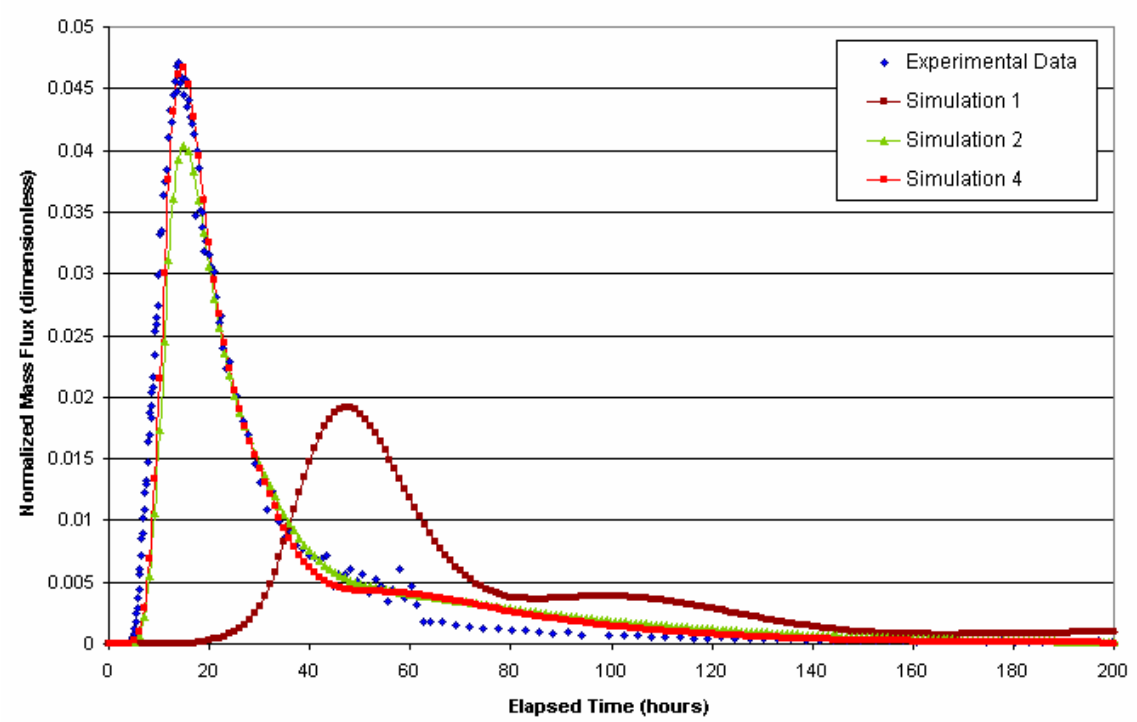

Figure 6-4 *B2g Pathway Napthionate breakthrough as compared to experimental data. Reference to Table 6-3 for input parameters.*

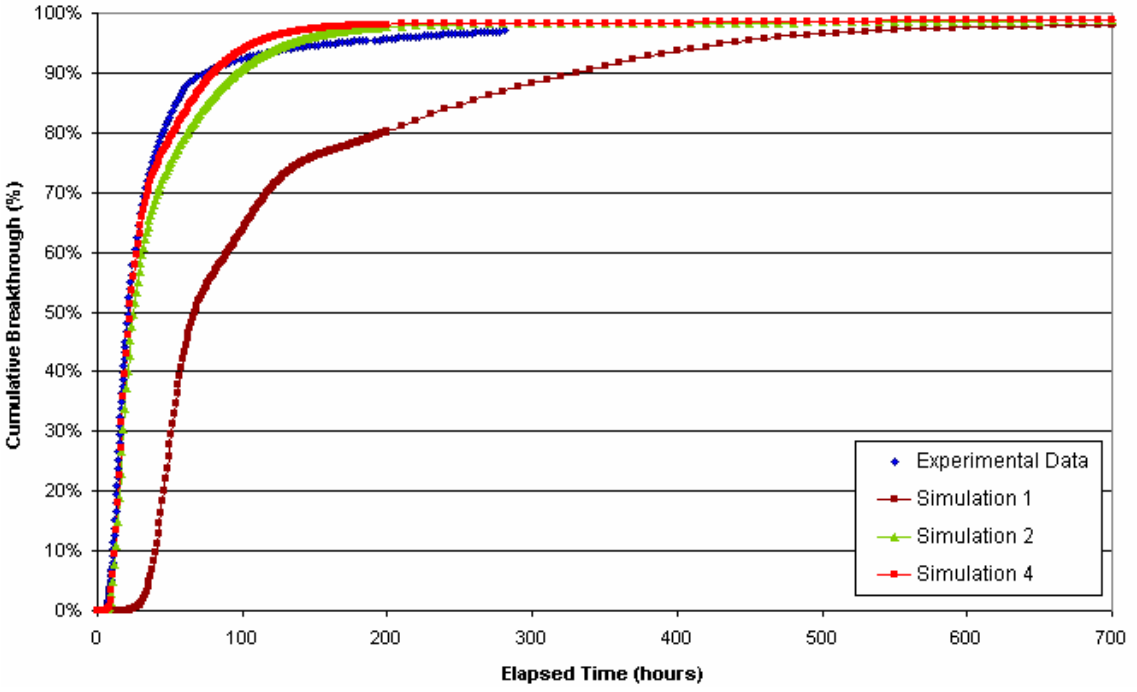

Figure 6-5 *B2g Pathway Napthionate cumulative breakthrough as compared to experimental data. Reference to Table 6-3 for input parameters.*

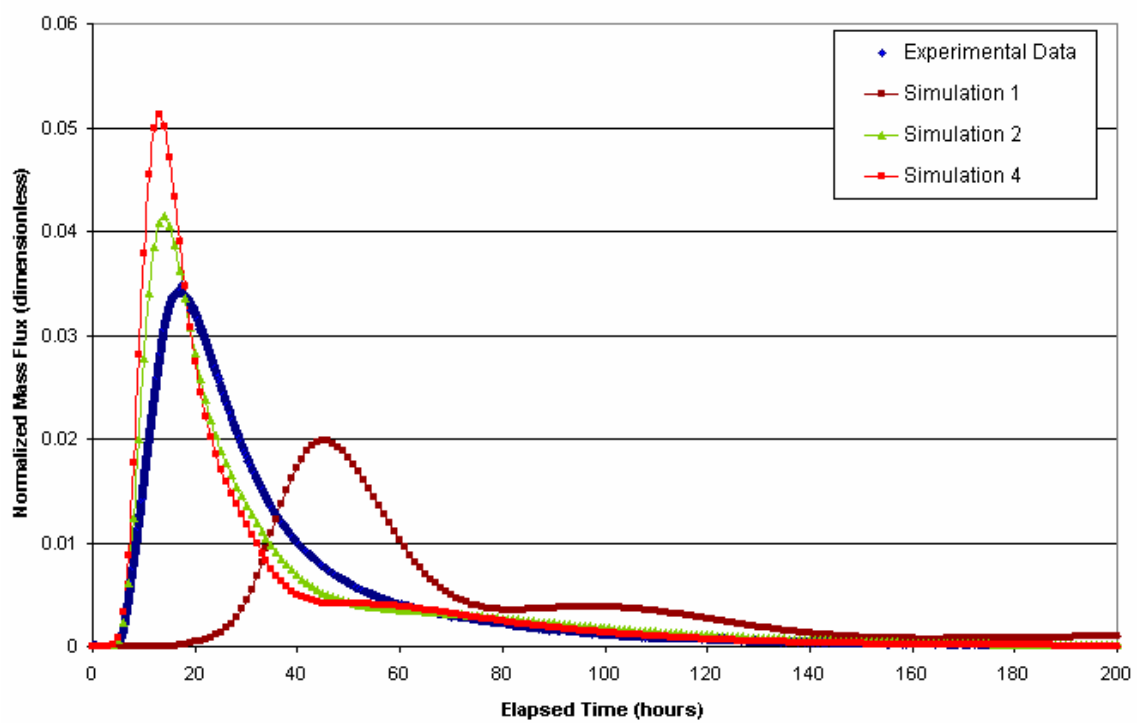

Figure 6-6 *B2g Pathway Helium-3 breakthrough as compared to experimental data. Reference to Table 6-3 for input parameters.*

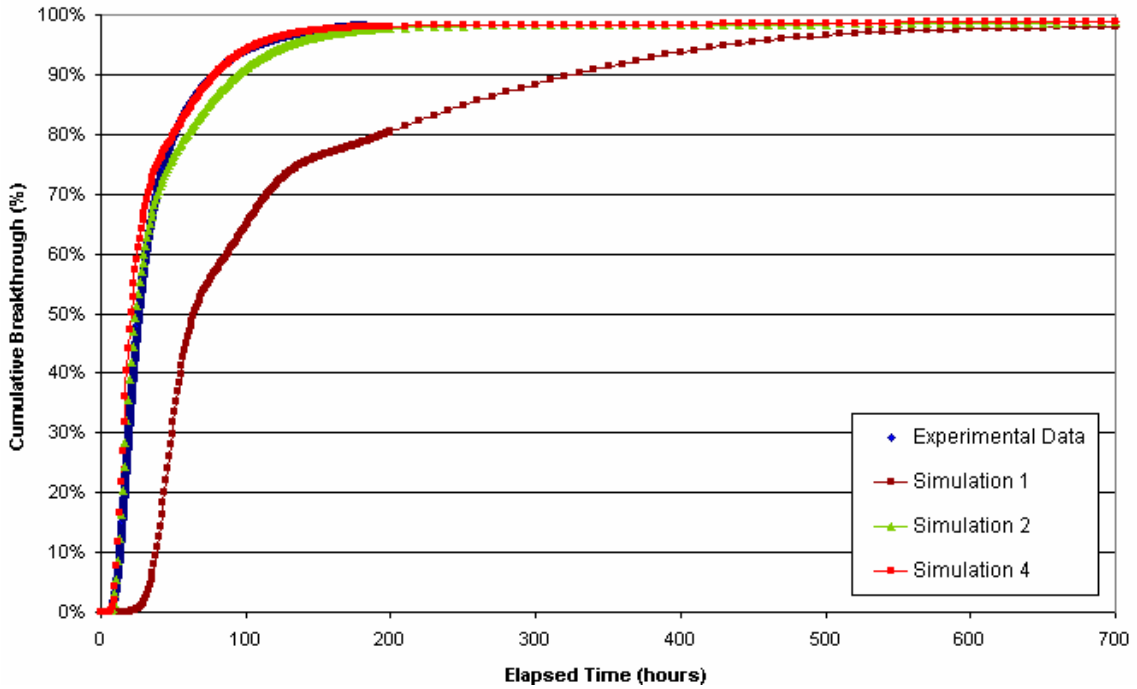

Figure 6-7 *B2g Pathway Helium-3 cumulative breakthrough as compared to experimental data. Reference to Table 6-3 for input parameters.*

The simulations of Napthionate and Helium transport produced good matches for the transport pathway using relatively low values of matrix porosity and large diffusion distance. The use of Helium as a tracer was very useful, because the high diffusivity resulted in sensitivity of results to matrix porosity and maximum diffusion distance. Helium has a diffusivity of $2.50 \cdot 10^{-9}$ m^2/s while Napthionate has a diffusivity of $1.00 \cdot 10^{-9}$ m^2/s. Napthionate matches the breakthrough curve quite well. The low diffusion distances and matrix porosity on both deterministic structures and background fractures suggest that small amounts of tracer are moving into the immobile zone. The diffusion length of 1 m is approximately 6% of the total flow path along deterministic structures from source to sink. A transport aperture equal to 25% of the flow aperture was calibrated by fitting the early time first arrival of the tracer at approximately 10 hours.

6.2.2 Pathway II (KI0025F03:P7 to KI0023B:P6) Test B2d

The B2d conservative tracer, Gadolinium, was simulated for this pathway. The tracer was injected into borehole KI0025F03 section P7 and pumped at borehole KI0023B section P6 (Table 6-2). Tracers used in this test travel from Structure 23 to Structure 20/21. In-situ conservative tracer recovery and breakthrough data was best matched by Simulation #17g (Table 6-4). This simulation had a matrix porosity of 0.5% for the background fractures and 0.001% for the deterministic structures. This is contrary to the result for Pathway I that found higher matrix porosity for the deterministic structures. The diffusion distance was 3mm on the background fractures and 0.01mm on the deterministic structures, also contrary to Pathway I results which found higher matrix porosity for the determinate structures. Transport aperture was calibrated to 13.5% of the flow aperture and the dispersion length was 0.25m. Table 6-4 displays the input parameters for the simulations. Figure 6-8 and Figure 6-9 present the breakthrough curves. Figure 6-10 illustrates channel pathways from the source to the sink locations. Figure 6-11 displays the CN model with pipes colored according to hydraulic head.

Table 6-4 Pathway II Simulations (TestB2d)

Simulation	Matrix Porosity (%)	Diffusion Distance (m)	Dispersion Length (m)	Transport Aperture (m)
10	1%	0.005	0.5	0.2•flow aperture
15	1%	0.001	0.25	0.1•flow aperture
16	1%	0.001	0.75	0.15•flow aperture
17	0.50%	0.003 on background fractures, 0.00001 on deterministic fractures	0.25	0.15•flow aperture
17g	0.5% on background fractures, 0.001% on deterministic fractures	0.003 on background fractures, 0.00001 on deterministic fractures	0.25	0.135•flow aperture

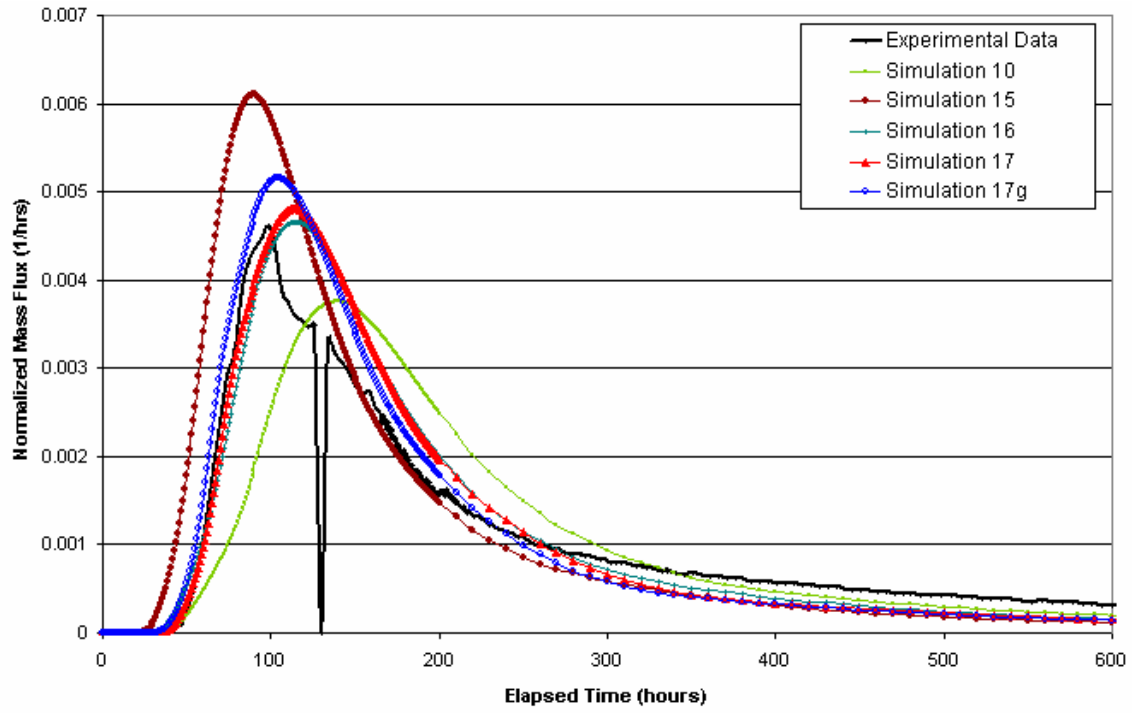

Figure 6-8 *Pathway II Gadolinium Breakthrough (Test B2d). Results of 5 simulations shown together with the experimental data. Reference to Table 6-4 for input parameters.*

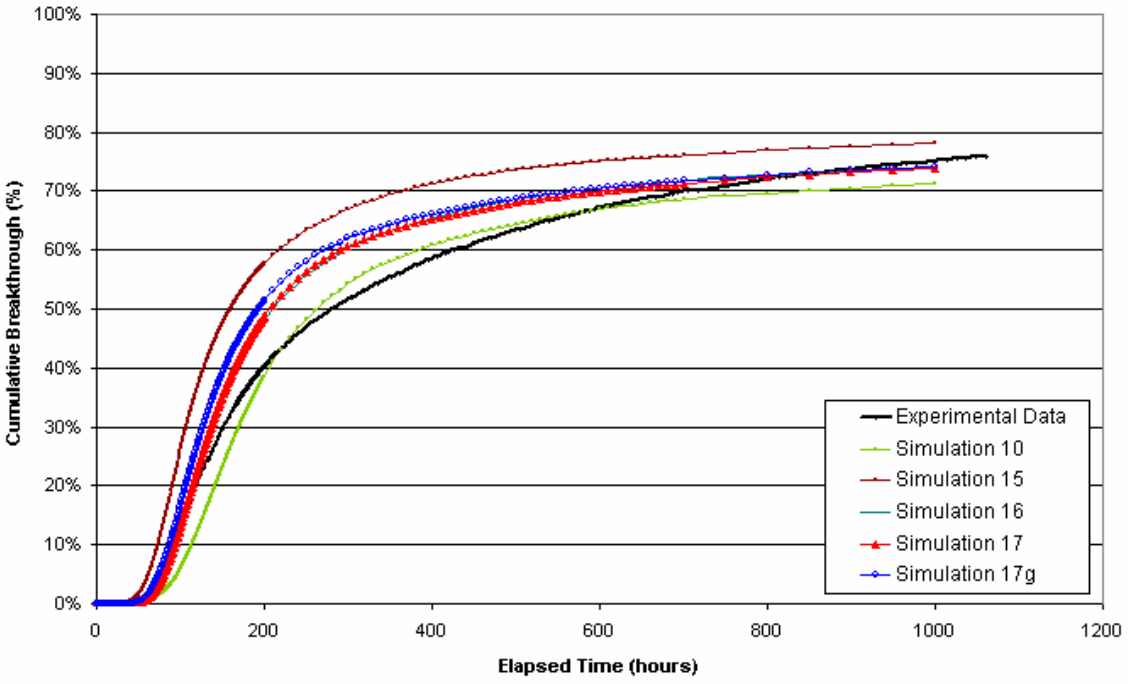

Figure 6-9 *Pathway II Gadolinium Cumulative Recovery (Test B2d). Results of 5 simulations shown together with the experimental data. Reference to Table 6-4 for input parameters.*

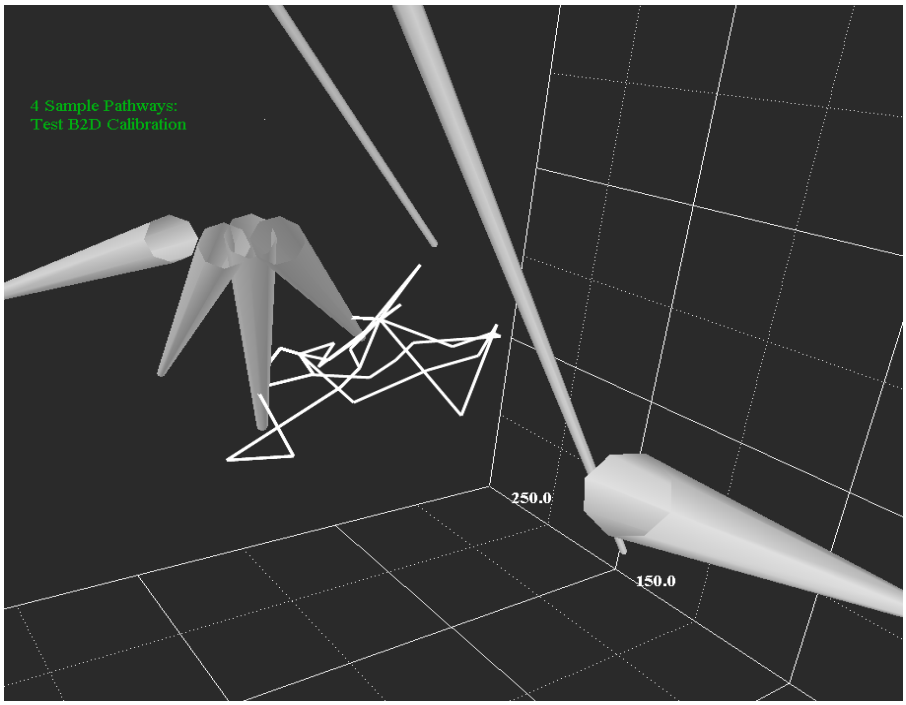

Figure 6-10 *Test B2D transport pathways. Visualization of 4 sample pathways of varying path lengths through the fracture network. Note: boreholes are not to scale.*

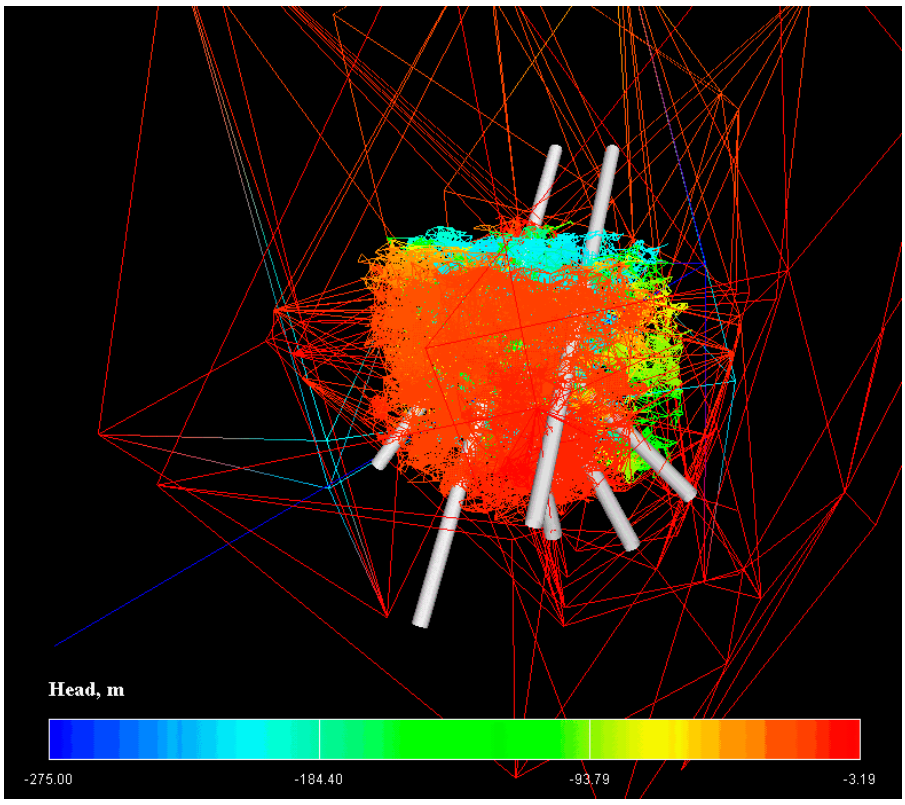

Figure 6-11 *TRUE Block Scale CN Model. Figure illustrates post-test hydraulic head distribution (masl) from Test B2d Simulation. Note: boreholes are not to scale.*

Test B2d experienced a 15% mass loss during the test. The simulated model for Test B2d allows for mass loss due to the 20/21 FIZ. The FIZ provides connection to lower pressures at the model boundaries, diverting mass away from the pumping location, and therefore decreasing the tracer recovery.

As shown in Figure 6-8 and Figure 6-9, the simulations carried out were able to identify transport properties which produced decent early and late time matches. However, the mid-time results and peak mass rate were not matched using these parameters. In simulation #17g, the short diffusion distances and low matrix porosity on both deterministic structures and background fractures suggest that little tracer was moving into the immobile zone. The small dispersion length, approximately 2% of the travel distance along deterministic structures, indicates the macroscopic dispersion along the pathway. The transport aperture is 13.5% of the flow aperture.

6.2.3 Pathway III (KI0025FO2:P3 to KI0023B:P6) Test PT4

The PT4 conservative tracer Amino G Acid was used to derive transport properties for this pathway. The tracer was injected into borehole KI0025F02 section P3 and was recovered at borehole KI0023B section P6 (Table 6-2). Pathway PT4 travels from Structure 21 to Structure 20. The in-situ conservative tracer recovery and breakthrough data was best matched by Simulation #22. Transport parameters from this simulation are as follows: matrix porosity equals 1%, diffusion distance of 1mm, transport aperture was 30% of the flow aperture, and the dispersion length was 2m. Figure 6-12 and Figure 6-13 show the comparison of measured and simulated tracer breakthrough and cumulative recovery respectively. Table 6-5 provides the transport parameters of those simulations.

Table 6-5 Pathway III Simulations (Test PT4)

Simulation	Matrix Porosity (%)	Diffusion Distance (m)	Dispersion Length (m)	Transport Aperture (m)
18	1%	0.01	10	flow aperture
19	1%	0.01	5	0.22•flow aperture
20	1%	0.01	5	0.3•flow aperture
21	1%	0.0001	2.5	0.3•flow aperture
22	1%	0.001	2	0.3•flow aperture

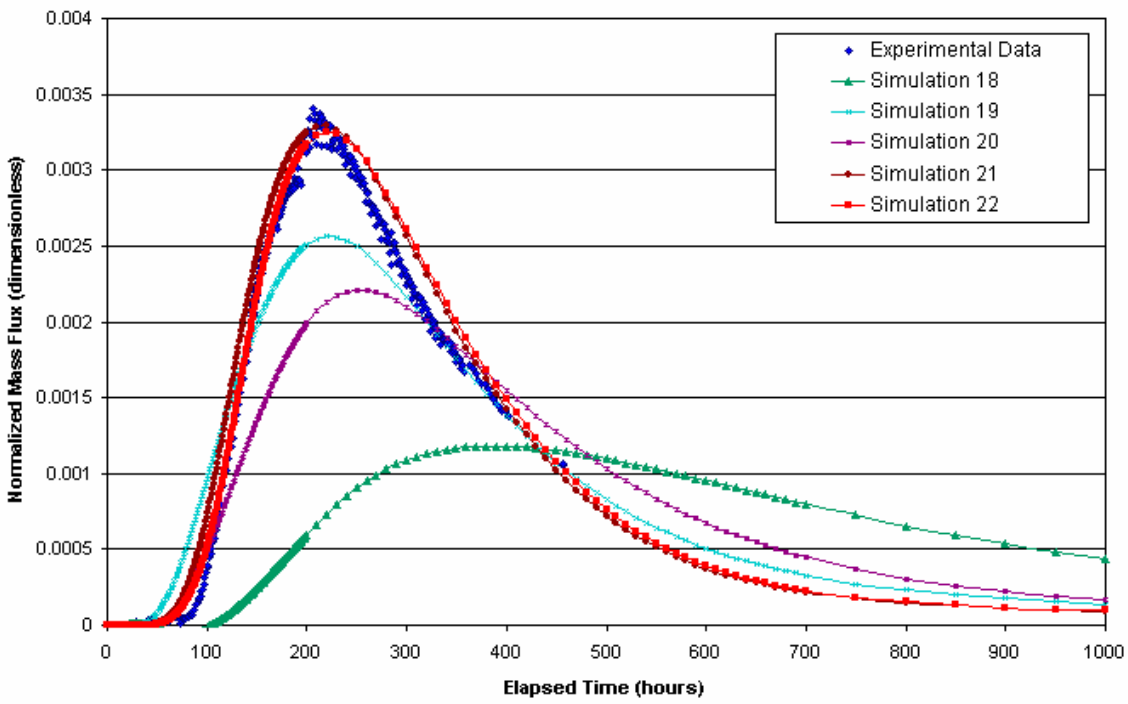

Figure 6-12 *Pathway III Amino G Acid Breakthrough (Test PT4). Results of 5 simulation shown with the experimental data. Reference to Table 6-5 for input parameters.*

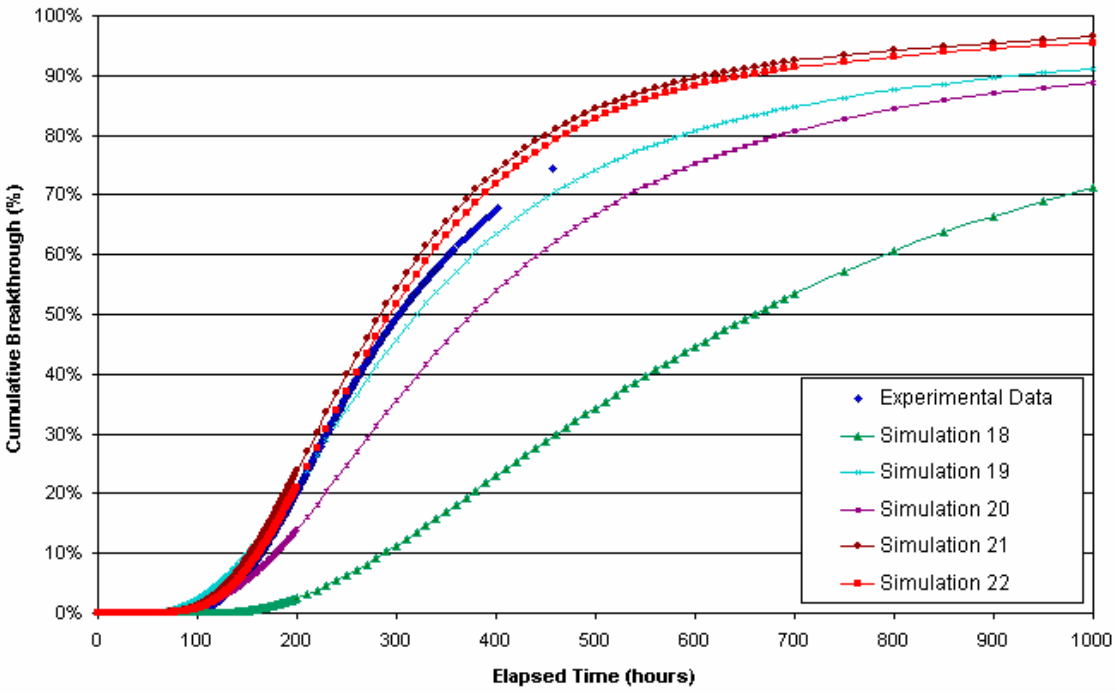

Figure 6-13 *Pathway III Amino G Acid Cumulative Recovery (Test PT4). Results of 5 simulations shown with the experimental data. Reference to Table 6-5 for input parameters.*

Simulations of the PT4 test resulted in a late time recovery higher than measured. The simulation of mass flux after the peak breakthrough was improved by decreasing the dispersion length. Simulation #22, which provided the closest match, has a dispersion length of 2 m, approximately 6% of the travel path along the deterministic structures from source to sink. The match to early time mass flux was improved with decreased diffusion into the matrix. The matrix porosity of 1% and diffusion distance of 1 mm was found to best fit the simulated data to the experimental data (Simulation #22).

6.2.4 Simulations using TRUE-1 calibrated In-situ parameters

To test the hypothesis that the TRUE-Block Scale pathways are similar to those studied in the TRUE-1 experiments, a series of simulations were carried out using the diffusion distance and matrix porosity from the TRUE-1 STT-2 (Task 4F) calibrations. Tracer Tests B2g, B2d, and PT4 were simulated, varying only the dispersion length and the aperture and using the Dershowitz et al. (2000) TRUE-1 STT-2 (Task 4F) values for all remaining transport parameters. Simulations using the TRUE-1 STT-2 (Task 4F) diffusion distance of 1cm and the matrix porosity of 3% were not able to achieve the high recoveries and high mass flux peak seen in the Phase C tests with realistic dispersion length and aperture values.

The results of these simulations are provided in Figures 6-11 through 6-16. Table 6-6 displays the input parameters (transport aperture and dispersion length) for the best match simulation using the TRUE-1 STT-2 (Task 4F) parameters. In general, the TRUE-1 immobile zone parameters did not provide a good match to in-situ measurements. This implies that either the internal structure (microstructure) of the structures tested in these experiments is significantly different from those of the feature tested in TRUE-1. As a result, the TRUE-1 immobile zone parameters are not "universal" for Äspö fractures. More research is clearly needed to develop methods for predicting immobile zone properties.

Table 6-6 Simulations Assuming TRUE-1 STT-2 (Task 4F) Transport Properties. Bold values are based on TRUE-1 STT-2 (Task 4F) simulation results

Pathway	Simulation	Matrix Porosity (%)	Diffusion Distance (m)	Transport Aperture (m)	Dispersion Length (m)
B2g	Simulation #4	0.001% Deterministic, 0.5% Background	0.0001 Deterministic, 0.01 Background	0.25•Transport Aperture	1
	Simulation using TRUE-1 STT-2 (Task 4F) parameters	**3%**	**0.01**	0.3•Transport Aperture	2.5
B2d	Simulation #17g	0.001% Deterministic, 0.5% Background	0.00001 Deterministic, 0.003 Background	0.135•Transport Aperture	0.25
	Simulation using TRUE-1 STT-2 (Task 4F) parameters	**3%**	**0.01**	0.025•Transport Aperture	10
PT4	Simulation #22	1%	0.001	0.3•Transport Aperture	2
	Simulation using TRUE-1 STT-2 (Task 4F) parameters	**3%**	**0.01**	0.37•Transport Aperture	10

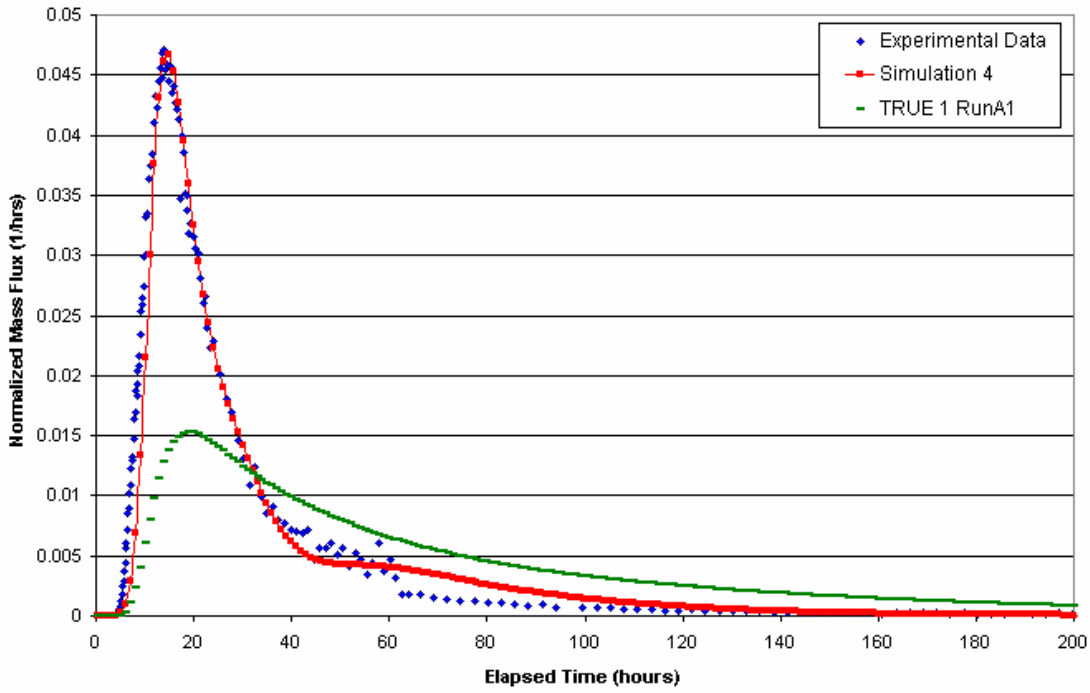

Figure 6-14 *Pathway I, Test B2g Napthionate Breakthrough. Comparision of experimental data, best-fit simulation (Run 4), and best-fit simulation with TRUE-1 STT-2 (Task 4F) diffusion distance and porosity (TRUE-1 Run A1). Reference to Table 6-6 for input parameters.*

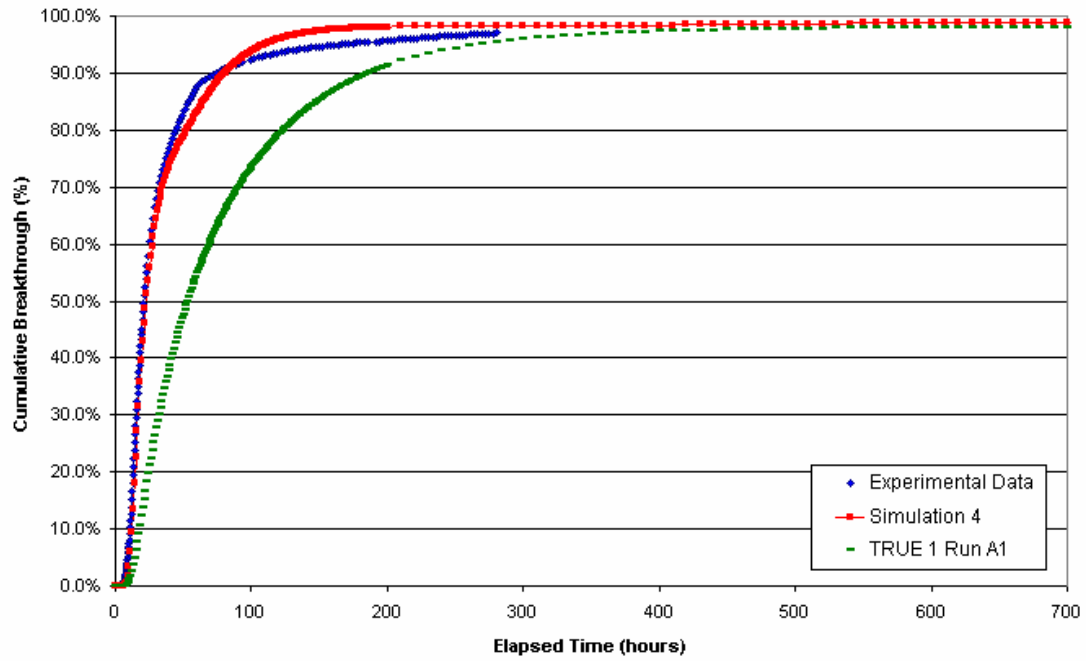

Figure 6-15 *Pathway I, Test B2g Napthionate Cumulative Breakthrough. Comparision of experimental data, best-fit simulation (Run 4), and best-fit simulation with TRUE-1 STT-2 (Task 4F) diffusion distance and porosity (TRUE-1 Run A1). Reference to Table 6-6 for input parameters.*

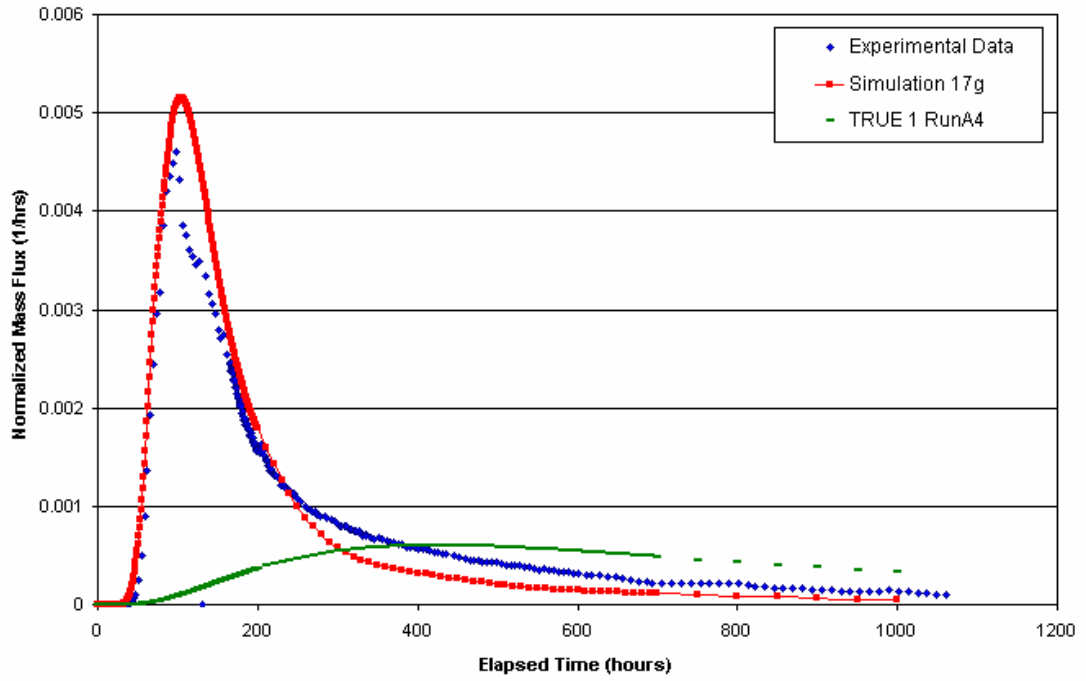

Figure 6-16 *Pathway II, Test B2d: Gadolinium Breakthrough. Comparision of experimental data, best-fit simulation (Run 17g), and best-fit simulation with TRUE-1 STT-2 (Task 4F) diffusion distance and porosity (TRUE-1 Run A4). Reference to Table 6-6 for input parameters.*

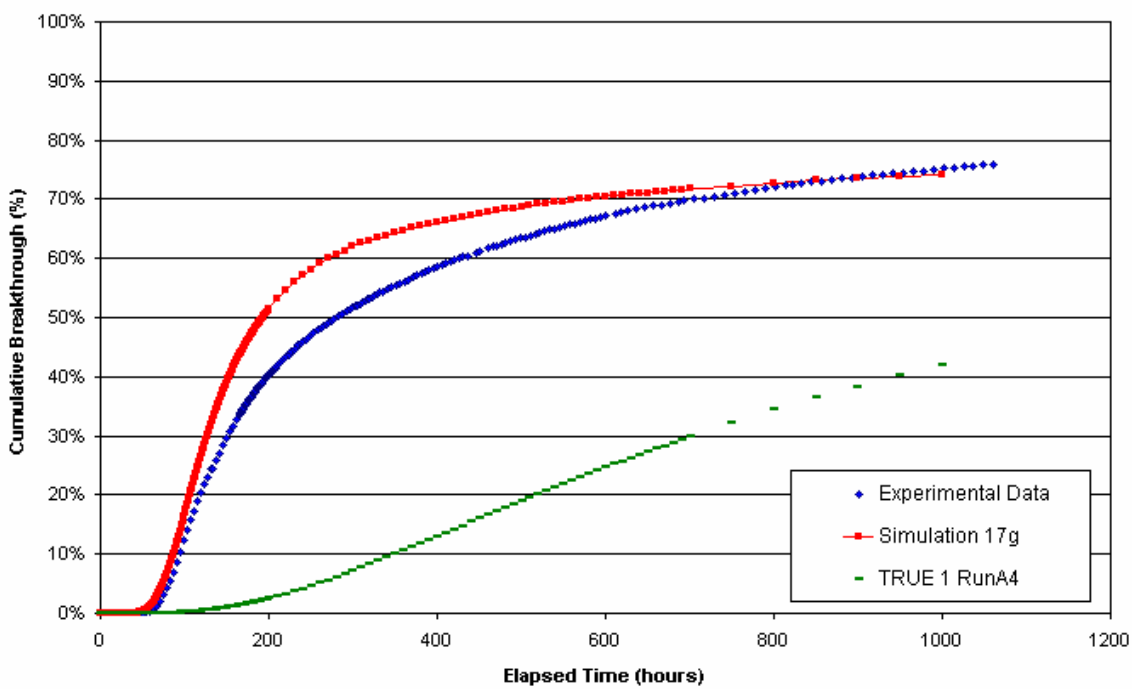

Figure 6-17 *Pathway II, Test B2d Gadolinium Cumulative Breakthrough. Comparision of experimental data, best-fit simulation (Run 17g), and best-fit simulation with TRUE-1 STT-2 (Task 4F) diffusion distance and porosity (TRUE-1 Run A4). Reference to Table 6-6 for input parameters.*

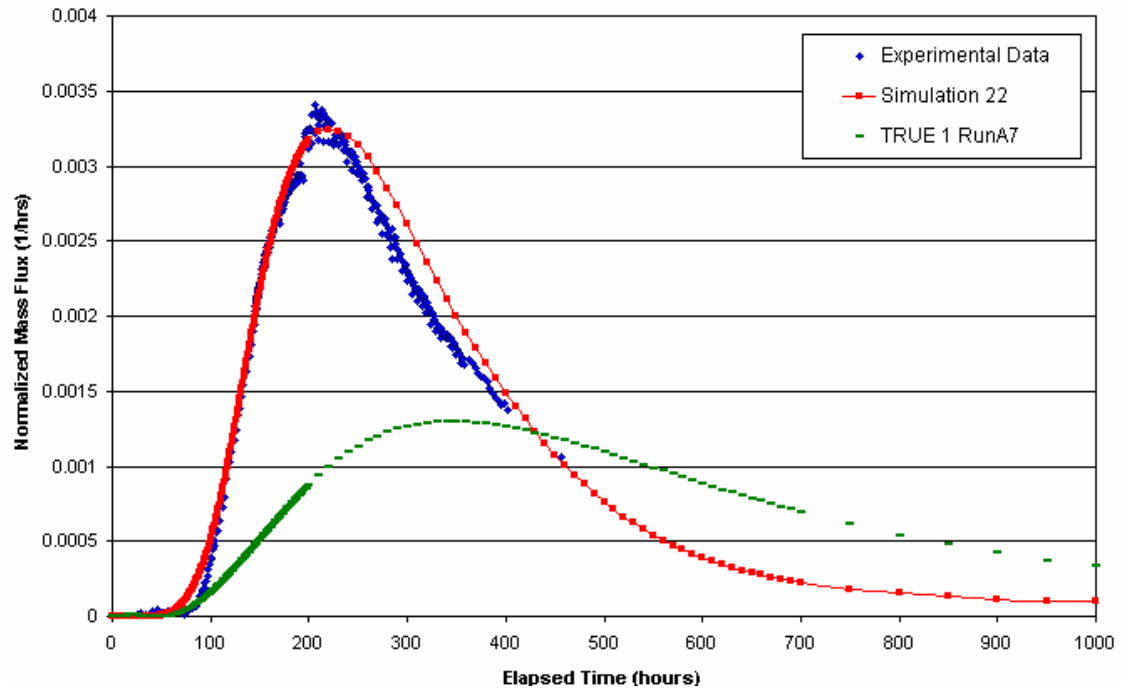

Figure 6-18 *PT4 Pathway III, Test PT4 Amino G Acid Breakthrough. Comparision of experimental data, best-fit simulation (Run 22), and best-fit simulation with TRUE-1 STT-2 (Task 4F) diffusion distance and porosity (TRUE-1 Run A7). Reference to Table 6-6 for input parameters.*

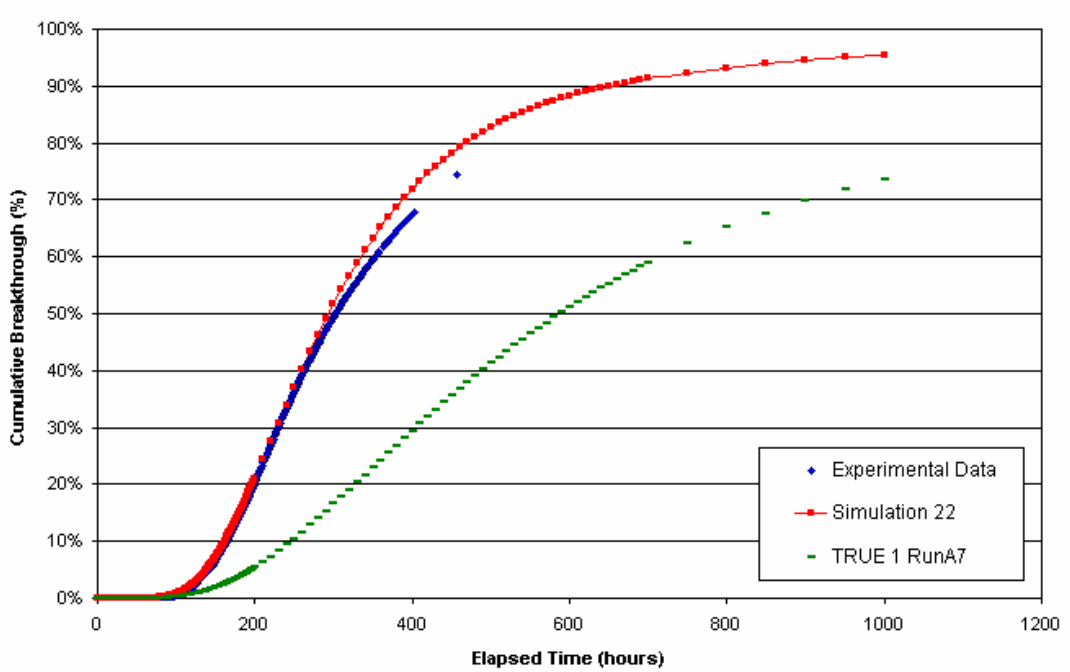

Figure 6-19 *Pathway III, Test PT4 Amino G Acid Cumulative Breakthrough. Comparision of experimental data, best-fit simulation (Run 22), and best-fit simulation with TRUE-1 STT-2 (Task 4F) diffusion distance and porosity (TRUE-1 Run A7). Reference to Table 6-6 for input parameters.*

6.2.5 Multiple realizations of background fractures

Multiple realizations of the stochastically generated background fractures were generated to compare the effects of background fractures on transport pathways. Four realizations were run for each tracer test (B2g, B2d, and PT4) based on the best-fit simulation (see Table 6-3, Table 6-4, and Table 6-5.). For each realization, only the stochastic background fracture generation was changed. Figure 6-20 through Figure 6-22 shows the four realizations for each of the tracer tests.

Simulations of Tracer Tests B2g, B2d, and PT4 show varying degrees of variability due to multiple realizations of background fractures. Simulations of B2g and B2d display approximate cumulative recoveries to the experimental data. The peak breakthrough time of Tests B2g simulations also approximates the peak time of the experiment. Test B2d peak breakthrough times are generally earlier than experimental data. Simulations of Test PT4 have higher cumulative recovery as compared to the experimental data. Peak breakthrough times of Test PT4 simulations are earlier than the experimental data. Pathway III (Test PT4) thus appear to be more sensitive to background fractures. This is reasonable, considering the greater length of that pathway.

For Pathway III (Test PT-4), between 90% and 100% of the injected mass travels through pipes associated with background fractures over the duration of the test. The large amount of tracer interaction with the background fractures accounts for the high variability in realizations associated with the background fractures.

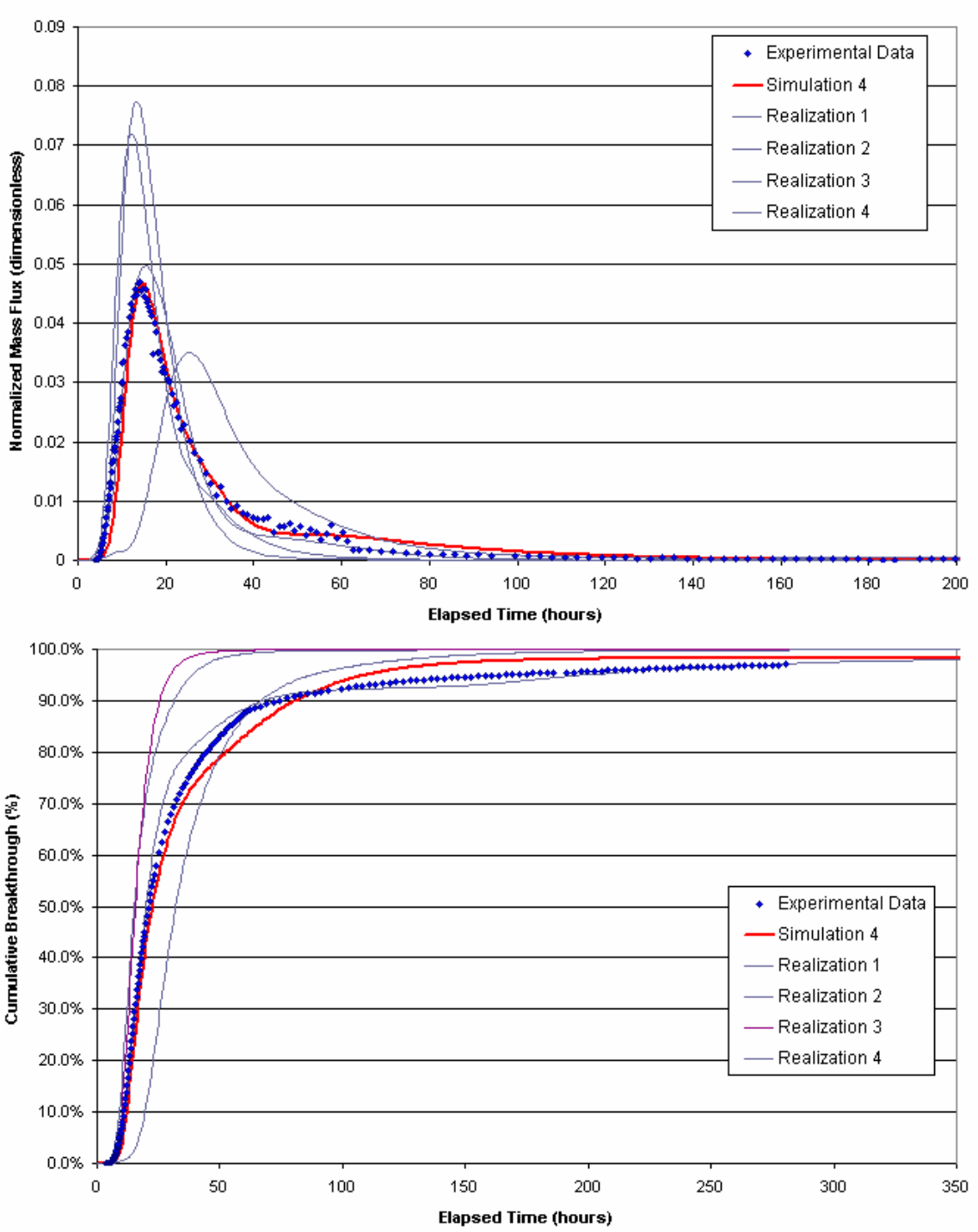

Figure 6-20 *Multiple Realizations of Background Fractures. Pathway I, Test B2g Napthionate Transport*

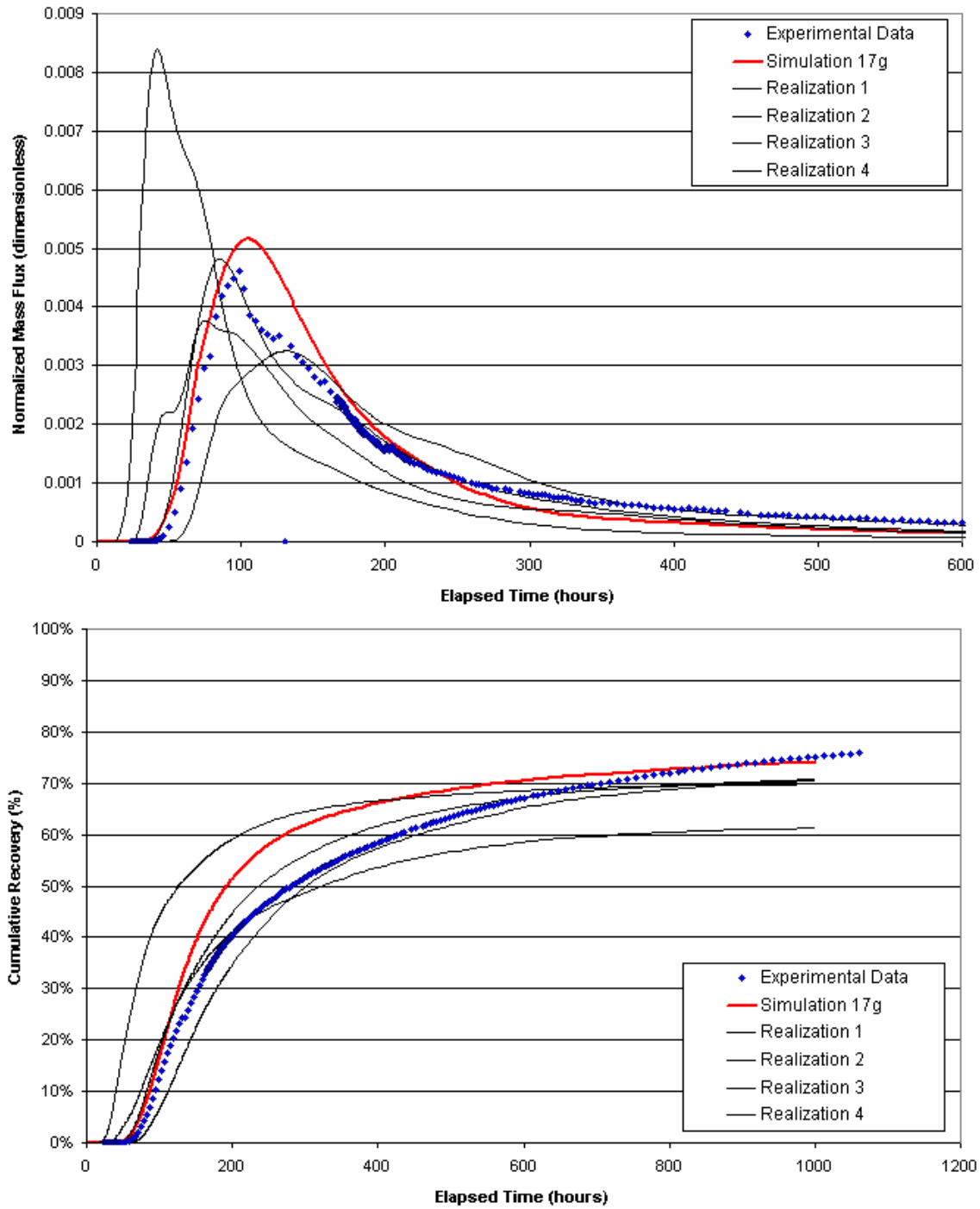

Figure 6-21 *Multiple Realizations of Background Fractures. Pathway II, Test B2d Gadolinium Transport*

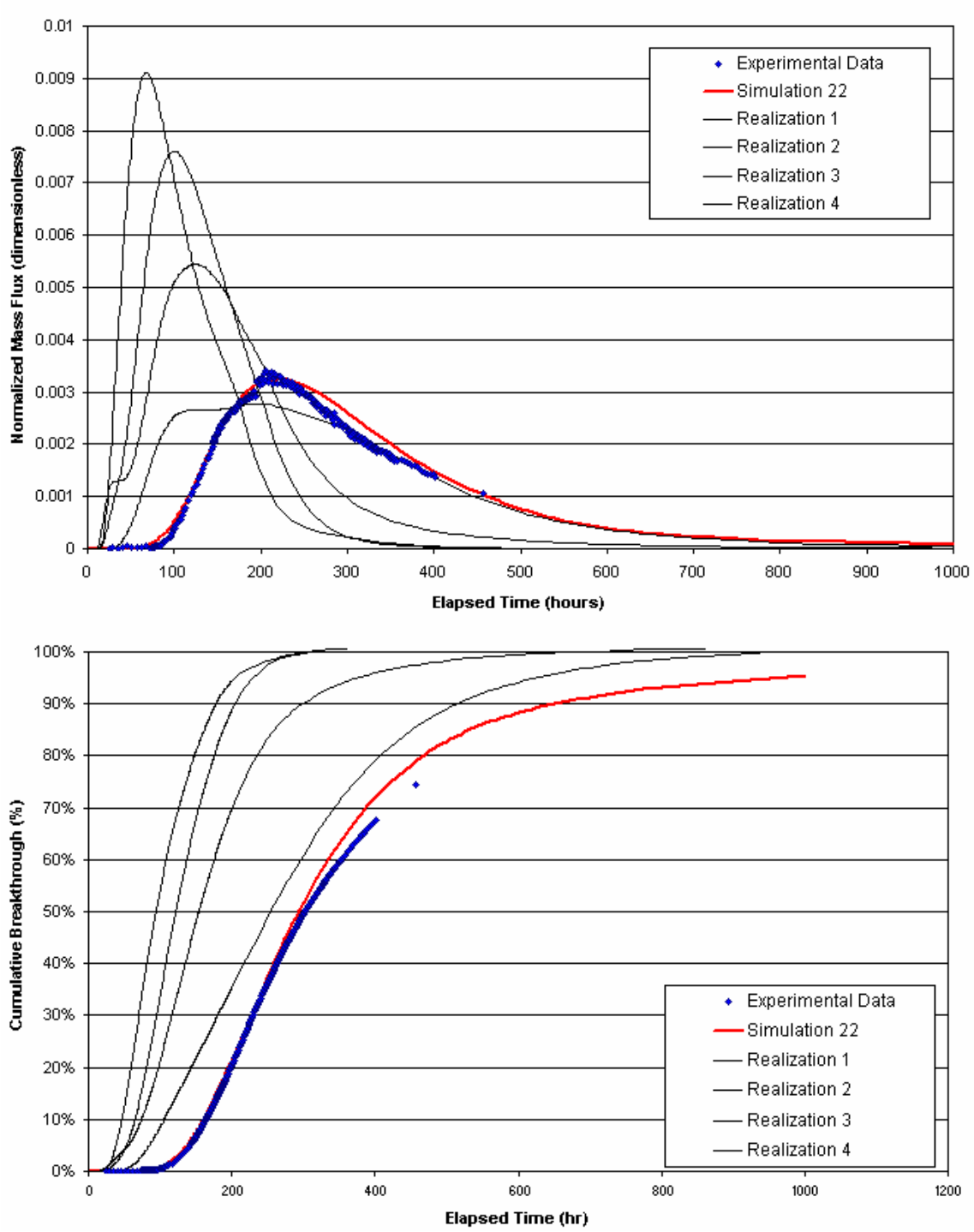

Figure 6-22 *Multiple Realizations of Background Fracture. Pathway III, Test PT4 Amino G Acid Transport*

6.2.6 Pathway assessment

The DFN/CN transport simulations carried out on the three transport pathways I, II, III (Tests B2g, B2d, and PT4) derived values for transport parameters that are fairly consistent between the pathways. These parameters are summarized in Table 6-7.

Table 6-7 Phase C Calibration Parameters.

Pathway	Simulation	Matrix Porosity	Diffusion Distance (m)	Transport Aperture (m)	Longitudinal Dispersion x_L (m)
Tests I C1 (B2g)	Simulation #4	0.001% Deterministic, 0.5% Background	0.0001 Deterministic, 0.01 Background	0.25•Flow Aperture	1
Tests II C2 (B2d)	Simulation #17g	0.001% Deterministic, 0.5% Background	0.00001 Deterministic, 0.003 Background	0.135•Flow Aperture	0.25
Tests III C3 (PT4)	Simulation #22	1%	0.001	0.3•Flow Aperture	2

- Diffusive processes are relatively weak along these pathways, with diffusion distances on the order of 0.01 to 0.0001 m and a matrix porosity of 0.001% to 0.5%.
- Advective transport is 4 to 6 times faster than would be expected from the transport aperture derived using A = 0.1 and B = 2 (Dershowitz et al, 2000) in Eq 1. The advective transport corresponds to A values between 0.1 and 2.
- Less longitudinal dispersion occurs on these pathways than would be expected based on 10% of path length. Pathway longitudinal dispersion are only 0.25 to 2 m, with the least dispersion on pathway B2d, which crosses a fracture intersection zone and has reduced recovery.

Surprisingly, in the CN/DFN model as implemented, a significant portion of the transport occurs along background fractures, and diffusive processes appear to be stronger along those pathways that include background fractures. Unfortunately, no systematic study was carried out to distinguish the role of background fractures more clearly.

6.3 Predictive simulations

6.3.1 Transport parameters

The pathway transport properties derived in the previous sections were used to model and predict the Phase C transport experiments. The parameters above include all those necessary for simulating conservative tracer transport. For sorbing tracer transport, additional sorption parameters are required. The parameters were taken from the values that successfully matched sorbing tracer transport at the TRUE-1 site at the north end of the Äspö laboratory (Dershowitz et al., 2000). These effective sorption parameters are based primarily on laboratory measurement (Byegård et al., 1998), adjusted based on tracer breakthrough observation in "Feature A" experiments (STT-1, STT-1b and STT-2). It is expected that these values reflect the influence of specific fracture infillings and coatings.

It should be noted that although the effective sorption parameters from TRUE-1 are the only parameters available that are calibrated on in-situ experiments, the simulations above for conservative tracers have already indicated that the TRUE-1 immobile zone parameters might not be directly applicable to the TRUE Block Scale experiment. Parameters are listed in Table 6-8.

Table 6-8: Blind Prediction Sorbing Parameters, K_d and K_a values from TRUE-1 Task 4F (Dershowitz et al, 2000)

Tracer	K_d (m^3/kg)	Surface Sorption K_a (m)	Free Water Diffusivity (m^2/s)
Ba-131	$1.25 \cdot 10^{-05}$	$6.08 \cdot 10^{-04}$	$8.30 \cdot 10^{-10}$
Ba-133	$1.25 \cdot 10^{-05}$	$6.08 \cdot 10^{-04}$	$8.30 \cdot 10^{-10}$
Br-82	0	0	$2.08 \cdot 10^{-09}$
Ca-47	$6.25 \cdot 10^{-07}$	$3.04 \cdot 10^{-05}$	$7.92 \cdot 10^{-10}$
Cs-134	$8.30 \cdot 10^{-05}$	$4.03 \cdot 10^{-03}$	$2.06 \cdot 10^{-09}$
Cs-137	$1.67 \cdot 10^{-04}$	$8.12 \cdot 10^{-03}$	$2.06 \cdot 10^{-09}$
HTO	0	0	$2.40 \cdot 10^{-09}$
K-42	$2.00 \cdot 10^{-04}$	$9.72 \cdot 10^{-03}$	$2.00 \cdot 10^{-09}$
Na-22	$2.70 \cdot 10^{-07}$	$1.31 \cdot 10^{-05}$	$1.33 \cdot 10^{-09}$
Na-24	$2.70 \cdot 10^{-07}$	$1.31 \cdot 10^{-05}$	$1.33 \cdot 10^{-09}$
Rb-83	$2.08 \cdot 10^{-05}$	$1.01 \cdot 10^{-03}$	$2.03 \cdot 10^{-09}$
Rb-86	$2.08 \cdot 10^{-05}$	$1.01 \cdot 10^{-03}$	$2.03 \cdot 10^{-09}$
Re-186	0	0	$1.00 \cdot 10^{-09}$
Sr-85	$1.04 \cdot 10^{-06}$	$5.05 \cdot 10^{-05}$	$7.89 \cdot 10^{-10}$

6.3.2 Phase C injection functions

The injection functions (tracer time history at source) measured for the Phase C tracer experiments are shown in Figure 6-23 through Figure 6-25. All of these injection curves were corrected for decay, and there was therefore no need to include decay in the transport modeling.

Injected activities reported for the experiments were not completely consistent with the injection curves shown in Figure 6-23 through Figure 6-25. Injection activities were therefore estimated by deriving an injection rate for C1, C2, and C3 injections to match the reported cumulative injections. The adjusted total injected activities are provided in Table 6-9, Table 6-10, and Table 6-11.

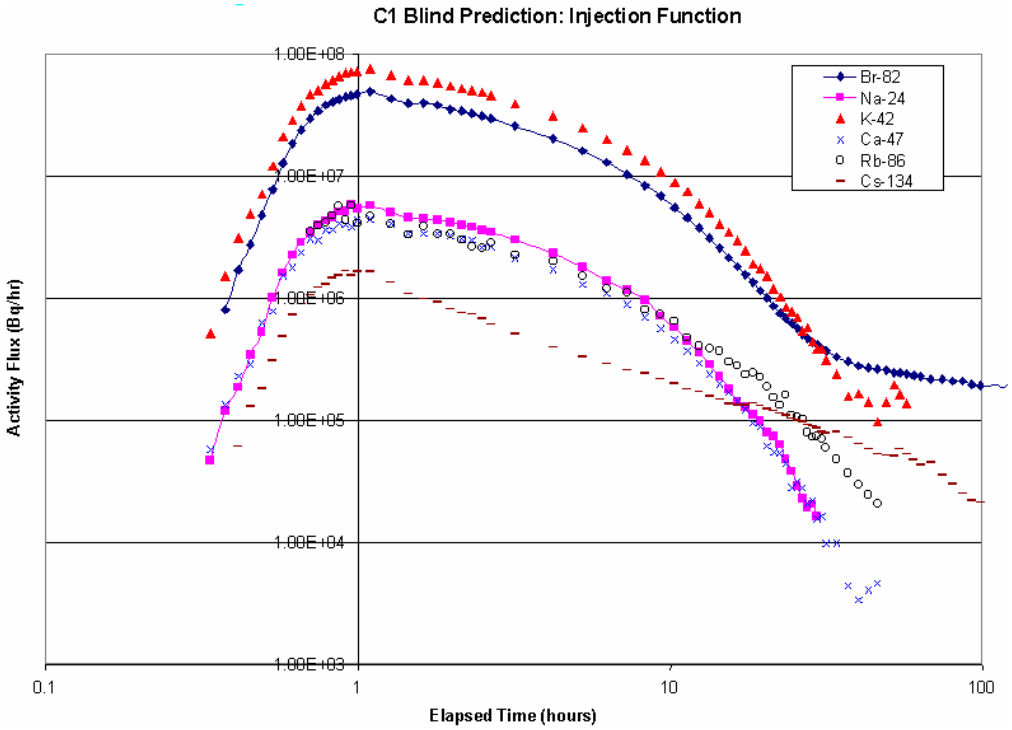

Figure 6-23 *Test C1: Injection Functions for Br-82, Na-24, K-42, Ca-47, Rb-86, and Cs 134*

Table 6-9 Test C1 Injection Activity: Measured and Estimated

Tracer	Injection Activity (Bq) - Measured	Injection Activity (Bq) - Estimated
Br-82	$1.38 \cdot 10^{8}$	$2.5129 \cdot 10^{8}$
Na-24	$1.56 \cdot 10^{7}$	$2.5523 \cdot 10^{7}$
K-42	$2.29 \cdot 10^{8}$	$3.6097 \cdot 10^{8}$
Ca-47	$1.07 \cdot 10^{7}$	$1.9730 \cdot 10^{7}$
Rb-86	$1.33 \cdot 10^{7}$	$2.3783 \cdot 10^{7}$
Cs-134	$7.79 \cdot 10^{6}$	$1.4418 \cdot 10^{7}$

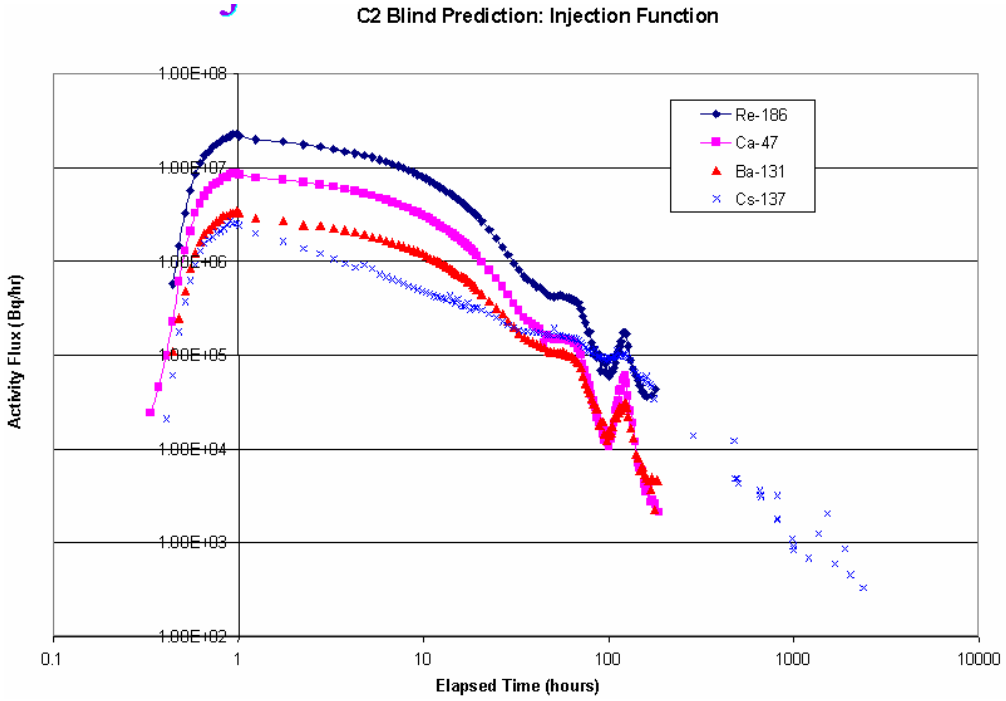

Figure 6-24 *Test C2: Injection Functions for Re-186, Ca-47, Ba-131, and Cs-137.*

Table 6-10 Test C2 Injection Activity: Measured and Estimated

Tracer	Injection Activity (Bq) - Measured	Injection Activity (Bq) - Estimated
Re-186	$1.71 \cdot 10^{8}$	$2.29 \cdot 10^{8}$
Ca-47	$5.64 \cdot 10^{7}$	$8.69 \cdot 10^{7}$
Ba-131	$2.57 \cdot 10^{7}$	$3.69 \cdot 10^{7}$
Cs-137	$2.35 \cdot 10^{7}$	$4.07 \cdot 10^{7}$

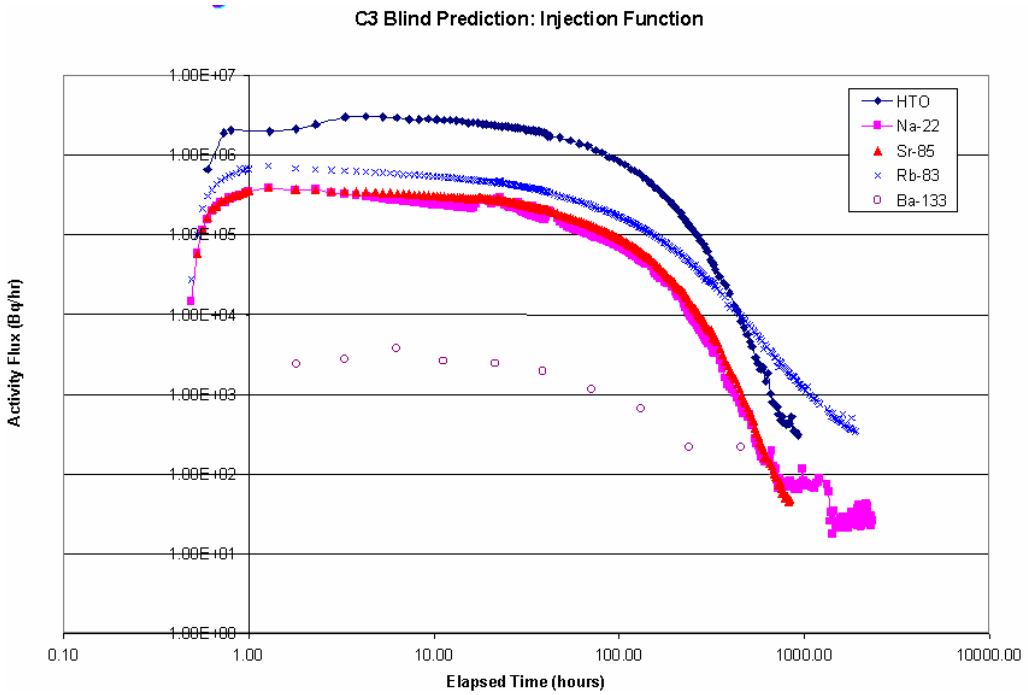

Figure 6-25 *Test C3: Injection Functions for HTO, Na-22, Sr-86, Rb-83, and Ba-133.*

Table 6-11 Test C3 Injection Activity: Measured and Estimated

Tracer	Injection Activity (Bq) - Measured	Injection Activity (Bq) - Estimated
HTO	$2.4394 \cdot 10^{8}$	$2.5235 \cdot 10^{8}$
Na-22	$2.1606 \cdot 10^{7}$	$2.2610 \cdot 10^{7}$
Sr-85	$2.2105 \cdot 10^{7}$	$2.6398 \cdot 10^{7}$
Rb-83	$4.5895 \cdot 10^{7}$	$5.4249 \cdot 10^{7}$
Ba-133	$5.5446 \cdot 10^{5}$	$3.4989 \cdot 10^{5}$

6.3.3 Prediction of Phase C tracer tests

The Phase C tracer experiments were simulated using the developed CN/DFN models and transport parameters described in the previous sections. The resulting “blind” predictions are presented in Figure 6-26 through Figure 6-31.

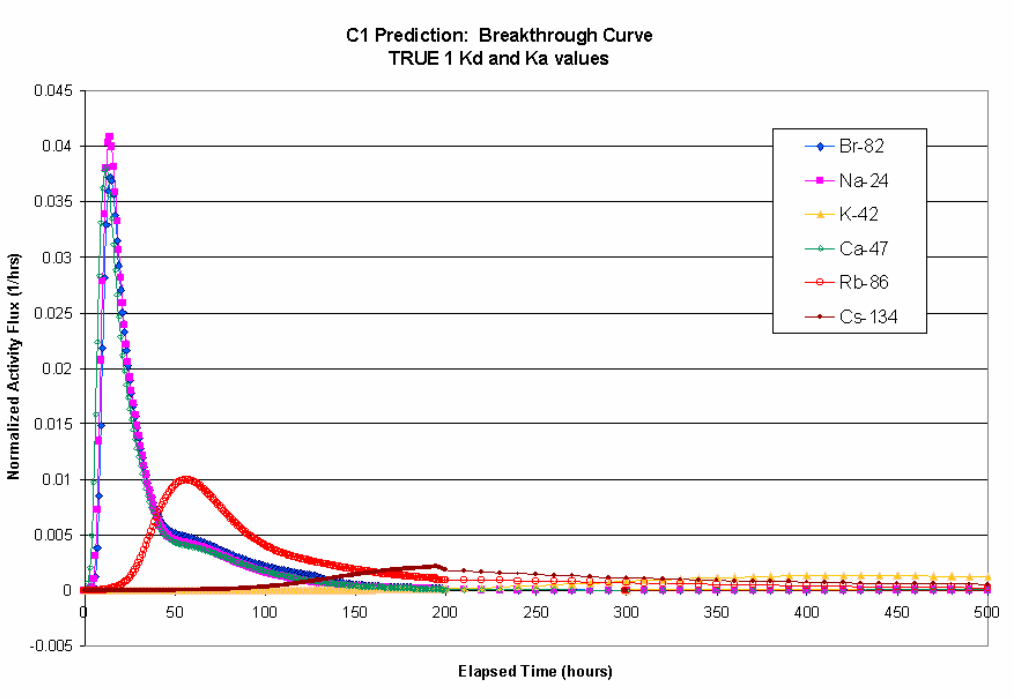

Figure 6-26 *Test C1: Blind Prediction Breakthrough. Predictions made with TRUE-1 K_d and K_a values.*

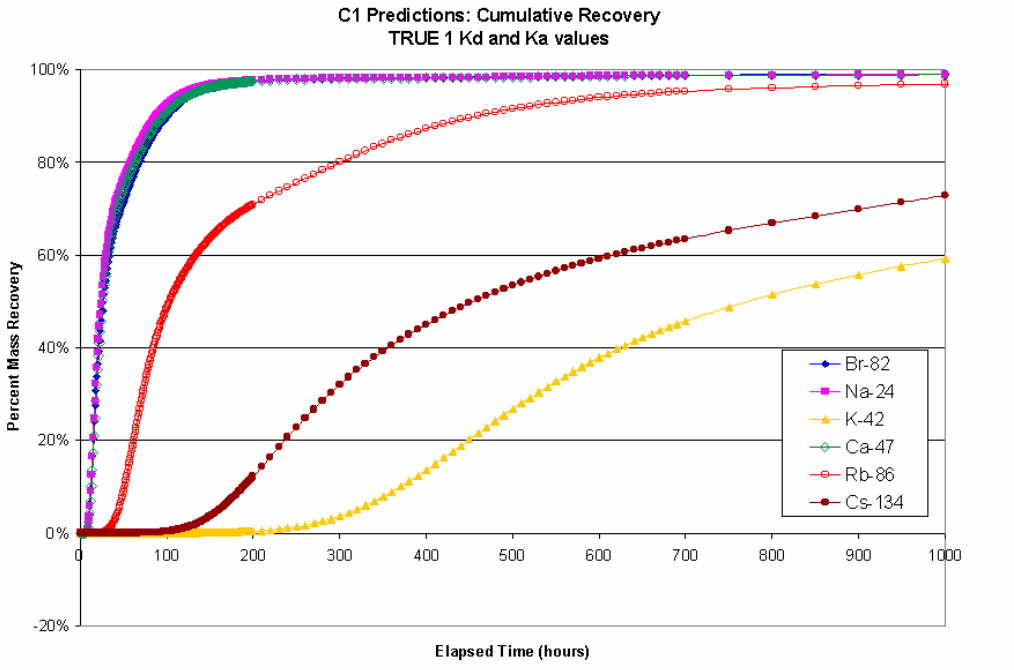

Figure 6-27 *Test C1: Blind Prediction Cumulative Breakthrough. Predictions made with TRUE-1 K_d and K_a values.*

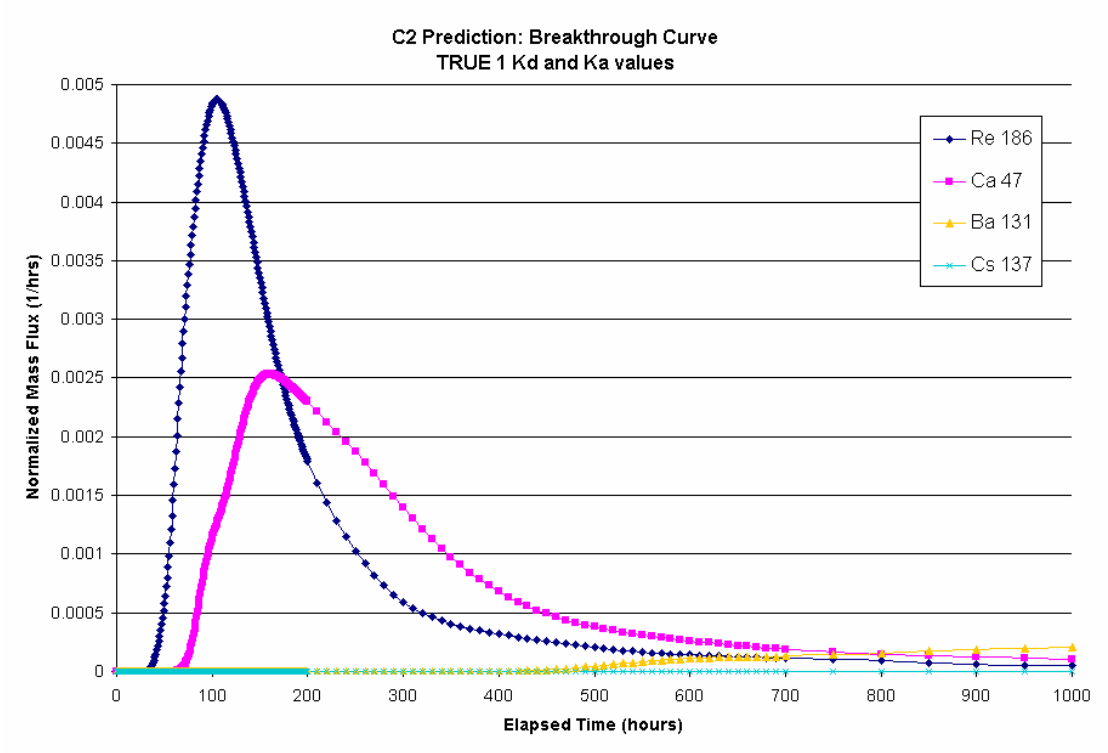

Figure 6-28 *Test C2: Blind Prediction Breakthrough. Predictions made with TRUE-1 K_d and K_a values.*

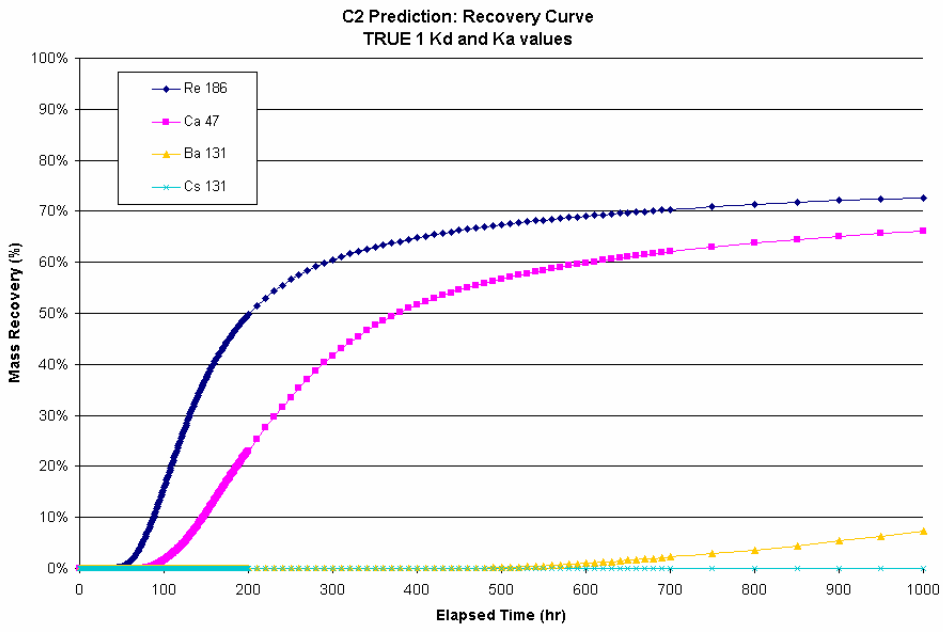

Figure 6-29 *Test C2: Blind Prediction Cumulative Breakthrough. Predictions made with TRUE-1 K_d and K_a values.*

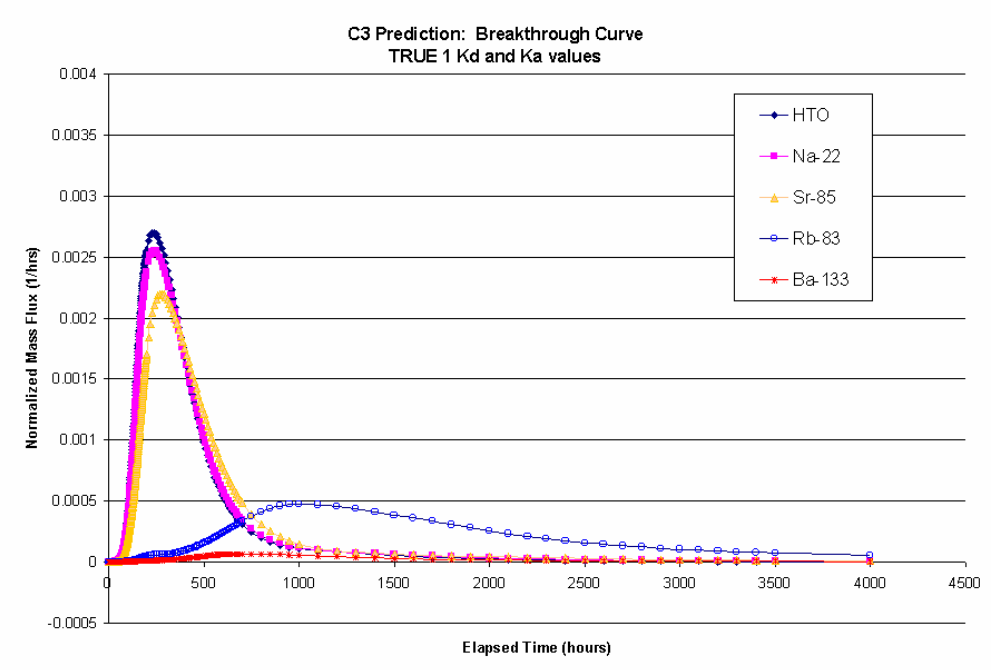

Figure 6-30 *Test C3: Blind Prediction Breakthrough. Predictions made with TRUE-1 K_d and K_a values.*

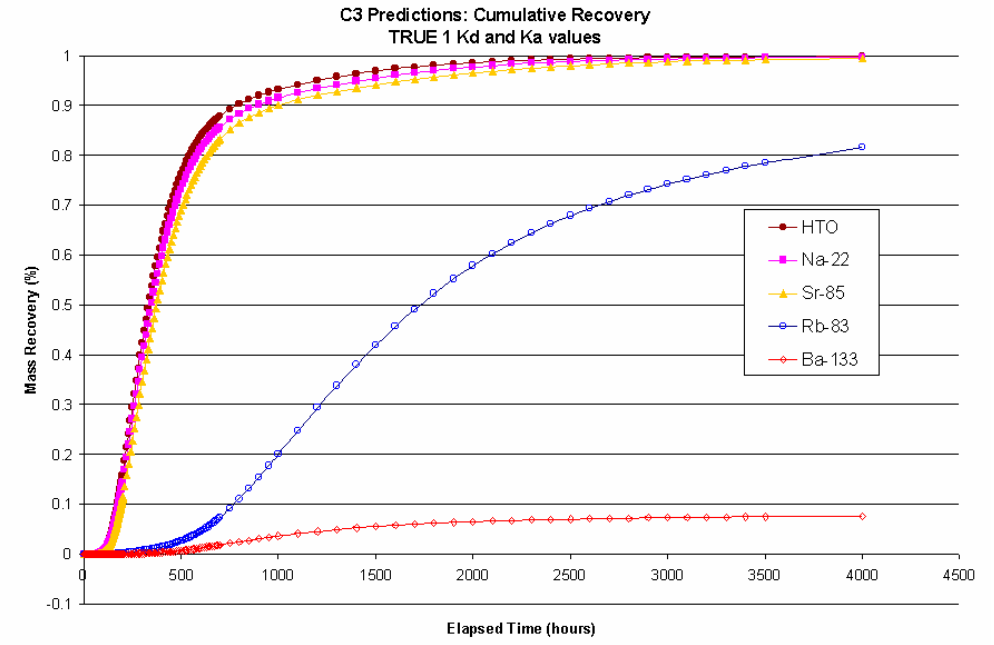

Figure 6-31 *Test C3: Blind Prediction Cumulative Breakthrough. Predictions made with TRUE-1 K_d and K_a values.*

6.3.4 Preliminary evaluation

After the predictions were made, in-situ data for sorbing tracers was released by the project. The T_5, T_{50}, T_{95} values from the measured data are compared to the blind prediction using TRUE-1 sorption parameters (See Table 6-8) T_5, T_{50}, T_{95} values in Table 6-12. Of the 15 tracers subjected to prediction simulations, 11 tracers show breakthrough and recovery in the experimental data. The remaining 4 tracer breakthroughs were below background levels. Of a total of 60 predictions 22 were within 20% of measurements. Predictions for conservative tracers were generally within the 20% criterion for the pathways of C1 and C2. Surprisingly, the pathway C3 transport of HTO was significantly slower than modeled based on tracer experiment PT4. We have no explanation for this at present and further study is required to analyze this discrepancy.

Table 6-12 Comparison of T_5, T_{50}, and T_{95} Values of Blind Predictions using TRUE-1 sorption parameters and In-situ Measurements

TEST/ TRACER		T_5	T_{50}	T_{95}	% Ultimate Recovery
C1 / Br-82 (Conservative)	In-situ	9.01	21.01	49.02	111%
	Blind Prediction	11	26	131	100%
C1 / Na-24	In-situ	11.01	27.01	104.68	96%
	Blind Prediction	11	24	121	100%
C1 / K-42	In-situ	21.01	104.68	Na	52%
	Blind Prediction	320	750	Na	92%
C1 / Ca-47	In-situ	15.01	46.02	262.71	98%
	Blind Prediction	11	26	131	100%
C1 / Rb-86	In-situ	67.54	403.42	Na	67%
	Blind Prediction	45	104	660	99%
C1 / Cs-134	In-situ	526.42	Na	Na	39%
	Blind Prediction	160	450	2600	97%
C2 / Re-186 (Conservative)	In-situ	92.88	255.18	Na	80%
	Blind Prediction	74	200	Na	73%
C2 / Ca-47	In-situ	377.013	721.32	Na	68%
	Blind Prediction	123	370	Na	66%
C2 / Ba-131	In-situ	Recovery below background levels			
	Blind Prediction	850	Na	Na	10%
C2 / Cs-137	In-situ	Recovery below background levels			
	Blind Prediction	Na	Na	Na	0%
C3 / HTO (Conservative)	In-situ	227.33	822.33	Na	73%
	Blind Prediction	148	330	1200	100%
C3 / Na-22	In-situ	336.33	1481.33	Na	70%
	Blind Prediction	152	350	1400	100%

TEST/ TRACER		T_5	T_{50}	T_{95}	% Ultimate Recovery
C3 / Sr-85	In-situ	640.08	2967	Na	52%
	Blind Prediction	173	400	1900	99%
C3 / Rb-83	In-situ	Recovery below background levels			
	Blind Prediction	630	1700	Na	85%
C3 / Ba-133	In-situ	Recovery below background levels			
	Blind Prediction	1300	Na	Na	10%

For sorbing tracers, differences between measured and simulated Phase C tracer breakthroughs can be expressed in terms of differences in effective sorption parameters K_d and K_a, matrix porosity, diffusivity and diffusion thickness. The first hypothesis is that differences in sorption are related to differences in fracture infilling minerals between "Feature A" of the TRUE-1 experiments and the structures encountered in the TRUE Block Scale experiments. This hypothesis was addressed by applying the TRUE –Block Scale reference sorption parameter of Winberg et al. (2000). The Winberg et al. (2000) sorption parameters are provided in Table 6-12.

Table 6-13: Sorption Parameters from TRUE-Block Scale. K_d and Diffusivity values are referenced to Winberg et al, 2000 (Appendix G). K_a of zero was assumed to allow evaluation of a single sorption porosity.

Tracer	K_d (m^3/kg)	Surface Sorption K_a (m)	Free Water Diffusivity (m^2/s)
Ba-131	$2.00 \cdot 10^{-04}$	0	$8.30 \cdot 10^{-10}$
Ba-133	$2.00 \cdot 10^{-04}$	0	$8.30 \cdot 10^{-10}$
Br-82	0	0	$2.08 \cdot 10^{-9}$
Ca-47	$5.20 \cdot 10^{-06}$	0	$7.92 \cdot 10^{-10}$
Cs-134	$8.00 \cdot 10^{-04}$	0	$2.06 \cdot 10^{-9}$
Cs-137	$8.00 \cdot 10^{-04}$	0	$2.06 \cdot 10^{-9}$
HTO	0	0	$2.40 \cdot 10^{-9}$
K-42	$2.00 \cdot 10^{-04}$	0	$2.00 \cdot 10^{-9}$
Na-22	$2.80 \cdot 10^{-05}$	0	$1.33 \cdot 10^{-9}$
Na-24	$2.80 \cdot 10^{-05}$	0	$1.33 \cdot 10^{-9}$
Rb-83	$1.40 \cdot 10^{-03}$	0	$2.03 \cdot 10^{-9}$
Rb-86	$1.40 \cdot 10^{-03}$	0	$2.03 \cdot 10^{-9}$
Re-186	0	0	$1.00 \cdot 10^{-9}$
Sr-85	$4.70 \cdot 10^{-06}$	0	$7.89 \cdot 10^{-10}$

For tracer tests where neither the TRUE-Block Scale nor the TRUE-1 sorption parameters established a good fit to the experimental data, the K_d and K_a values were calibrated to the sorbing tracer breakthrough. Since the conservative tracer transport parameters were derived from analysis of previous conservative tracer experiments, only K_d and K_a were studied – all other parameters including transport aperture, path width, diffusivity, porosity, etc were kept fixed.

Table 6-14 details the K_d and K_a values that were necessary to provide a good fit to measured breakthrough. Tracers Br-82 or Na-24 in Test C1 achieved a good fit with the TRUE-1 sorbing parameters. All other simulated tracer breakthrough and recovery data improved by increasing effective K_d and K_a values. The percent change in K_d value is based on the TRUE-1 Task 4F K_d value. T_5, T_{50}, and T_{95} for all sorbing tracer test simulations, predicted and calibrated, are compared to the in-situ measurement in Table 6-15.

Very large increases in sorption parameters are necessary to obtain adequate fits to tracer breakthrough. For Pathways I (C1) and II (C2), these changes may indicate that TRUE-1 sorption values were not applicable to the tested pathways as modeled. For Pathway III (C3), the conservative tracer HTO was considerably slower than indicated by the previous tracer tests, indicating an issue possibly related to test boundary conditions.

Table 6-14: Sorbing Tracer Calibration Parameters. Calibration of sorbing parameters to fit tracer breakthrough. Calibration values compared to TRUE-1 sorption parameters

Test / Tracer	K_d (m^3/kg)	Surface Sorption K_a (m)	% Change from Blind Prediction Sorbing Parameters (TRUE-1)
C1 / Br-82	0	0	0%
C1 / Na-22	$8.75 \cdot 10^{-06}$	$1.58 \cdot 10^{-07}$	+3241%
C1 / K-42	$1.00 \cdot 10^{-05}$	$1.80 \cdot 10^{-07}$	+5%
C1 / Ca-47	$6.25 \cdot 10^{-06}$	$1.13 \cdot 10^{-07}$	+1000%
C1 / Rb-86	$1.03 \cdot 10^{-04}$	$1.85 \cdot 10^{-06}$	+495%
C1 / Cs-134	$4.57 \cdot 10^{-04}$	$8.23 \cdot 10^{-06}$	+550%
C2 / Re-186	$3.00 \cdot 10^{-07}$	$5.40 \cdot 10^{-09}$	Na (prediction $K_d = 0$)
C2 / Ca-47	$6.25 \cdot 10^{-06}$	$1.13 \cdot 10^{-07}$	+1000%
C2 / Ba-131	No in-situ data given		
C2 / Cs-137	No in-situ data given		
C3 / HTO	$5.00 \cdot 10^{-06}$	$9.00 \cdot 10^{-08}$	Na (prediction $K_d = 0$)
C3 / Na-24	$2.70 \cdot 10^{-07}$	$1.31 \cdot 10^{-05}$	0%
C3 / Sr-85	$3.34 \cdot 10^{-04}$	$6.01 \cdot 10^{-06}$	+32115%
C3 / Rb-83	No in-situ data given		
C3 / Ba-133	No in-situ data given		

Table 6-15: Comparison of Experimental Data, Predictions using TRUE-1 and TRUE-Block Scale sorption parameters (Prediction TRUE-1 and Prediction TRUE-BS), and Sorbing Tracer Calibrations where sorption parameters were calibrated to obtain the best-fit to breakthrough experimental data (STC).

Test	Tracer		T5	T50	T95	% Recovery
C1	Br-82	Experimental Data	9.01	21.01	49.02	111%
		Prediction TRUE-1	11	26	131	100%
		Prediction TRUE-BS	10	26	131	100%
		SCT	no calibration			
	Na-24	Experimental Data	11.01	27.01	104.68	96%
		Prediction TRUE-1	11	24	121	100%
		Prediction TRUE-BS	10	25	200	100%
		SCT	no calibration			
	K-42	Experimental Data	21.01	104.68	Na	53%
		Prediction TRUE-1	320	750	Na	92%
		Prediction TRUE-BS	12	32	850	99%
		SCT	27	61	380	99%
	Ca-47	Experimental Data	15.01	46.02	262.71	98%
		Prediction TRUE-1	11	26	131	100%
		Prediction TRUE-BS	10	24	130	100%
		SCT	13	46	280	99%
	Rb-86	Experimental Data	67.54	403.42	Na	67%
		Prediction TRUE-1	45	104	660	99%
		Prediction TRUE-BS	15	74	Na	94%
		SCT	171	410	2800	97%
	Cs-134	Experimental Data	526.42	Na	Na	39%
		Prediction TRUE-1	160	450	2600	97%
		Prediction TRUE-BS	18	123	3400	96%
		SCT	1300	3300	Na	57%
C2	Re-186	Experimental Data	92.88	255.18	Na	80%
		Prediction TRUE-1	74	200	Na	73%
		Prediction TRUE-BS	74	200	Na	73%
		SCT	100	280	Na	69%
	Ca-47	Experimental Data	377.01	721.32	Na	68%
		Prediction TRUE-1	123	370	Na	66%
		Prediction TRUE-BS	102	400	Na	67%
		SCT	310	Na	Na	44%
C3	HTO	Experimental Data	227.33	822.33	Na	73%
		Prediction TRUE-1	148	330	1200	100%
		Prediction TRUE-BS	148	330	1200	100%
		SCT	260	660	Na	94%
	Na-22	Experimental Data	336.33	1481.3	Na	70%
		Prediction TRUE-1	152	350	1400	100%
		Prediction TRUE-BS	183	430	2200	99%
		SCT	340	900	Na	91%
	Sr-85	Experimental Data	640.08	2967	Na	52%
		Prediction TRUE-1	173	400	1900	99%
		Prediction TRUE-BS	153	350	1400	100%
		SCT	850	2500	Na	71%

In general, sorbing tracer transport for Pathway I was reasonably well matched using the TRUE-1 sorption parameters (Table-6-8). There was not a significant difference between results obtained using TRUE –Block Scale sorption parameters (Table 6-13) as compared to TRUE-1 sorption parameters. While improvements were possible using larger sorption values, the fit using TRUE-1 sorption parameters was generally reasonable. Some improvements were achieved by increasing K_d and K_a to increase sorption. Future studies will need to address the possibility of greater porosity for the immobile zone related to the C1 pathway to explain these lower recoveries.

Pathway II (Test C2) was reasonably well predicted for the conservative tracer Re-186. Mass recovery was within 10% of the predicted value of 73%, supporting the use of FIZ pipe to model tracer loss to alternative sinks. The travel times for sorbing tracers were approximately 2-3 times longer than predicted using either TRUE-1 or TRUE-Block Scale sorption parameters. However, increases in sorption parameters also reduced recoveries to below measured levels.

The maximum recovery for the conservative tracer HTO used in Pathway III, Test C3 was 73%. This is inconsistent with the CN/DFN model that did not include any alternative sinks. The predicted recoveries for both sorbing and conservative tracers were all approximately 100%, while measured recoveries were only 50 to 73%. In addition the advective travel time t_{50} for HTO was over twice that expected from PT4 results. This indicates that the boundary condition of Test C3 were such that the effective gradient along the transport path was greatly reduced during the Phase C experiment. It was possible to improve the fit of the breakthrough curve for Test C3 by assuming sorption. However, this is not very realistic. The sorbing tracer breakthrough for Pathway III could also be matched by increasing the K_d sorption parameter. However, it is doubtful whether this is a correct approach, given the low recovery of HTO.

7 Discussion and conclusions

The JNC/Golder team implemented and tested the Revised March 2000 Hydro-structural model (Hermanson and Doe, 2000) for use in "blind" predictions of sorbing tracer tests at the TRUE Block Scale site. The hydro-structural model was implemented to include both background fractures and fracture intersection zones (FIZ) as indicated by the site characterization data.

The hydro-structural model was first tested against experimental distance-drawdown data. The hydro-structural model was generally acceptable according to this data. However, minor changes were made to the structure transmissivity and connectivity to account for discrepancies in connectivity of a few structures. Fracture intersection zones (FIZ) were included for the intersection of deterministic Structures 13 and 21 and Structures 20 and 21 to establish connections for possible mass loss within the models.

Tracer transport parameters were obtained from conservative tracer tests B2g, B2d, and PT4 along the same pathways (I, II and III) used for the C1, C2, and C3 tracer tests. The parameters obtained based on these experiments were matrix porosity, diffusion distance, dispersion length, and transport aperture. Phase C "blind" predictions of conservative and sorbing tracer transport were made using the CN/DFN implementation of the project hydro-structural model with the pathway specific transport parameters, and in-situ calibrated sorption parameters obtained from the TRUE-1 experiments (Dershowitz et al., 2000).

Once predictions were made, experimental data was released to compare the "blind" predictions with in-situ breakthrough data to evaluate the hypotheses related to the hydro-structural model, FIZ effects, and transport parameters. In general the TRUE-1 transport parameters were not sufficient for adequate transport prediction.

Where neither the TRUE-1 nor the TRUE-Block Scale sorption parameters resulted in good matches to the experimental data supplementary simulations were carried out to determine whether better fit could be obtained by modifying K_a and K_d. In these preliminary studies, matrix porosity, diffusion distance, dispersion length and transport aperture were not altered. In general, modification of K_a and K_d was sufficient to obtain significant improvement to matches. However, future studies need to address the possibility that different sets of pathway parameters are responsible for observed delays in breakthrough, particularly for pathway C3.

8 References

Andersson, P., Personal communication, November, 2000.

Andersson, P., Byegård, J., Dershowitz, W., Doe, T., Hermanson, J., Meier, P., Tullborg, E-L., Winberg, A., 2002a. TRUE Block Scale Project Final Report 1. Characterization and model development. Swedish Nuclear Fuel and Waste Management Company. SKB Technical Report TR-02-13.

Andersson, P., Byegård, J., Winberg, A., 2002b. TRUE Block Scale Project Final Report 2. Tracer tests in block scale. Swedish Nuclear Fuel and Waste Management Company. SKB Technical Report TR-02-13.

Byegård, J., Johansson, H., Skålberg, M., Tullborg, E-L., 1998. The interaction of sorbing and non-sorbing tracers with different Äspö rock types. Sorption and diffusion experiments in the laboratory scale. SKB TR-98-18. ISSN 0284-3757, 1998.

Dershowitz, W., Cladouhos, T. and M.Uchida, Tracer Tests with Sorbing Tracers. Golder Associates Inc., January 2001. Swedish Nuclear Fuel and Waste Management Company. Äspö Hard Rock Laboratory International Cooperation Report ICR-01-02.

Dershowitz, W., Fox, A. and M.Uchida, 2000. Understanding of Sorbing Transport in Fracture Networks at the 10 Meter Scale. Unpublished document.

Dershowitz, W., Foxford, T., Sudicky, E., Shuttle, D.A. and T. Eiben. 1998. PAWorks: Pathways analysis for discrete fracture networks with LTG solute transport. User Documentation, Version 1.5. Golder Associates Inc.

Dershowitz, W., Lee, G., Geier, J., Foxford, T.and E. Ahlstrom, 1999. FracMan Interactive Discrete Feature Data Analysis, Geometric Modeling, and Exploration Simulation. User Documentation, Version 2.6. Golder Associates Inc.

Hermanson, J. and T. Doe, 2000. Updated March 1999 Hydro-structural Model. TRUE Block Scale Project Correspondence. Swedish Nuclear Fuel and Waste Management Company.Äspö Hard Rock Laboratory International Progress Report IPR-00-34.

Holton, D., 2001. Boundary conditions for sub-models at the Äspö TRUE Block site. . Swedish Nuclear Fuel and Waste Management Company Äspö Hard Rock Laboratory International Progress Report IPR-01-50.

Miller, I., Lee, G. and W. Dershowitz 1999. MAFIC: Matrix/Fracture Interaction Code with heat and solute transport. User Documentation Version 1.6, Golder Associates Inc.

Oila, E., Siitari-Kauppi, M., 2001. Investigation of porosity and microfracturing in granitic rock using the C-PMMA technique . Swedish Nuclear Fuel and Waste Management Company. Äspö Hard Rock Laboratory International Progress Report IPR-01-27.

Winberg, A., Andersson, P., Hermanson, J., Byegård, J., Cvetkovic, V. and L. Birgersson 2000. Final report of the first stage of the tracer retention understanding experiments. Swedish Nuclear Fuel and Waste Management Company (SKB), Technical Report TR-00-07. ISSN 1404-0344.

Winberg, A., (ed), 2000. Final Report, TRUE Block Scale Project, Characterization and Model Development Swedish Nuclear Fuel and Waste Management Company. Äspö Hard Rock Laboratory International Cooperation Report ICR-00-02.